NASA-CR-173679
19840020041

A Reproduced Copy

OF

Reproduced for NASA

by the

NASA Scientific and Technical Information Facility

PURDUE UNIVERSITY
SCHOOL OF AERONAUTICS AND ASTRONAUTICS

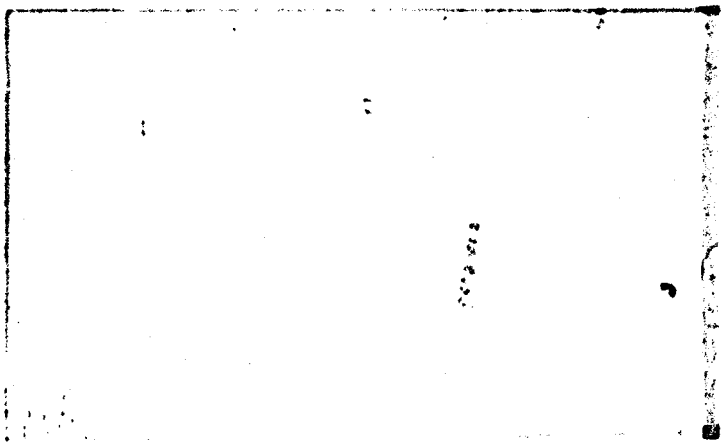

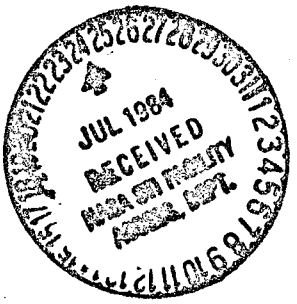

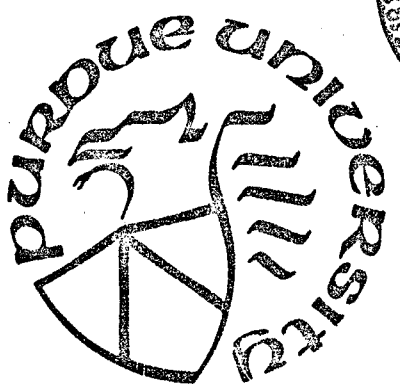

West Lafayette, Indiana 47907

Three-Dimensional Measurements of Fatigue Crack Closure

by

S.K. Ray and A. F. Grandt, Jr.

Final Report

for

NASA Grant No. NAG-1-321

School of Aeronautics and Astronautics

Grissom Hall

Purdue University

West Lafayette, Indiana 47907

July 1984

1. Report No.	2. Government Accession No.	3. Recipient's Cat. No.
4. Title and Subtitle Three-Dimensional Measurements of Fatigue Crack Closure		5. Report Date July 1984 6. Performing Org. Code
7. Author(s) S.K. Ray and A.F. Grandt, Jr. 9. Performing Organization Name and Address School of Aeronautics & Astronautics Purdue University W. Lafayette, IN 47907 12. Sponsoring Agency Name and Address National Aeronautics & Space Administration Langley Research Center, Hampton, VA 23665 15. Supplementary Notes		8. Performing Org. Rept. N 10. Work Unit No. 11. Contract or Grant No. NAG-1-321 13. Type of Rept. & Per. Covered Final Report June 83 - June 84 14. Sponsoring Agency Code

16. Abstract

Results are described for fatigue crack growth and retardation experiments conducted in polycarbonate test specimens. The transparent test material allows optical interferometry measurements of the fatigue crack opening (and closing) profiles. Crack surface displacements are obtained through the specimen thickness and are discussed in terms of three-dimensional aspects of fatigue crack closure.

17. Key Words (Suggested by Author(s))	18. Distribution Statement
Fatigue Crack Closure Polycarbonate Fracture Mechanics	Unclassified - unlimited
19. Security Classif. (of this report) Unclassified	20. Security Classif. (of this page) Unclassified
21. No. of Pages 124	22. Price

TABLE OF CONTENTS

LIST OF ILLUSTRATIONS

THREE-DIMENSIONAL MEASUREMENTS OF FATIGUE CRACK CLOSURE

S.K. Ray* and A.F. Grandt, Jr.**
School of Aeronautics and Astronautics
Purdue University
West Lafayette, IN 47907

SUMMARY

Fatigue cracks were grown in polycarbonate specimens under constant cyclic stress intensity factors and were subjected to tensile overloads to determine the fatigue crack retardation behavior. The cracks were examined under a monochromatic light source to create optical interference fringe patterns, which were used to measure crack surface separation in the test specimens. These crack opening profiles were obtained as a function of applied load and were compared before and after the tensile overload. These results are discussed in terms of the fatigue crack closure mechanism, and provide a more thorough understanding of the three dimensional nature of crack closure.

A tensile overload was shown to significantly delay subsequent fatigue crack growth in polycarbonate specimens. The increased difference between crack growth rates at the surface and interior of the specimen resulted in more tunneling following the overload. The crack opening load at the specimen surface is significantly higher than that in the interior, which explains the difference in crack growth rates between the surface and the interior of the specimen.

---

* Research assistant
** Professor of Aeronautics and Astronautics

NOTATION

a:	Average crack length
2D:	Crack surface separation at a specific fringe location
E:	Elastic modulus
K:	Stress intensity factor
ΔK:	Cyclic range in stress intensity factor
n:	Fringe order
N:	Number of applied load cycles
Q:	K_{max} of overload cycle/ΔK_b
r:	Distance from crack tip
R:	Stress ratio = minimum/maximum stress per cycle
ν:	Poisson's ratio
λ:	Wave length of light (sodium vapor)
ΔK_b:	Applied ΔK for steady state crack growth
K_o:	K needed to separate the crack faces at the tip.
K_{oe}:	K value which gives elastic crack opening-force relation
N_d:	Increase in cyclic life caused by the overload

CHAPTER 1

BACKGROUND

1.1 INTRODUCTION

One important measure of fatigue damage is the current fatigue crack size and its associated propagation rate. It has been observed that crack tip plasticity due to tensile overloads may significantly delay (retard) fatigue crack propagation in many materials [1-4]. Figure 1 represents a typical crack length versus cycles curve showing the overload effect on the growth rate of a fatigue crack. Since many structures are subjected to complex load histories which may include these overloads, understanding the retardation effect is of great importance. Explanation for fatigue crack retardation has included crack tip blunting and the fatigue crack closure approaches.

The blunting mechanism describes retardation in terms of crack reinitiation [5]. When an overload is applied, the crack tip is blunted by the local plastic deformation, and additional cycles must be applied to reinitiate small flaws at the blunted site. Note in Figure 2 how small surface cracks form along the notch in a polycarbonate fatigue specimen (2b), and eventually coalesce (2c) into a single crack front. Following the application of a tensile overload in the transparent test specimen, small cracks again form along the blunted crack tip (Figure 2e) during the retardation period. Thus, in this case, the overload blunted the sharp crack tip and the retardation period involved reinitiation of fatigue cracks along the blunted crack front.

The crack closure phenomenon [1,6] explains retardation in terms of compressive residual stresses behind the crack tip. These stresses are due to the plastically deformed region ahead of the crack tip, and the size of this deformed region is proportional to the stress level and the crack length. As a crack grows through this plastic zone, a plastic wake is formed which contains the compressive residual stresses. These stresses hold the crack faces closed during portions of positive load cycles and reduce the effective load for the remainder of the cycle. Figure 3 schematically shows the crack tip plastic zone and the resulting plastic wake. Figure 4 shows how the effective stress range is reduced in a typical load cycle by crack closure. The crack growth rate is decreased as a result of the closure effect and in some cases crack arrest is caused by complete closure [7]. It has been proposed that the overloads increase the magnitude of the residual compressive stresses, resulting in a reduction of the effective stress level, and lowering of the crack growth rate (retardation). A recent review paper [8] points out the importance of fatigue crack closure in characterizing variable amplitude loading, threshold fatigue crack growth, and extension of short cracks.

It is well known that the crack tip plastic zone is larger at free surfaces, where plane stress occurs, than at the center of a thick specimen where plane strain conditions prevail [9].

Figure 5 shows how the plastic zone size varies through the thickness of a thick specimen. This through-the-thickness plastic zone size variation has been used to explain, among other things, thickness dependent fracture toughness and thickness related fatigue crack behavior. The larger plastic zone at the specimen surface would imply that the closure effect is more profound at the surface than at the interior, resulting in a slower crack growth rate at the free surface. This through-thickness variation in crack growth rates is commonly called the tunneling effect. The effect of the state of stress on plastic zone size, and the resulting fatigue crack growth rate has been demonstrated with variable amplitude loading experiments, where thin specimens have longer crack growth lives than thick specimens [10-16].

In addition to crack closure associated with the plastic wake behind the crack tip, two other closure mechanisms have been proposed: asperity induced closure and oxide induced closure. The asperity induced closure model [17-19] states that crack surface roughness keeps the crack faces propped open under zero load. The maximum plastic zone size in this model is smaller than the grain size, while the size of the fracture surface roughness is on the same order as the crack tip displacement. To satisfy the requirement for a small plastic zone size, asperity induced closure is generally observed at low crack growth rates (on the order of 10^{-6} mm/cycle). When the fracture surface size is the dominant factor, the crack tends to grow in a zig-zag, out of plane path, leading to significant Mode II displacements and to asperity induced closure. Models used to predict asperity induced closure include the single asperity model [20], spring clip model [21], and the fracture surface roughness model [22].

In the oxide induced closure mechanism [23,24], the formation of an oxide layer just behind the crack tip prevents the crack surfaces from closing. As before, the thickness of the oxide layer is comparable to the crack tip displacements. During the closing phase of the load cycle, early contact occurs between the two crack faces due to the presence of the oxide layer, resulting once more in the closure phenomenon. Oxide induced closure, like the asperity model, has also been observed at low crack growth rates. Since both asperity and oxide induced closure mechanisms keep the crack faces open under zero load, they are sometimes referred to as "Non-closure" models. A more detailed discussion of the various closure mechanisms, as well as other factors contributing to closure, is presented in a recent literature review [25].

1.2 PRIOR WORK

This section reviews techniques that have been developed to characterize fatigue crack closure. Both numerical and experimental methods are briefly discussed.

Some analytical crack closure models [26-27] have been shown to be effective in predicting the crack growth rates in thin metal specimens. The model used in Reference 26, for example, employed the Dugdale concept but allowed plastically deformed material to be left in the wake of the extending crack tip. This model was used to study a central crack in a finite-width specimen subjected to uniform load. The crack surface displacements were obtained by the superposition of two elastic solutions: a crack in a finite plate subjected to a remote stress and a uniform stress applied over a portion of the crack surfaces. This crack closure model was used to correlate the fatigue crack growth rates under constant-amplitude loading and to predict the crack behavior under variable-amplitude loading. Experiments performed with 2219-T851 aluminum alloy specimens agreed well with the analytical predictions.

The closure model described in Reference 27 is based on a cycle-by-cycle analysis of the fatigue crack growth and assumes that crack extension only occurs during the increasing portion of the applied load cycle. The effective stress intensity factor range that the central crack in a plate experiences is based on the plasticity behind the crack tip. This model was used to analyze crack growth rate behavior under variable amplitude loading, and the results were comparable to the experimental behaviors.

Another numerical study analyzed crack closure in a center-cracked panel under cyclic loading using a two-dimensional, non-linear, finite element model with changing boundary conditions [28]. In this study the material was assumed to be elastic-perfectly plastic, and the model was composed of two-dimensional constant-strain triangular elements. It was observed that the element-mesh size near the crack tip influenced the prediction of the magnitude of crack closure and opening loads. By choosing an appropriate finite-element-mesh, the actual experimental crack growth rate could be simulated. Using this finite element analysis, the simulated crack growth rate was consistent with some of the experimental results. Although the finite-element method may work well for closure predictions, the analysis is often complicated and may require long computation times.

Most experimental measurements of fatigue crack opening have been performed on metal specimens, employing techniques such as crack mouth opening displacement (CMOD) measurements, strain gages, push rods, etc. Some detailed aspects of these methods are discussed below.

The CMOD gage [29-31] measures the displacement from a clip gage mounted across the mouth of the precracking notch. A plot of displacement versus load is obtained, and the transition point (where the curve changes from non-linear to linear) represents the closure load. The closure load measured by this technique represents an average value for the crack opening through the specimen thickness. Extreme care must be taken with this technique since misalignment and friction in the loading fixtures and the clip gage may alter the results considerably.

The strain gage measurements [29,32-33] involve bonding one or more strain gages at various locations across the crack surfaces. In some cases strain gages are also mounted on the back face of the specimen. The signal from the strain gages are then recorded as a function of the applied load, and the closure load is again determined at the point where the load versus strain record becomes linear.

Ultrasonic methods [34-36] measure the changing acoustic resistance of a specimen as the crack opens or closes. The intensity of the ultrasonic signal reflected from the fatigue crack varies depending on the amount of closure present. In this technique, an ultrasonic transmitter is placed on the top of the cracked test specimen, and a receiver is placed opposite the transmitter on the bottom of the specimen. As before, the received signal intensity is plotted against the load or the stress intensity, and the closure load is determined. The closure load obtained in this fashion is not, however, always consistent with the CMOD or the strain gage measurements [25].

The potential difference approach [25,29,31,37,38] measures the electric resistance of a specimen, which is also proportional to the opening of the crack. In this instance the metal specimen acts as a part of an electrical circuit. A constant current supply is provided across the specimen, and the signal obtained from potential probes placed on both sides of the crack is recorded as a function of the applied load. It has been observed in some applications that the received signal may be misled by the presence of a layer of insulating oxide on the crack faces which prevents electrical contact. Other difficulties with this technique are associated with the change of the electrical properties of the material in the crack tip yield zone.

The interferometric displacement gage [39-40] uses a laser to measure the relative displacement between two shallow reflecting indentations [39], or grooves [40], located across the crack (the separation distance varying from 0.5 to 1.0 mm). Interference fringe patterns are created by the diffracted laser beams, and the motion of these fringes represent the crack surface displacements. This technique has proven to be an effective method for measuring crack surface displacements and is essentially a non-contact method.

The push-rod displacement gage technique [7,41] has been used to determine the closure at a single point inside the specimen. For this method a push-rod assembly is fastened to the specimen by drilling two parallel holes just behind the fatigue crack front. The relative displacement of the hole bottoms is measured with a twin cantilever clip gage via the push-rods. The closure load is then determined by locating the linear point on the load/displacement curve.

Other methods used to obtain the closure loads include special displacement gages [42], direct observation using electron microscopy [43], and a vacuum infiltration technique [44]. It should be noted that all of these techniques only determine the closure loads at the specimen surface or at a single point inside the specimen [7] and can not determine the complete through-the-thickness variation of closure. Also note that since an acoustically or electrically open crack is not the same as a mechanically open flaw, these methods can give different measures of crack closure [45].

Optical interferometry has been employed to measure stress intensity factors from crack surface displacements in glass specimens [46-47] and to measure crack closure in polymethylmethacrylate (PMMA) [48]. Although PMMA is fairly brittle, crack retardation was not observed in this earlier work, but it was possible to determine that fatigue crack closure was more significant at the surface than in the specimen interior.

1.3 OBJECTIVE OF CURRENT RESEARCH

The objective of the current research is to determine through-the-thickness variations in fatigue crack closure. Complete three-dimensional crack opening profiles are measured by the use of optical interferometry. In this technique, a monochromatic light source is directed onto the crack plane in an optically transparent specimen. The reflection of the light rays from the crack surfaces form a fringe pattern which can be related to the crack surface displacements. Crack closure can then readily be observed from the behavior of the surface displacements.

Crack opening results are described for optical interferometry measurements with cracked polycarbonate (a transparent, ductile polymer) specimens. Since the specimens are transparent, optical interferometry provides three-dimensional measurements of crack surface displacements. These displacements were then related to fatigue crack retardation and closure. Fundamental questions addressed in this report include the following:

What is the complete through-the-thickness crack opening profile assumed by a fatigue crack in a thick member?

Does the crack opening profile measured on the specimen surface (plane stress) differ from that which occurs in the plane strain interior?

Does the crack opening load differ in the specimen interior from that measured at the free surface?

What is the effect of tensile overloads on crack opening profiles, and what is the subsequent effect on fatigue crack growth?

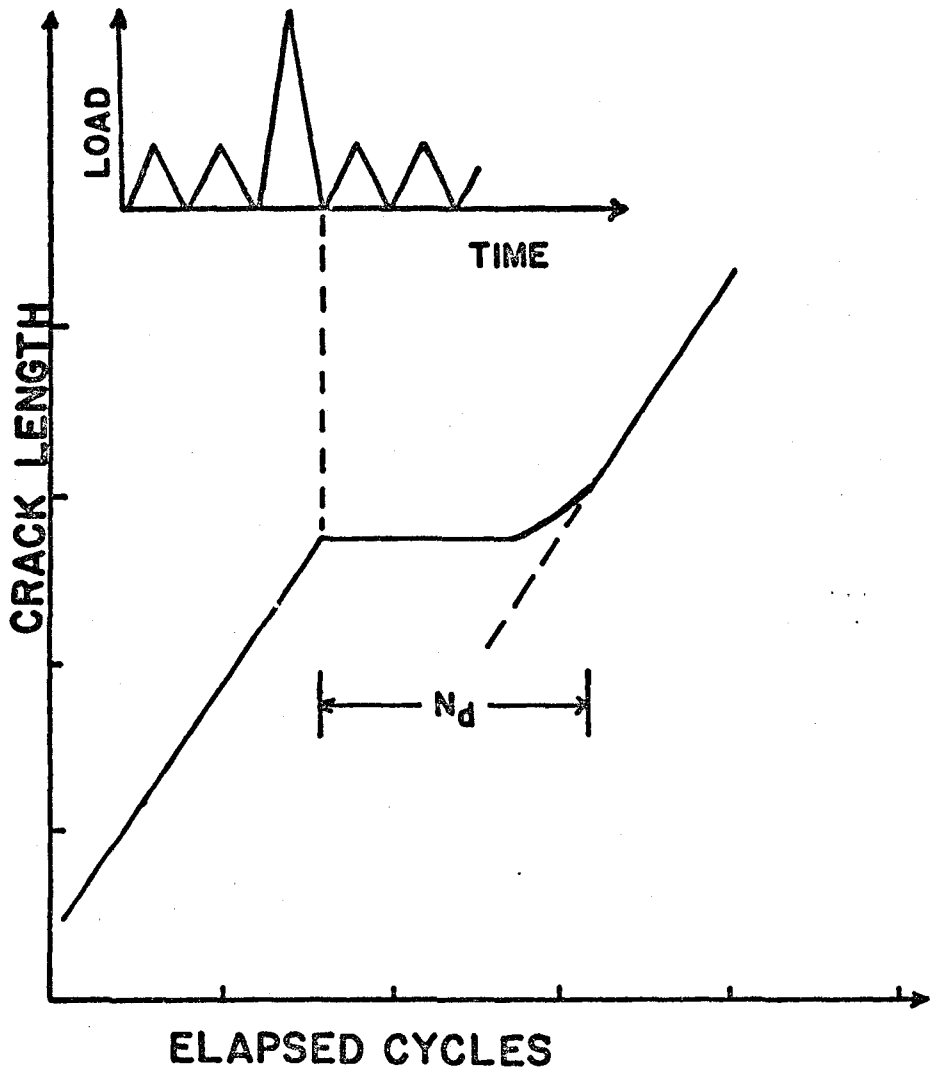

Figure 1: Schematic view of the crack growth under constant cyclic stress intensity showing the retardation of a single peak overload.

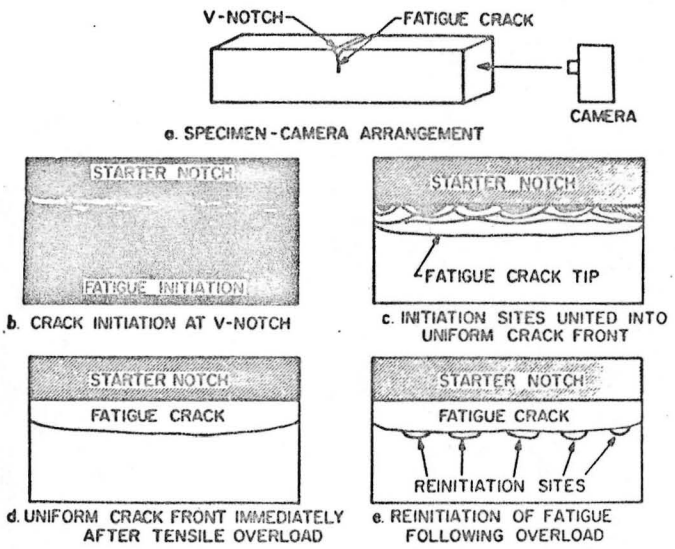

Figure 2: Schematic view of fatigue crack initiation at original V-notch and reinitiation following the overload [Ref. 5].

Figure 3: Schematic view of the crack tip plastic zone and plastic wake formation behind the crack tip, resulting in compressive residual stresses, which hold the crack faces closed during portions of positive applied load.

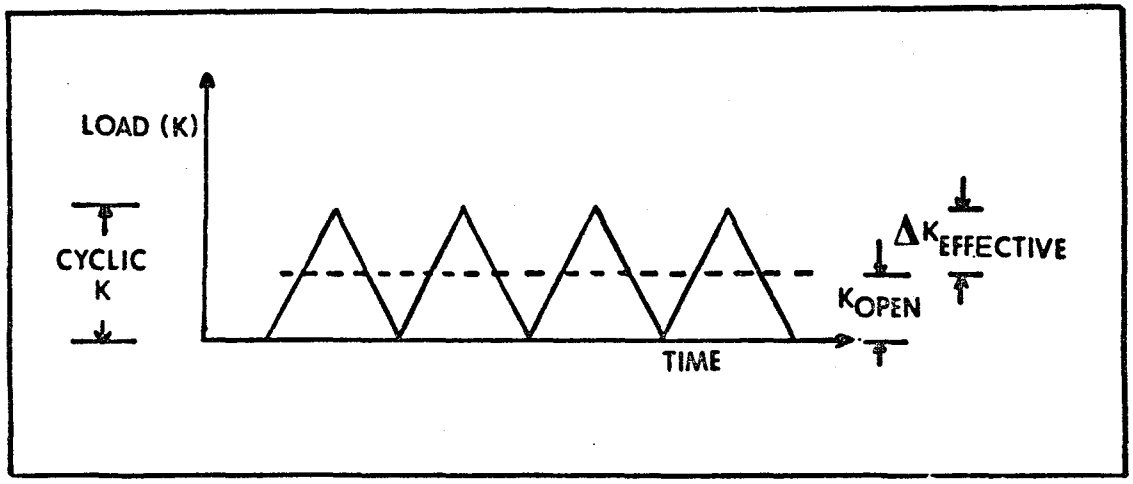

Figure 4: A schematic representation of the effective cyclic K level that the specimen experiences in a typical load cycle.

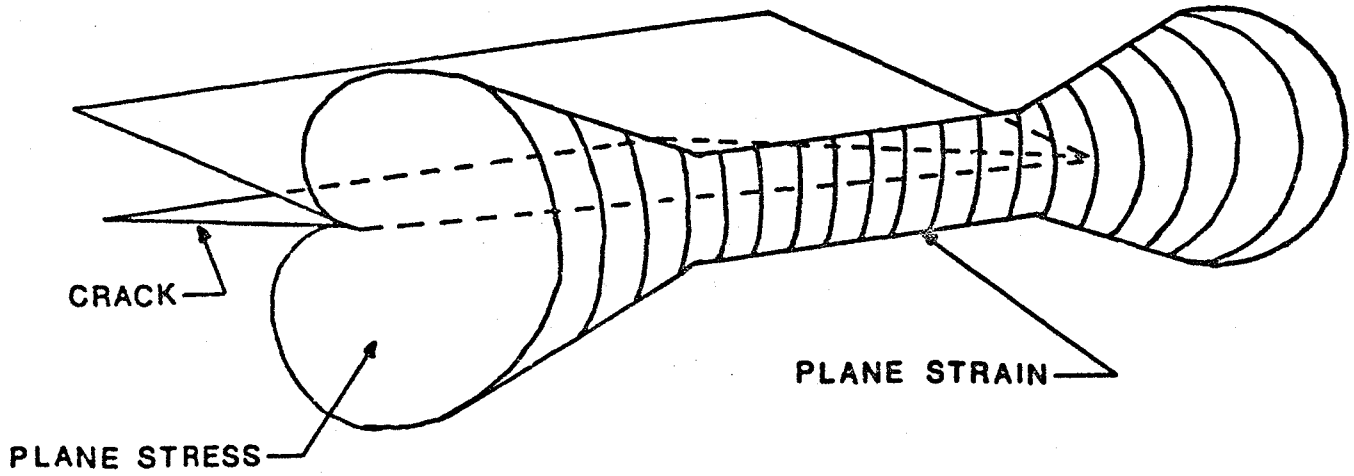

Figure 5: Schematic presentation of three-dimensional crack tip plastic zone showing transition from large plane stress plastic zone at specimen surface to smaller plane strain zone size at the center of the specimen.

CHAPTER 2

EXPERIMENTAL PROCEDURE

2.1 INTERFEROMETRIC TECHNIQUE

Optical interference occurs in a thin transparent wedge when the reflection of light rays from the top and the bottom of the faces of the wedge have different path lengths [49-50]. When a crack is present in a transparent material, an air film wedge is formed between the two crack surfaces and may cause optical interferometry to take place. As schematically presented in Figure 6, some light waves travel through the transparent specimen and are reflected back by the top surface of the crack, whereas other waves, following a different path, penetrate the top surface and are reflected by the bottom surface of the crack. This difference in path lengths causes interference fringes to form. Each fringe represents a locus of points which have the same displacement between the crack surfaces [50]. If the wavelength of the light source is known, the crack surface displacements may be computed using the following optics equation [50].

For destructive interference:

$$D=\frac{2n+1}{4}\lambda \qquad (1)$$

Here D is half the crack surface separation at a specific fringe location, n is the fringe order (n = 0, 1, ...), and λ is the wave length of the monochromatic light source. The 0-order fringe is defined here as the first destructive fringe and corresponds to a total crack separation $2D = \lambda/2$.

Note that Equation 1 demonstrates that destructive fringes occur when the path difference between the top and the bottom faces of the crack equals an odd number of half wavelengthes [49].

In addition to crack closure measurements [48], other applications of the interferometric technique described in the literature include stress intensity factor measurements [46-47,51], study of crack propagation at material interfaces [52], and measurements of the J-integral for arbitrary geometry and loading [53].

2.2 SPECIMEN PREPARATION

Polycarbonate was chosen as the model material because of its optical transparency and relatively large ductility (hence the ability to develop residual stresses that causes crack retardation). The test specimens were 4.6cm. x 2.0 cm. x 17.8 cm. (1.5 in. x 0.8 in. x 7.0 in.) and contained 0.25 cm. (0.1 in.) deep V-notches as shown in Figure 7. All specimen were cut from a single sheet of polycarbonate, and the notches were oriented in the same direction to maintain a constant crack growth direction for all tests. To remove potential initial residual stresses, the specimens were annealed at $138^{o}\pm3^{o}C$ ($280^{o}\pm3^{o}F$) for 24 hours and then slowly cooled to room temperature. A razor blade was used to sharpen the V-notch across the specimen thickness to ensure that small naturally occurring fatigue cracks developed in the same plane, and coalesced to form a single through-the-thickness crack. For observation purposes, one end of the specimen was polished with increasingly finer grade polishing wheels and finally buffed to transparency. Specimen transparency was further improved by placing a cover slip coated with a thin film of oil over the viewing surface (Figure 7).

2.3 FATIGUE CRACK GROWTH MEASUREMENTS

Cyclic loads (haversine function) were applied in a four-point bend configuration at 4 Hz. The specimen experienced a minimum bending moment of 2.33 N-m (20.63 lb-in) during the load cycle to minimize the specimen movement on the four-point bend fixtures. Loads were applied with a 20-000 lb capacity closed loop electrohydraulic MTS machine. The crack plane was photographed through the transparent specimen with a 35 mm. camera as a function of elapsed cycles. The crack photographs were measured by projecting the negatives onto a digitizing board. Since the crack fronts are often curved, five measurements at different locations across the specimen thickness were averaged for the through-thickness crack length.

Load shedding techniques were used to grow the cracks under constant ΔK conditions for the fatigue crack retardation experiments. The resulting linear crack length versus cyclic response simplified the task of determining the retardation cycles caused by overloads (Figure 2). For load shedding purposes, the crack length was measured by viewing a 0.25 cm. (0.1 inch) gradient scale mounted on a transparent piece of specimen material attached to the side of the test specimen. By this arrangement, it was possible to maintain ΔK constant to within $\pm 7\%$ during the experiments. It was necessary to grow the cracks at small cyclic loads to avoid rough crack surfaces which prevented interference fringe formation by scattering the reflected light rays.

2.4 FRINGE OBSERVATION

Interference fringe patterns were obtained by shining a sodium vapor light source through the polished end of the specimen. The wavelength of the sodium light source is 5.89×10^{-7} cm. (2.319×10^{-7} in.). The sodium light was projected at an right angle to the crack plane by one or more small mirrors. The resulting fringe patterns were then photographed for different applied loads with a 35 mm. camera equipped with a 135 mm. lens and bellows adjusted to give the desired magnification of the crack plane. A high contrast technical film (Kodak technical pan film 2415) was used to enhance the fringe photographs. The fringe patterns were photographed under different loads for the steady state crack growth case, the overload cycle, and for periodic cycles following the overload. The fringe pattern photographs were measured by projecting the 35 mm. negatives on to a digitizing table.

A three-point bend static load frame was constructed for the purpose of photographing the interference fringes under small applied loads. The fringes could not be easily photographed while the specimen was mounted on the MTS machine due to the vibration of the hydraulic system and the low light level from the light source. These vibrations, in conjunction with the long exposure times required to photograph the low light level fringe patterns, prevented distinct interference fringe photographs in the fatigue (MTS) machine.

Tensile overloads were applied to the test specimen on the three-point bend static load frame. After photographing the resulting fringe patterns caused by the overloads, further crack growth was carried out at the original baseline stress intensity factors on the MTS machine.

2.5 STRAIN GAGE AND CMOD MEASUREMENTS

One objective of these experiments was to correlate fringe pattern data with results from the strain gage and CMOD techniques. For this purpose, two EA-41-125-120 type strain gages (whose length=0.15 cm.) were mounted across the crack on one test specimen as shown in Figure 8. One of the strain gages was mounted at 0.10 cm. (.04 in.) behind the crack tip at the surface, while the second gage was mounted just ahead of the crack tip. The signals from both strain gages were recorded as a function of applied load at the same time the fringe patterns were photographed. Since the specimen was loaded in three-point bending for the fringe photographs, it was not possible to locate a strain gage on the top surface perpendicular to the crack plane.

A clip gage was mounted at the mouth of the crack by means of two metal tabs glued very close to the notch as shown in Figure 8. The crack mouth displacement was then monitored as a function of applied load. In one experiment, the reading from the strain gage and the clip gage were monitored while the fringe patterns were photographed for increasing load.

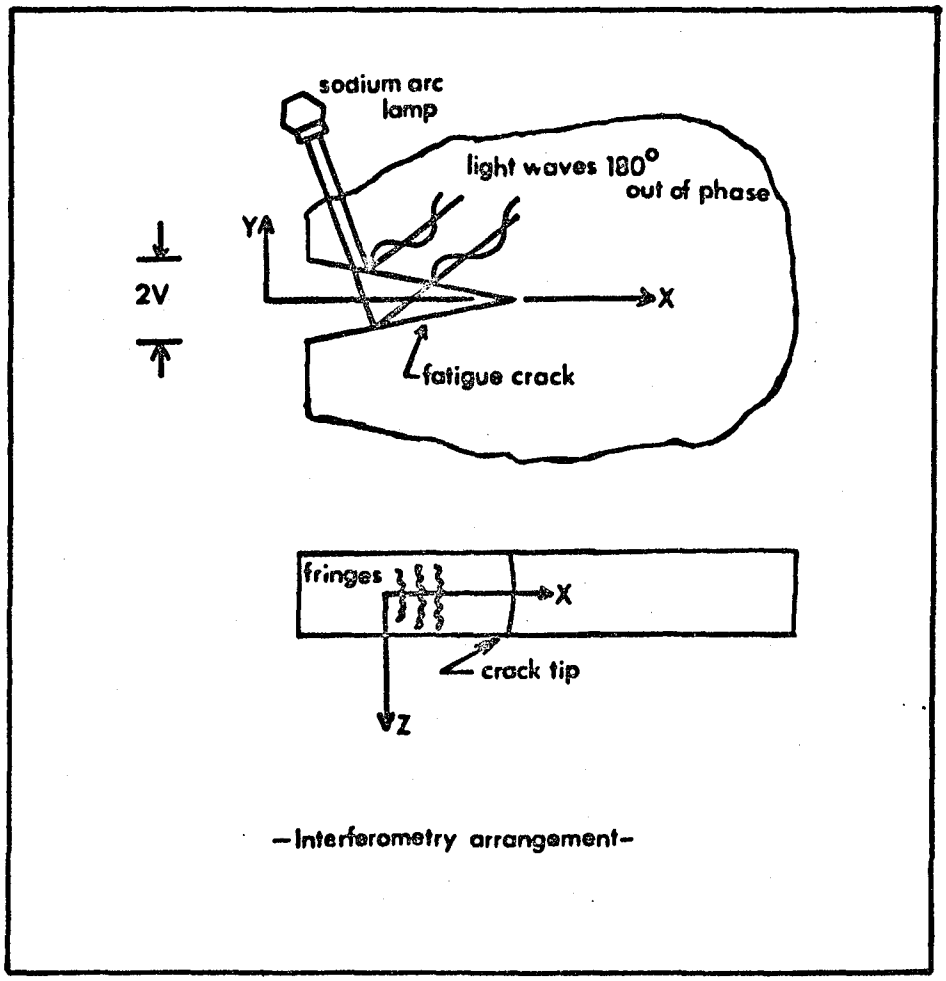

Figure 6: Schematic of interferometry method which gives three-dimensional crack surface displacements in transparent specimens [Ref. 47].

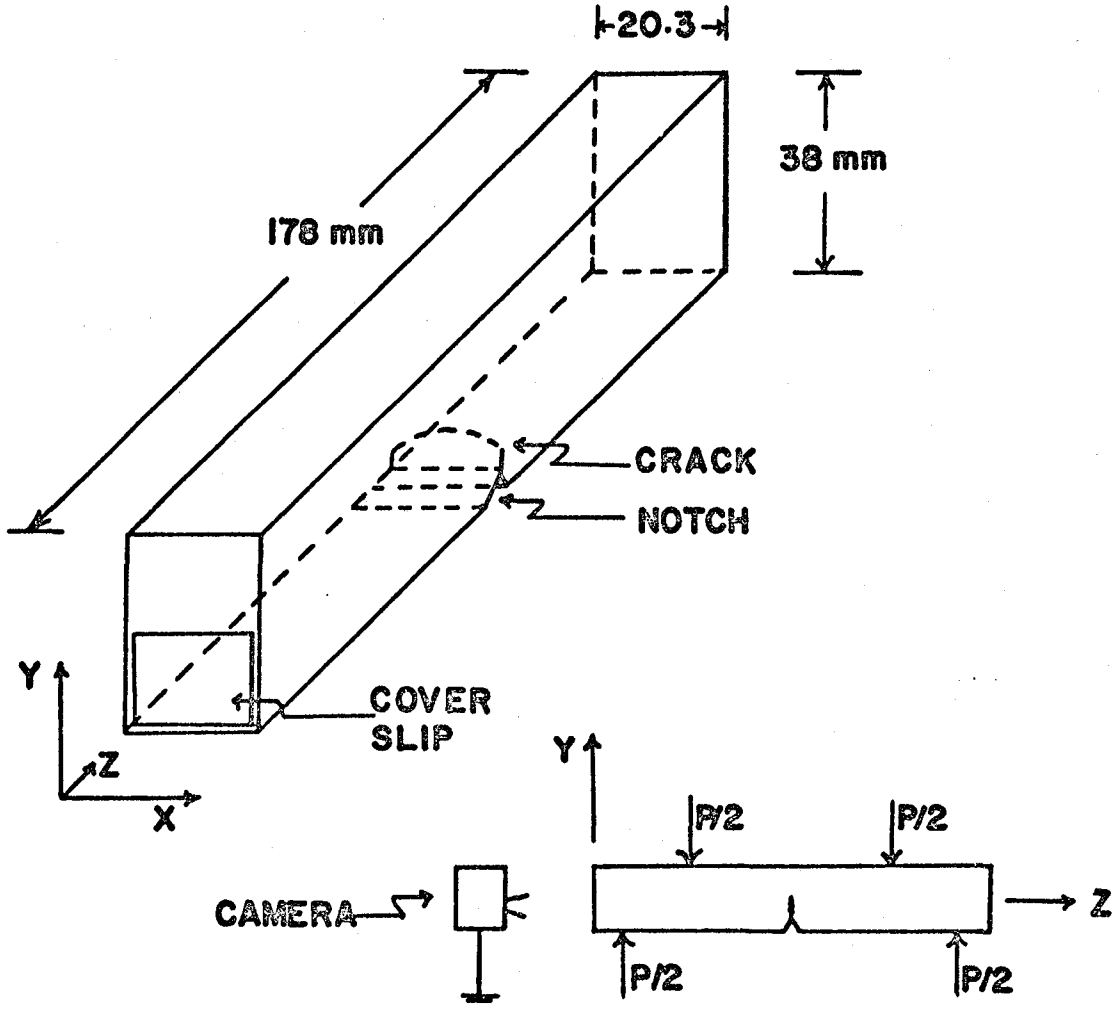

Figure 7: Four point bend test specimen configuration, showing specimen dimensions and experimental setup.

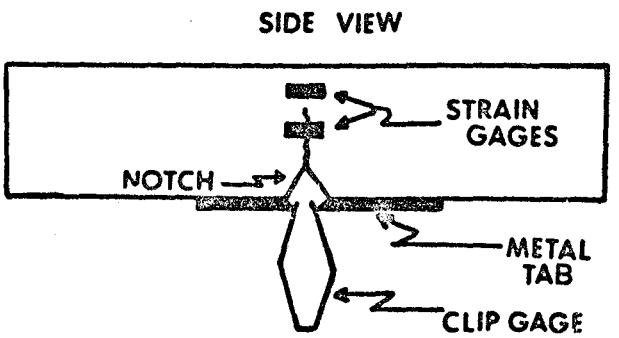

Figure 8: Schematic view of the strain gage and clip gage locations on the test specimen.

CHAPTER 3

RESULTS

3.1 MATERIAL PROPERTIES

Fatigue crack growth rate data for the polycarbonate test material are shown in Figure 9. This plot contains data from six constant load and five constant ΔK tests. All specimens were edge cracked beams loaded in four-point bending as before. The five constant ΔK specimens were conducted at low ΔK levels and are indicated by the solid circles at the lower end of the curve. A least squares straight line fit through the da/dN versus ΔK gave the following crack growth rate relation.

$$\frac{da}{dN} = C\Delta K^m \qquad (2)$$

When da/dN is expressed in inch/cycle, and the units of ΔK are psi-in$^{1/2}$ in Equation 2, m equals 3.89 and C equals 1.62×10^{-17}. If da/dN is in terms of mm/cycle, and the units for ΔK are KPa-m$^{1/2}$, m equals 3.89 and C equals 2.85×10^{-16}.

Tensile tests reported in Reference 5 for polycarbonate gave an elastic modulus of 2.234×10^6 KPa (3.24×10^5 psi), a 0.2% offset yield strength of 4.136×10^4 KPa (6.0×10^3 psi), a yield point of 6.342×10^4 KPa (9.2×10^3 psi), and a fracture toughness of 3637 KPa-m$^{1/2}$ (3310 psi-in$^{1/2}$). Equipment problems prevented measurement of stress-strain curves and fracture toughness at the time of this report although speci-

mens with the current material have been prepared and will be tested at a later date.

3.2 FATIGUE CRACK CLOSURE MEASUREMENTS

This section describes the individual fatigue crack retardation, closure experiments and presents the measured data. The significance of these results is discussed in Chapter 4. Six specimens were tested as described below and are summarized in Table 1.

TEST B-12

Test B-12 was conducted at a baseline stress intensity factor (ΔK_b) of 330 KPa-$m^{1/2}$ (300 psi-$in^{1/2}$). After the steady state fringe patterns were photographed as a function of applied load, an overload factor of 4 ($Q = K_{max} / \Delta K_b = 4$) was applied to the specimen. Figure 10 shows the average crack length versus elapsed cycles for Test B-12. Note that the delay in the cyclic life caused by the overload (N_d) for this specimen is approximately 43 000 cycles.

The presence of the crack tip plastic zone enables the crack surfaces to separate without causing measurable crack extension. This relative movement of the crack faces (crack-opening displacements) may be accurately determined by analyzing the interference fringe patterns. The displacement is expressed in fringe order units in this report, although other dimensions may be obtained by Equation 1.

Figure 11 presents a typical set of fringe patterns for the steady state case while Figure 12 presents the patterns for the first cycle

following the overload. Note in Figure 11 (the steady state case) that as the applied load is increased, the 0-order fringe reached the crack tip at the middle of the specimen at a K value of 46.4 KPa-$m^{1/2}$ (42.3 psi-$in^{1/2}$). As the load is further increased, the 0-order fringe reaches the crack tip at the specimen surface at a K value of 83.4 KPa-$m^{1/2}$ (76.2 psi-$in^{1/2}$). The load, at which the outer-most fringe reaches the crack tip, is referred as the K_o for that particular location and is a measure of the load required for the crack surfaces to separate. In Test B-12, the K_o for the surface of the specimen is 83.4 KPa-$m^{1/2}$ (76.2 psi-$in^{1/2}$), while the crack opened in the interior at 46.4 KPa-$m^{1/2}$ (42.3 psi-$in^{1/2}$). Also note in Figure 11 that as the applied load is increased, the number of fringes increases and the spacing among the fringes decreases, indicating that the crack faces become further separated. The last photograph in Figure 11 shows the fringe pattern photographed at the maximum load (ΔK_b = 330 KPa-$m^{1/2}$). It can be seen that under this applied load, the fringes become straight across the specimen, indicating little difference in crack separation between the specimen surface and interior.

Figure 12 shows that following the overload, the outer-most fringe reaches crack tip at the specimen interior under zero load although some positive load is necessary to open the crack tip at the surface. This fact suggests that the crack tip faces are separated at the specimen interior under zero load following the overload application.

One method for analyzing the crack opening profiles is to plot the fringe order as a function of distance from the crack tip for different

loads showing the crack surface separation as a function of position. Two such plots were obtained for each load sequence; crack opening profiles measured at the specimen surface and another measured along the interior (middle) plane of the specimen. In these crack opening profile plots, the crack tip is used as the plot origin. Figure 13 presents the opening profile measured at the surface for Specimen B-12 after steady state loading. Each curve in this Figure represents a different applied load and gives the total separation between the two crack surfaces as a function of distance from the crack tip. The load for which the curve passes through the origin, causing complete crack tip separation, is referred to here as the opening load (K_o) for the particular crack location. In Figure 13, an applied K of 83.69 KPa-$m^{1/2}$ causes complete crack separation and is called the opening stress intensity (K_o) measured at the specimen surface.

A K_o value may also be obtained for the specimen interior in a similar fashion. Figure 14 presents the crack opening profile for the middle (interior) of Specimen B-12 for the steady state case. Note that the opening load is much smaller in this instance than that at the free surface. The crack surfaces are completely open at an applied K of 46.4 KPa-$m^{1/2}$ at the specimen interior while a value of 83.4 KPa-$m^{1/2}$ was required to separate the crack faces at the specimen surface. This difference in crack tip opening at the specimen interior and surface is due to the larger plastic zone at the specimen surface.

Figure 15 presents crack separation profiles for the surface of the specimen in the steady state case as the applied load is removed. It was observed that the closing load (Figure 15) equals the opening load

(Figure 13) in this case. Figure 16 presents the crack closing profiles measured in the specimen interior, and again, the opening load is equal to the closing value.

Figure 17 presents the crack closing profiles for the overload cycle measured at the surface of the specimen (load is decreasing in this case). The opening load for the overload cycle is, of course, the same value as for the steady state case. Upon examination of Figure 17, it may be noted that the closing load (where the crack surfaces come into contact) for the overload cycle equals 74.4 KPa-$m^{1/2}$ as compared to the opening K of 83.7 KPa-$m^{1/2}$. Figure 18 presents the closing profiles (load is decreasing) for the specimen interior during the overload cycle. The closing K (where the crack faces at the tip come into contact) for the specimen interior is zero as compared to 46.4 KPa-$m^{1/2}$ for the steady state case. Thus, the crack tip remains open in the specimen interior after the overload is removed.

Figures 19-22 present the crack opening profiles measured at the specimen surface during the 1st, 10th, 100th, and 1000th cycles following the overload. There was no significant difference between the opening and the closing K values for these cases. Figures 23-26 present the crack opening profiles measured at the interior (middle) of the specimen for the 1st, 10th, 100th, and 1000th cycles following the overload. Again, it was observed that the specimen interior remained open under zero load for all these cases.

Thus far the opening stress intensity factor (K_o) has been defined as the K value where the crack faces separate at the crack tip as meas-

ured from the fringe pattern. Another interpretation of the opening load often employed is the load at which the crack opens and closes in a linearly elastic manner. When observing the COD, strain gage, or other similar compliance techniques, the opening load is defined as the value where the crack behaves linearly. This linear elastic value is obtained by observing the transition point on the load versus displacement curve. For comparison purposes, load versus displacement curves were obtained from the interference fringes at both interior and surface points on the specimen for different distances from the crack tip.

The data for the applied K versus crack displacement (2D) curves were obtained from the fringe plots (crack opening and crack closing profiles, Figures 11-26) by measuring the displacements (fringe order) at a fixed distance from the crack tip for different applied loads. Figures 27-30 present these elastic opening plots for different locations at both the side and the middle of the specimen for steady state crack growth. The elastic opening K values (K_{oe}) were then obtained by determining the point where the curve changes from non-linear to linear. Figures 31-36 present the load versus displacements curves measured at different locations from the crack tip for the 10th cycle following the overload. It may be noted from Figures 27-36 that the K_{oe} values following the overload are higher than for the steady state cases. The above procedure was carried out for different cycles following the overload as well as for crack opening and closing. Table 2 summarizes the K_{oe} values for different cases for Test B-12. Note that it was not practical to determine K_{oe} for distances less than 0.19 mm (0.0075 in) from the crack tip, since it was not possible to resolve the displace-

ment versus load curves from Figures 13-26 at such small distance from the origin.

TEST B-13

Test B-13 was carried out with ΔK_b set equal to 313 KPa-$m^{1/2}$ (285 psi-$in^{1/2}$) and employed an overload factor of 3. Figure 37 presents the average crack length versus cycles for this test. The delay caused by the overload in this case was 37 500 cycles. In this instance, portions of the crack plane were not smooth enough to form interference fringes through the thickness of the specimen, therefore no crack closure data are available for this test.

TEST B-14

This test employed a baseline ΔK_b of 297 KPa-$m^{1/2}$ (270 psi-$in^{1/2}$) with an overload factor of 5. Figure 38 presents the average crack length versus elapsed cycles for test B-14. The delay caused by the overload in this case equals 54 000 cycles. Figure 39 presents the crack opening profiles for the steady state case at the specimen interior, and Figure 40 represents the corresponding surface profiles. The crack tip opening load for the interior of the specimen was 14.2 KPa-$m^{1/2}$ (12.9 psi-$in^{1/2}$) whereas the opening load for the specimen surface was 37.9 KPa-$m^{1/2}$ (34.5 psi-$in^{1/2}$). It was also observed that the crack tip opening and closing loads were equal for Test B-14. It should be noted that for Test B-14, the opening load (K_o) was considerably lower than the crack tip opening load for Test B-12 (83.4 KPa-$m^{1/2}$).

Figures 41-43 present the specimen interior opening profiles for the 1st, 10th, and 1000th cycles following the overload. Following the overload application, it was observed that the interior crack tip was again open under zero load. Figures 44-45 show the crack opening profiles for the 1st and 10th cycle following the overload at the surface of the specimen. The crack tip opening load at the surface following the overload was 25 KPa-$m^{1/2}$ which is below the 37.9 KPa-$m^{1/2}$ value measured prior to the overload application.

Strain gages were also mounted across the crack at the surface of specimen B-14 (Figure 8). The crack opening profile photographs with and without the strain gages for the steady state case are presented in Chapter 4.

TEST B-15

This test was conducted at a baseline ΔK_b of 269 KPa-$m^{1/2}$ (245 psi-$in^{1/2}$) with an overload factor of 4. Figure 46 presents the average crack length versus applied cycles for test B-15. For this test, only the steady state crack length versus elapsed cycles is plotted since the crack growth pictures following the overload were lost due to difficulties with the photo developing. Figure 47 shows the crack opening profiles for the steady state case at the middle of the specimen, and Figure 48 represents the profiles at the surface. For test B-15, the opening load for the surface is 39.8 KPa-$m^{1/2}$ (36.3 psi-$in^{1/2}$) whereas the opening value for the specimen interior equals 15.1 KPa-$m^{1/2}$ (13.8 psi-$in^{1/2}$). Figures 49-52 present crack opening profiles for the 1st, 10th, 100th, and 1000th cycle following the overload at the surface of the

specimen. Figures 53-56 show the opening profiles for the middle of the specimen for the above conditions. The opening load following the overload at the free surface equals 19.9 KPa-$m^{1/2}$ (18.1 psi-$in^{1/2}$) whereas the crack tip surfaces remain open at zero load for the interior (middle) of the specimen following the overload.

TEST B-16

Test B-16 was conducted at a ΔK_b of 352 KPa-$m^{1/2}$ (320 psi-$in^{1/2}$) with an overload factor of 6. Figure 57 presents the average crack growth versus elapsed cycles for Test B-16. The delay in crack growth caused by the overload in this test equals 50 000 cycles. No fringe patterns were obtained for this test due to crack plane roughness at the relatively high ΔK_b which prevented formation of the interference fringes.

TEST B-17

One objective of this test was to determine whether the region well behind the crack tip influences the crack tip opening loads. Previous work done with thick X7090-T6 powder aluminum alloy specimens has shown that the removal of successive lengths of the plastic wake material behind the crack tip reduces the tip opening load [54]. Although there was a reduction in the crack opening load due to removal of material behind the crack tip, it was observed in Reference 54 that the near-tip closure influences the crack growth behavior much more than the closure away from the tip. This test (B-17) attempted to determine if similar behavior would occur through the specimen thickness in the transparent polycarbonate specimens.

In order to check for variance in crack opening load due to the removal of plastically deformed material behind the crack tip, successive lengths of crack contact surface were removed in Test B-17, and the resulting crack opening profiles were studied. Figure 58 shows a schematic view of this test matrix. Test B-17 was conducted at a baseline ΔK of 297 KPa-$m^{1/2}$ (270 psi-$in^{1/2}$). No overload was applied to this specimen, but the crack opening loads for the steady state case were determined at the specimen middle (Figure 59) and at the free surface (Figure 60). In this test, the free surface steady state opening load (K_o) equals 46.1 KPa-$m^{1/2}$ (42 psi-$in^{1/2}$) and for the middle equals 21.8 KPa-$m^{1/2}$ (19.8 psi-$in^{1/2}$). The effect of the contact surface removal on the crack opening profiles is discussed in Chapter 4.

TEST	ΔK_b (KPa$\sqrt{m}$)	$K_{OVERLOAD}$	TEST DESCRIPTION
B-12	330	1326	CRACK RETARDATION, FRINGE OBSERVATION
B-13	313	939	CRACK RETARDATION
B-14	297	1485	CRACK RETARDATION, FRINGE OBSERVATION, STRAIN GAGE MEASUREMENTS
B-15	269	1076	CRACK RETARDATION, FRINGE OBSERVATION
B-16	352	2112	CRACK RETARDATION
B-17	297	—	FRINGE OBSERVATION, CONTACT SURFACE REMOVAL EFFECT

Table 1: Summary of fatigue crack retardation and closure experiments.

DISTANCE FROM TIP (mm)	S S K_{oe} midplane	S S K_{oe} surface	1st cycle AO midplane	1st cycle AO surface	10th cycle AO midplane	10th cycle AO surface	10^3 cycles AO midplane	10^3 cycles AO surface
0·19	39·55	81·30	65·92	—	73·61	83·50	65·92	—
0·38	36·26	74·71	64·82	69·22	69·12	81·30	64·82	73·61
0·76	36·26	71·42	64·82	68·12	68·12	74·71	64·82	71·42
1·52	36·26	65·92	64·82	68·12	68·12	74·71	64·82	70·32
2·09	—	63·72	—	65·92	—	74·71	—	69·22
3·05	—	63·72	—	65·92	—	74·71	—	68·12

S S : STEADY STATE CONDITIONS

AO : POST OVERLOAD CONDITIONS

Table 2: Summary of the elastic, crack opening values (K_{oe}) for before and after overload for specimen B-12. All K_{oe} units are expressed in KPa-$m^{1/2}$.

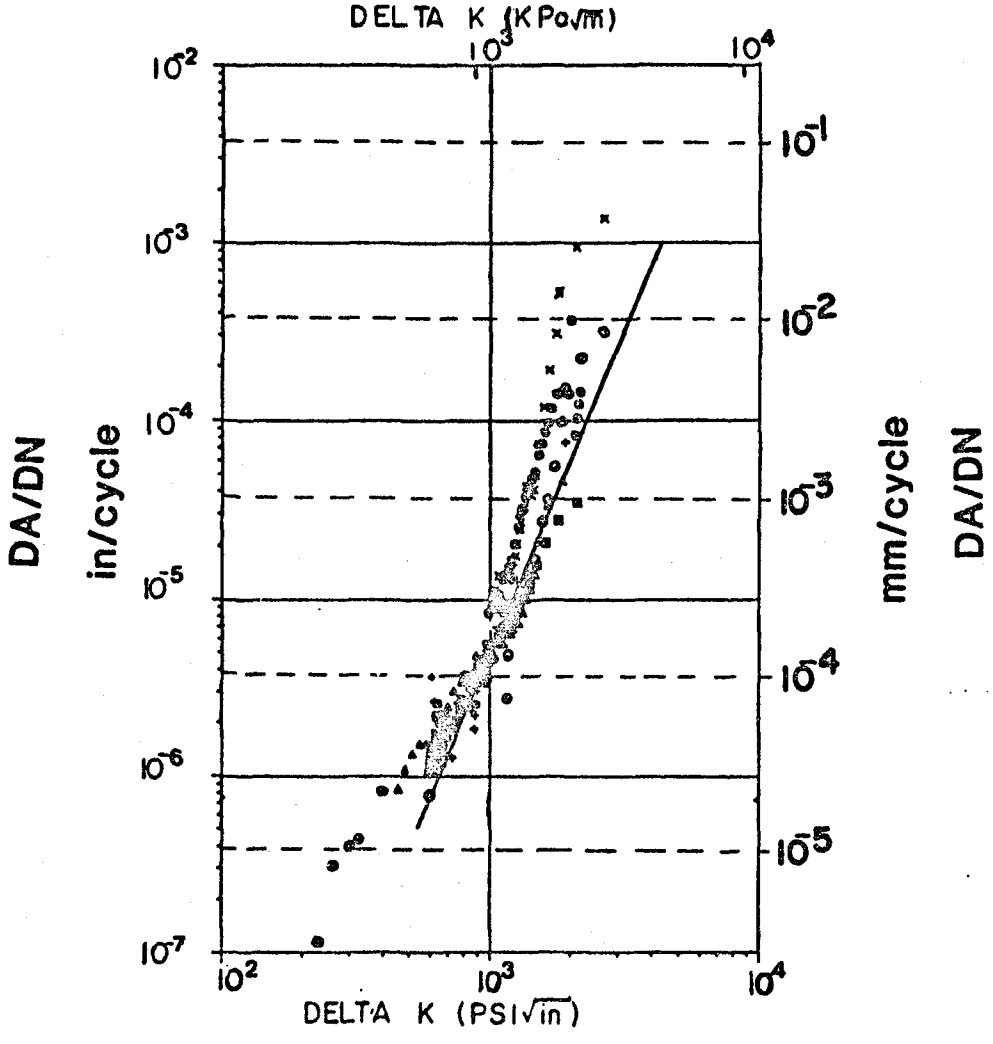

Figure 9: Polycarbonate fatigue crack growth rate data.

ORIGINAL PAGE IS
OF POOR QUALITY

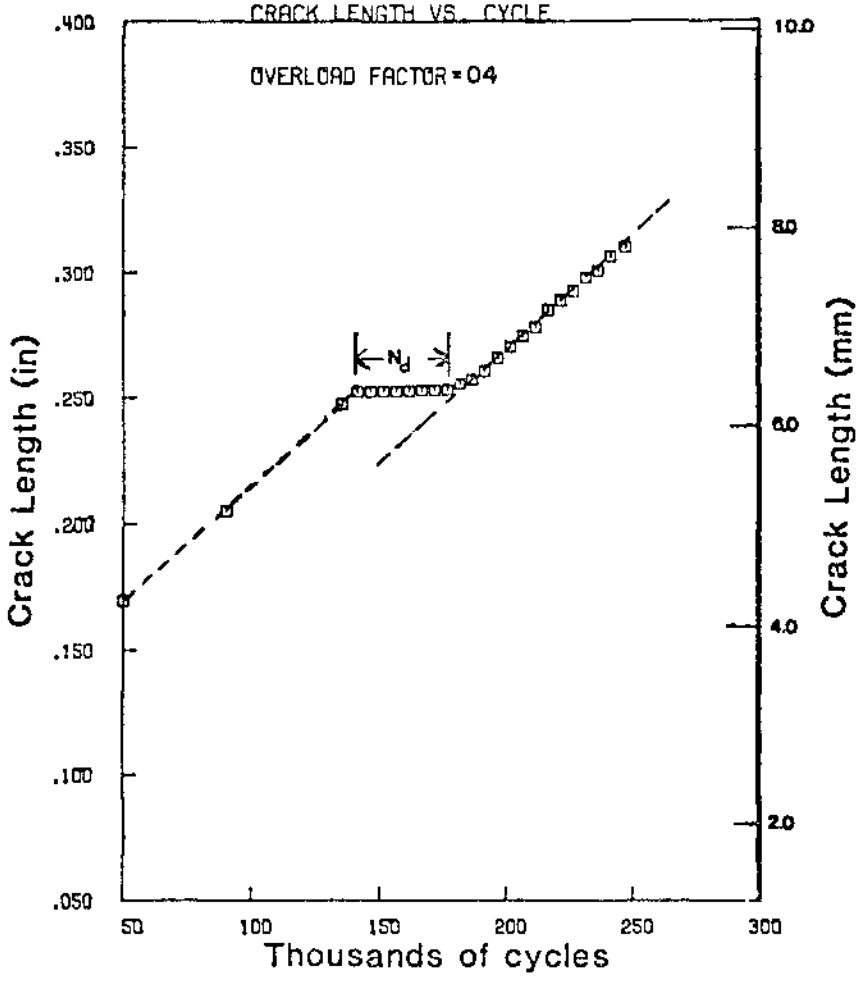

Figure 10: Average through-the-thickness fatigue crack length versus cycles for specimen B-12 (ΔK = 330 KPa-$m^{1/2}$, single peak overload = 1320 KPa-$m^{1/2}$).

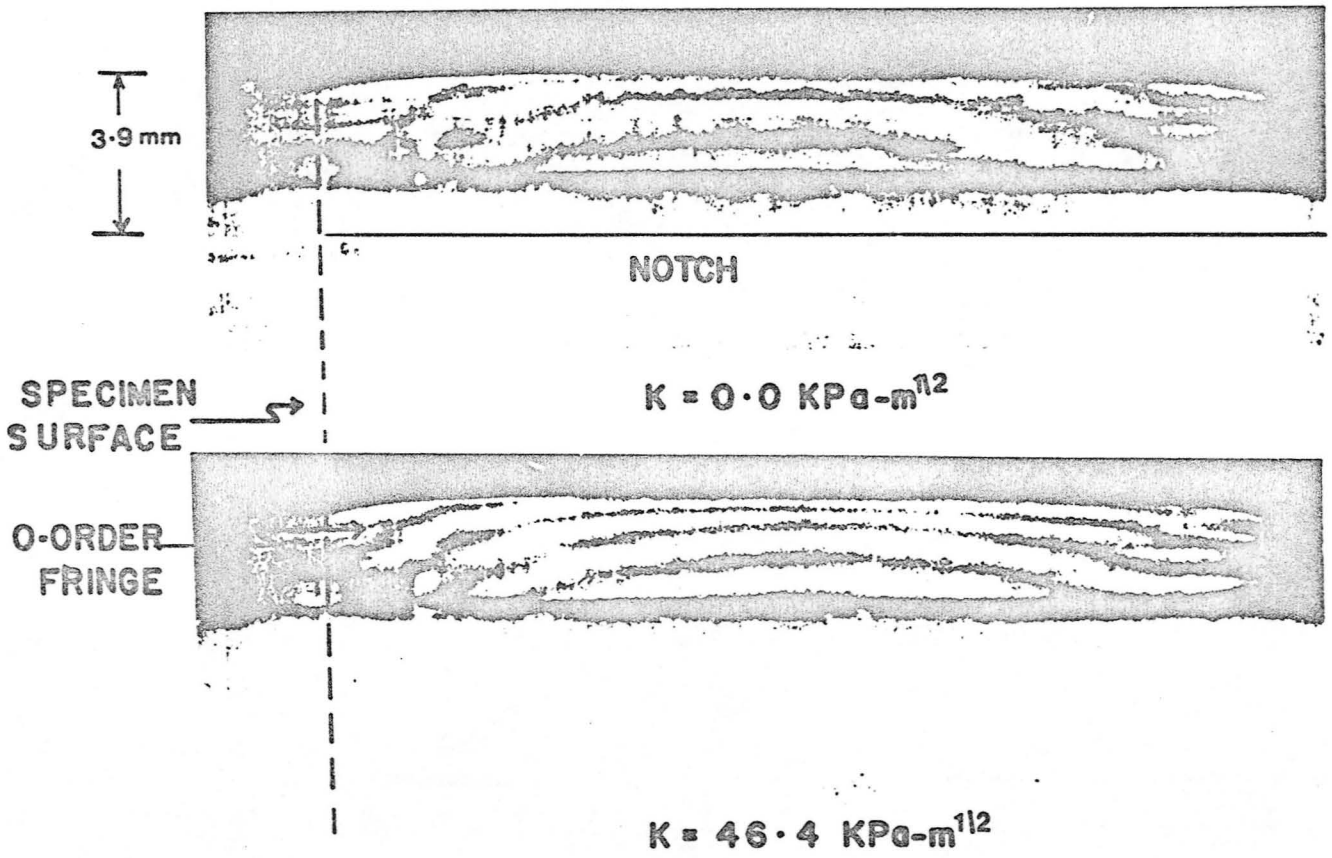

Figure 11: Steady state fringe patterns for Test B-12 at applied load of 0.0 and 46.4 KPa-$m^{1/2}$.

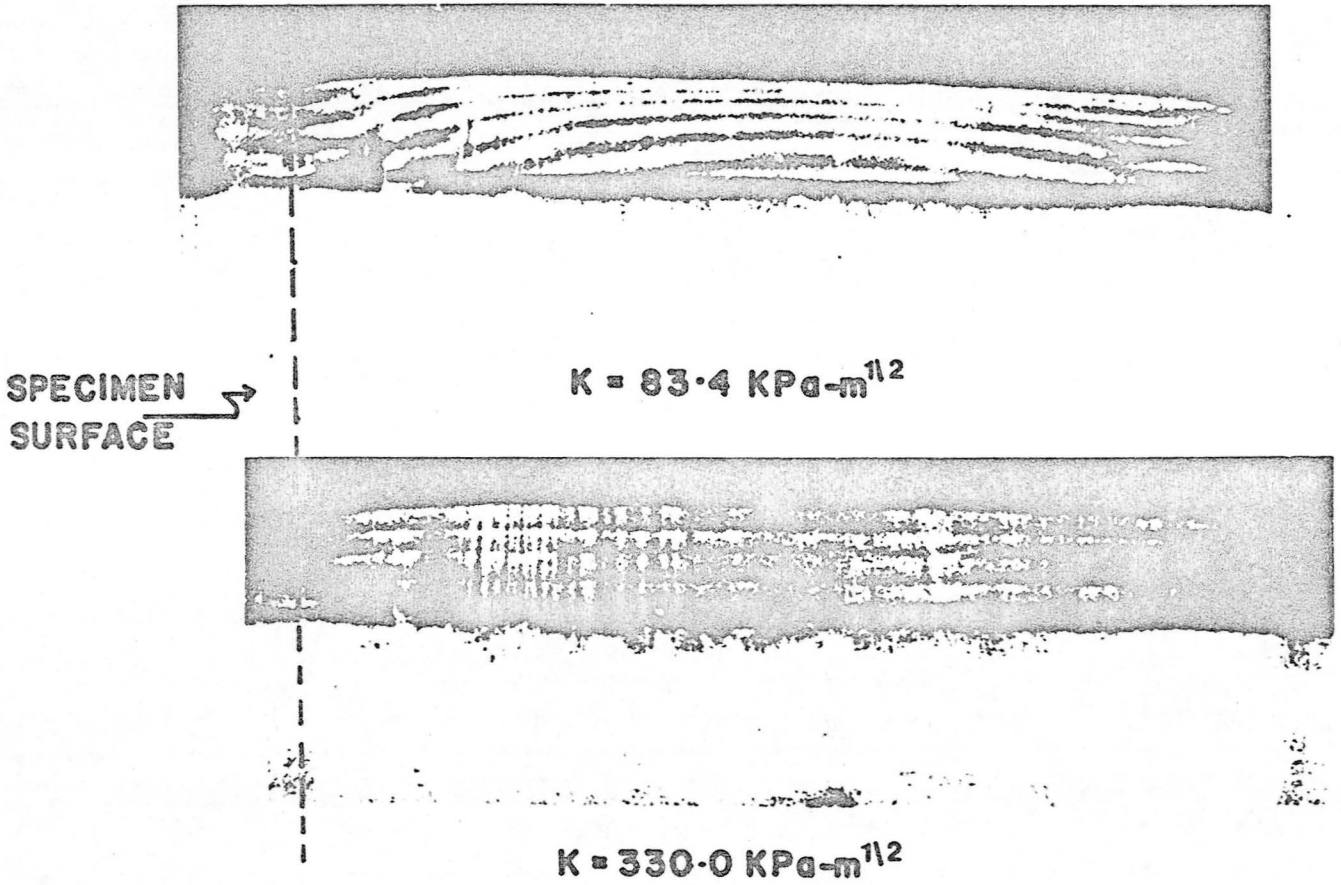

ORIGINAL PAGE IS OF POOR QUALITY

Figure 11 concluded: Steady state fringe patterns for Test B-12 at loads of 83.4 and 330 KPa-$m^{1/2}$.

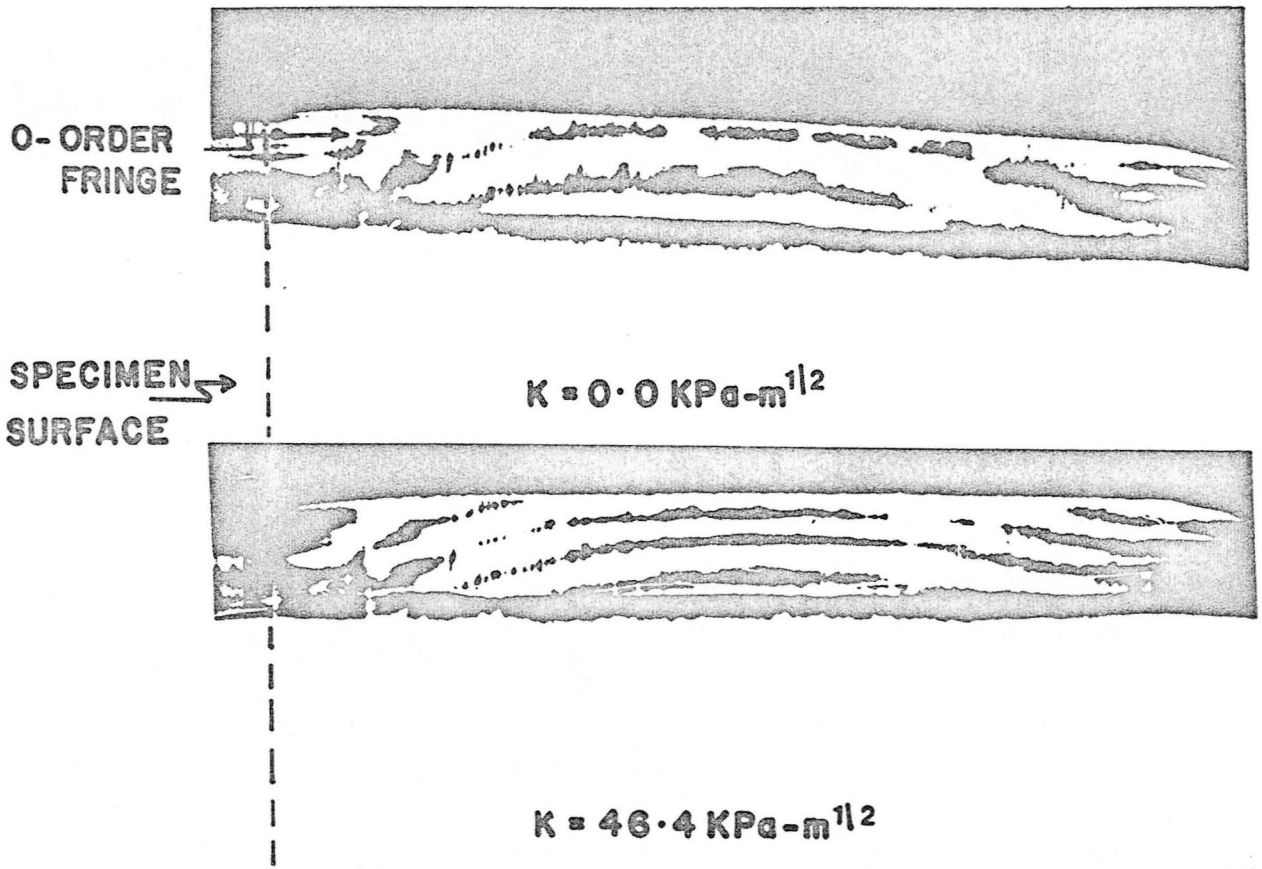

Figure 12: Fringe patterns following the overload for Test B-12 at applied loads of 0.0 and 46.4 KPa-$m^{1/2}$.

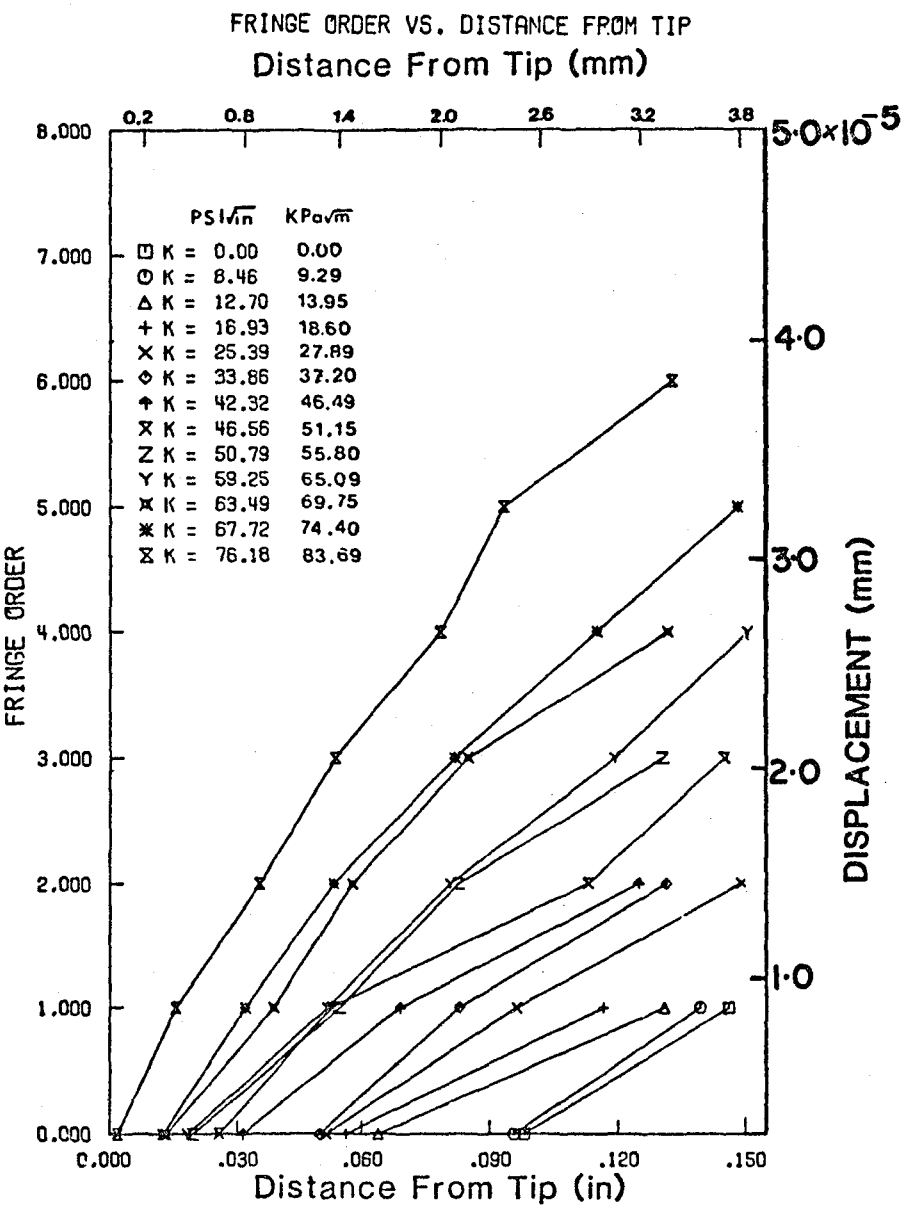

Figure 13: Free surface crack opening profiles as a function of applied load for specimen B-12 (steady state condition).

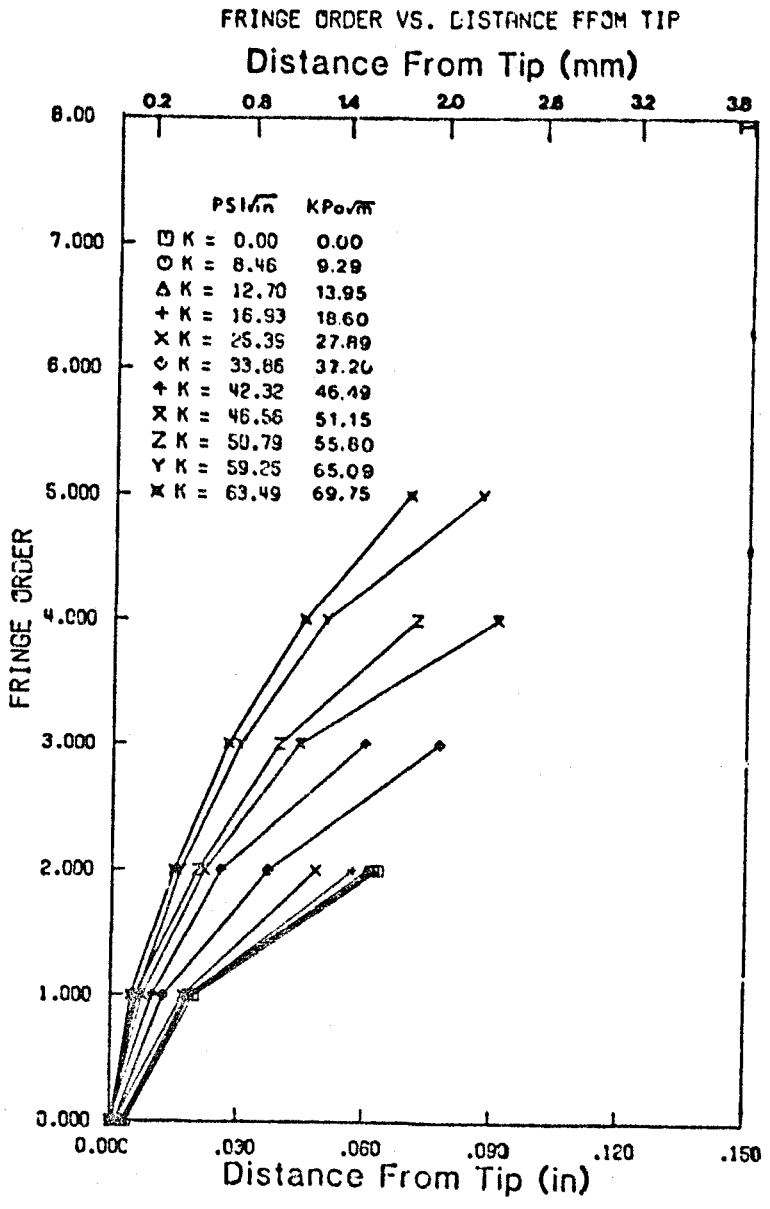

Figure 14: Midplane crack opening profiles as a function of applied load for Specimen B-12 (steady state conditions).

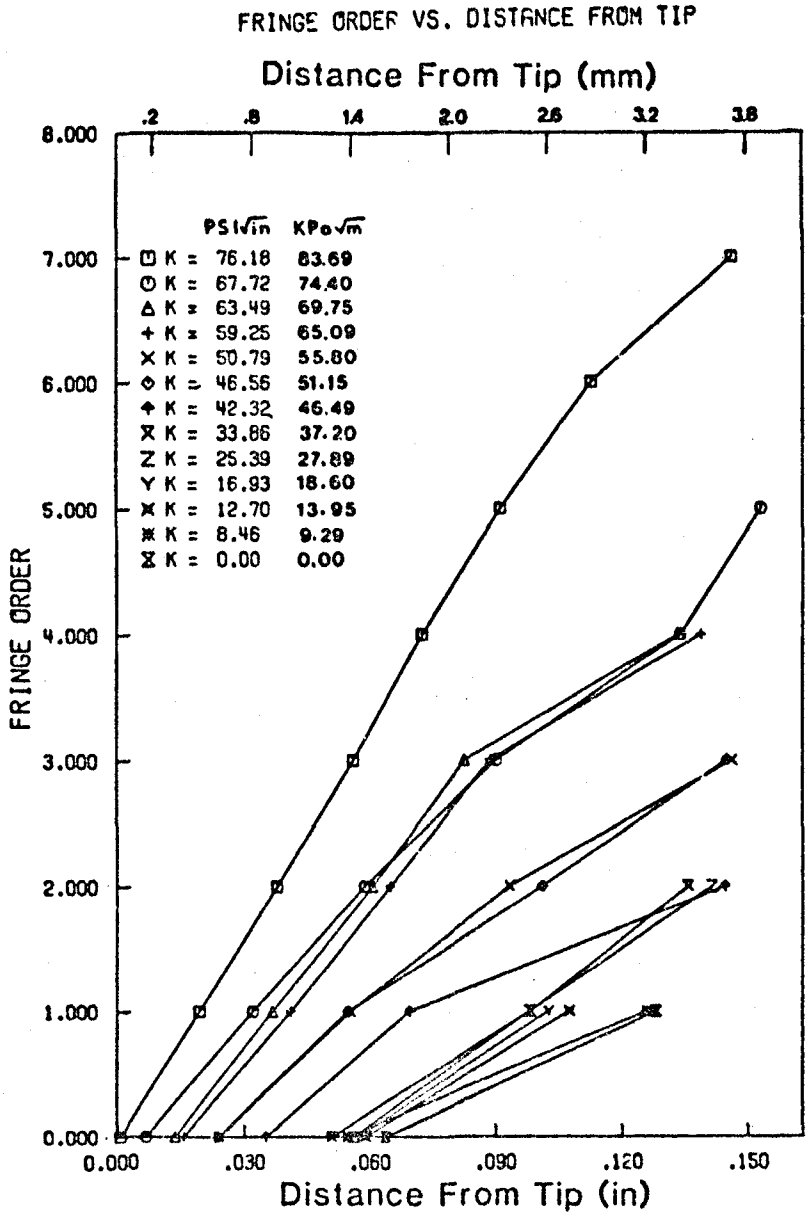

Figure 15: Free surface crack closing profiles as a function of applied load for specimen B-12 (steady state conditions).

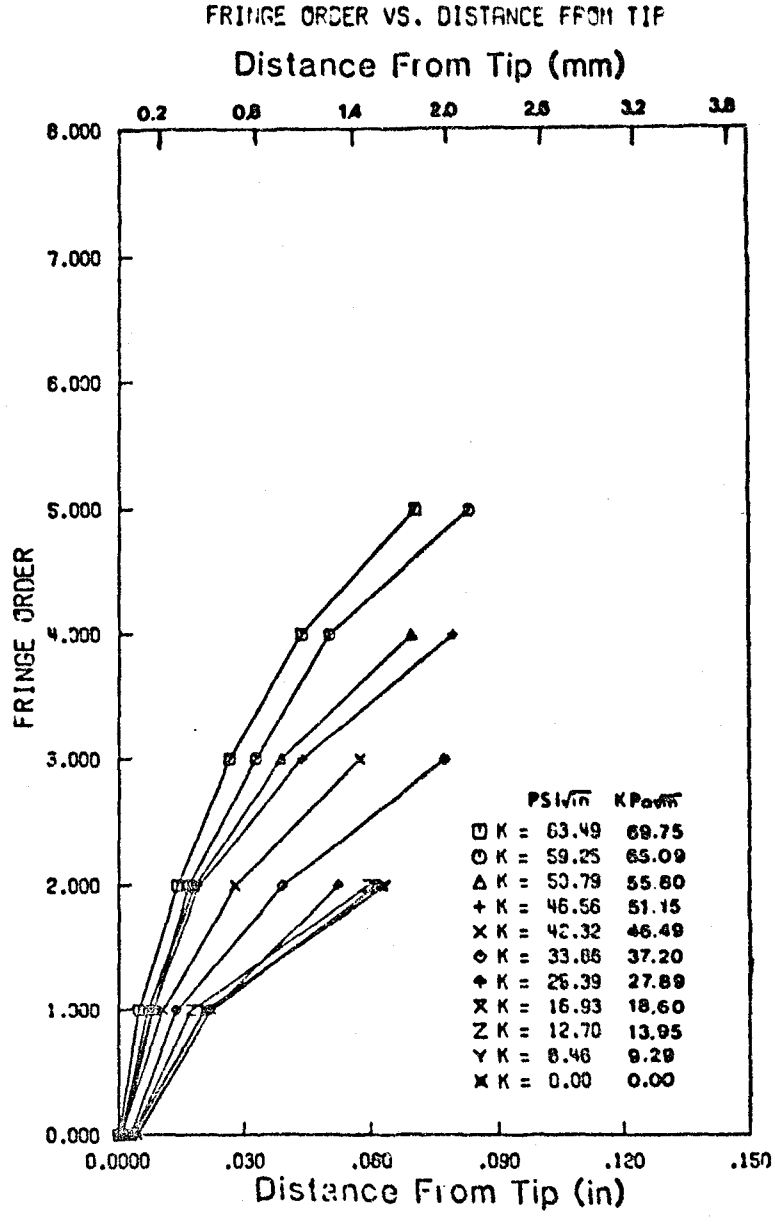

Figure 15: Midplane crack closing profiles as a function of applied load for specimen B-12 (steady state conditions).

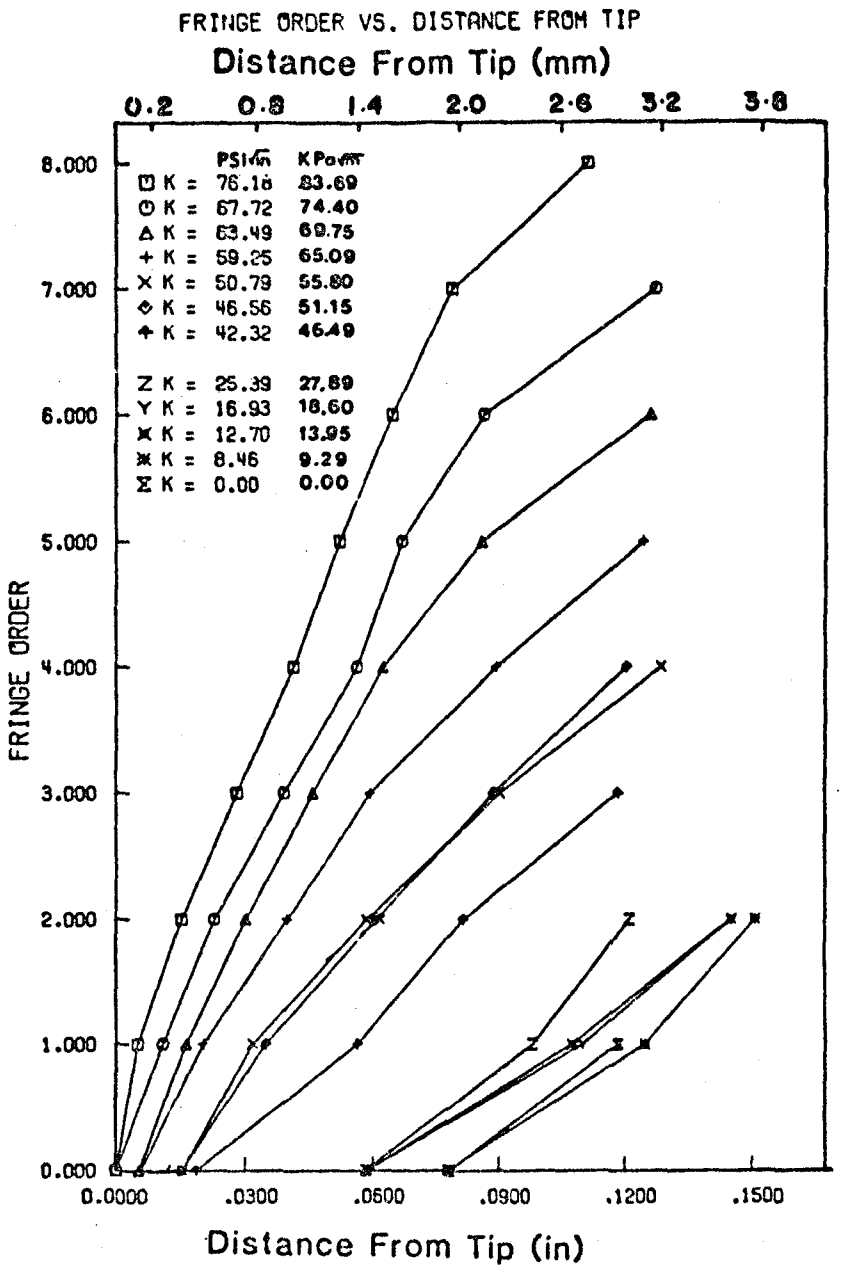

Figure 17: Free surface crack closing profiles as a function of applied load for specimen B-12 (overload cycle).

ORIGINAL PAGE IS
OF POOR QUALITY

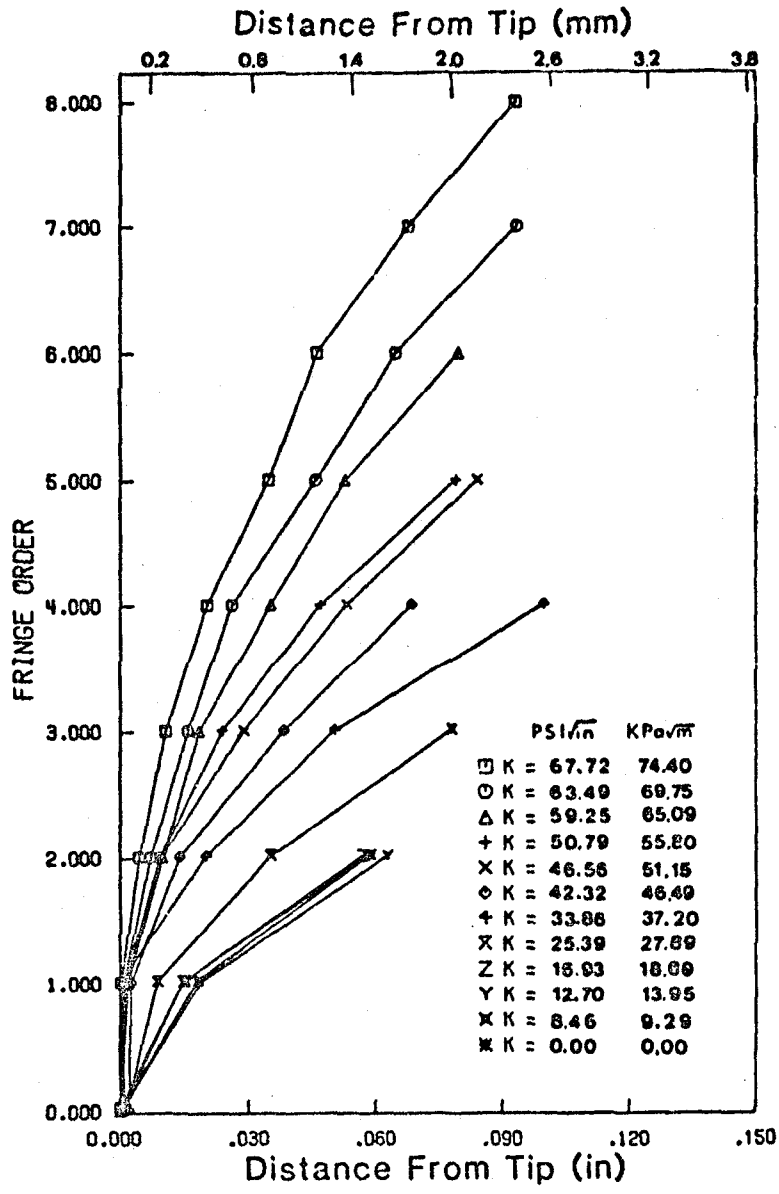

Figure 18: Midplane crack closing profiles as a function of applied load for specimen B-12 (overload cycle).

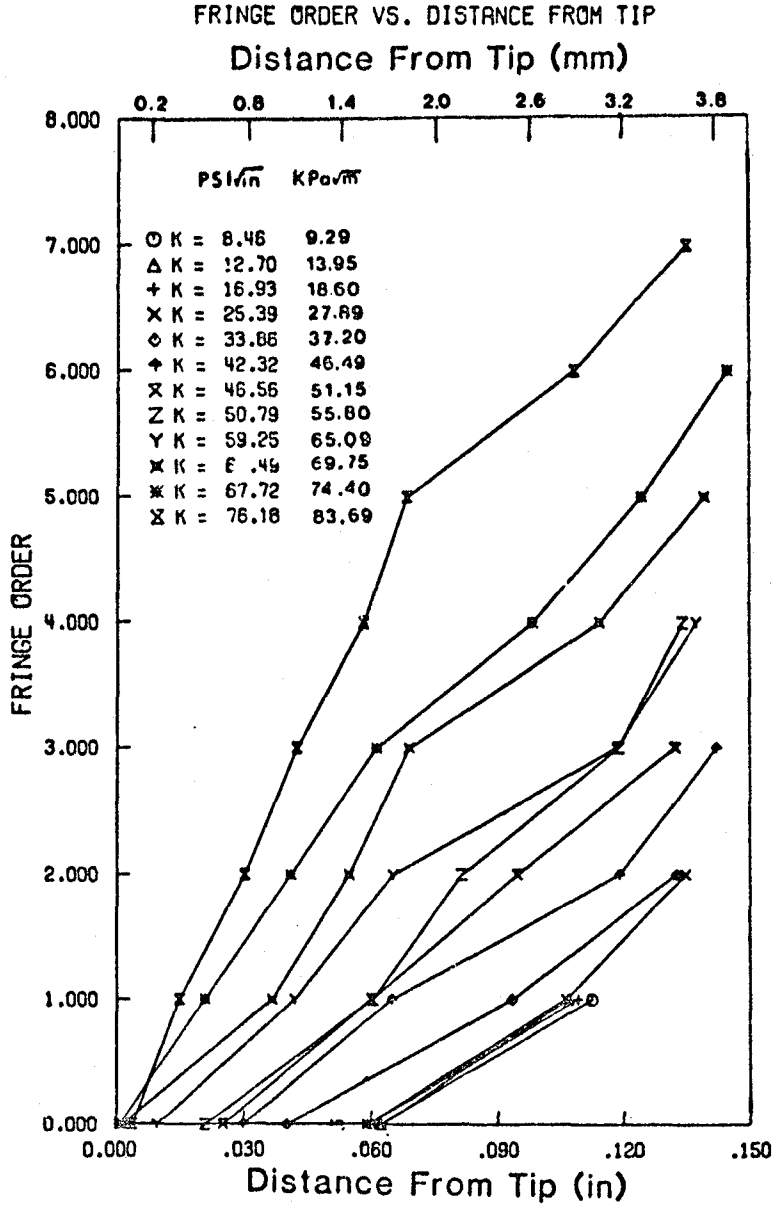

Figure 19: Free surface crack opening profiles as a function of applied load for specimen B-12 (1st cycle following the overload).

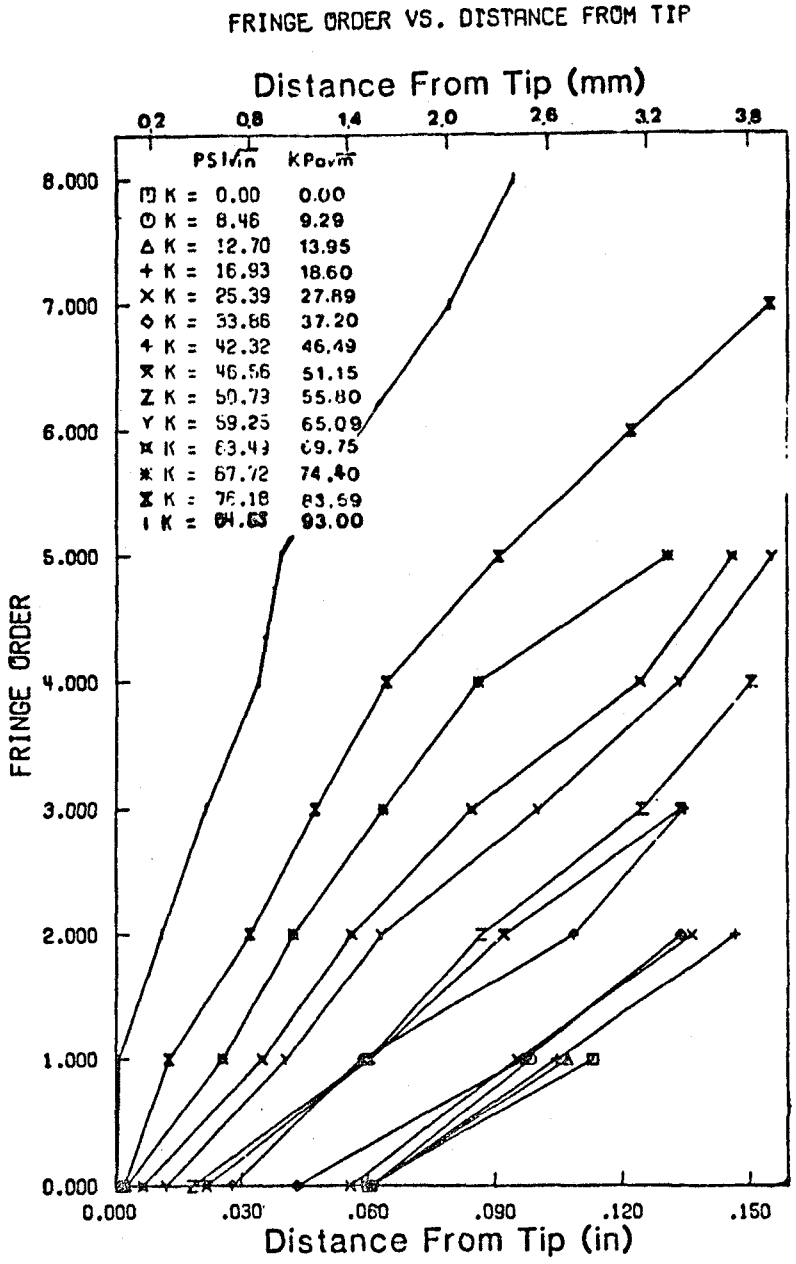

Figure 20: Free surface crack opening profiles as a function of applied load for Specimen B-12 (10th cycle following the overload).

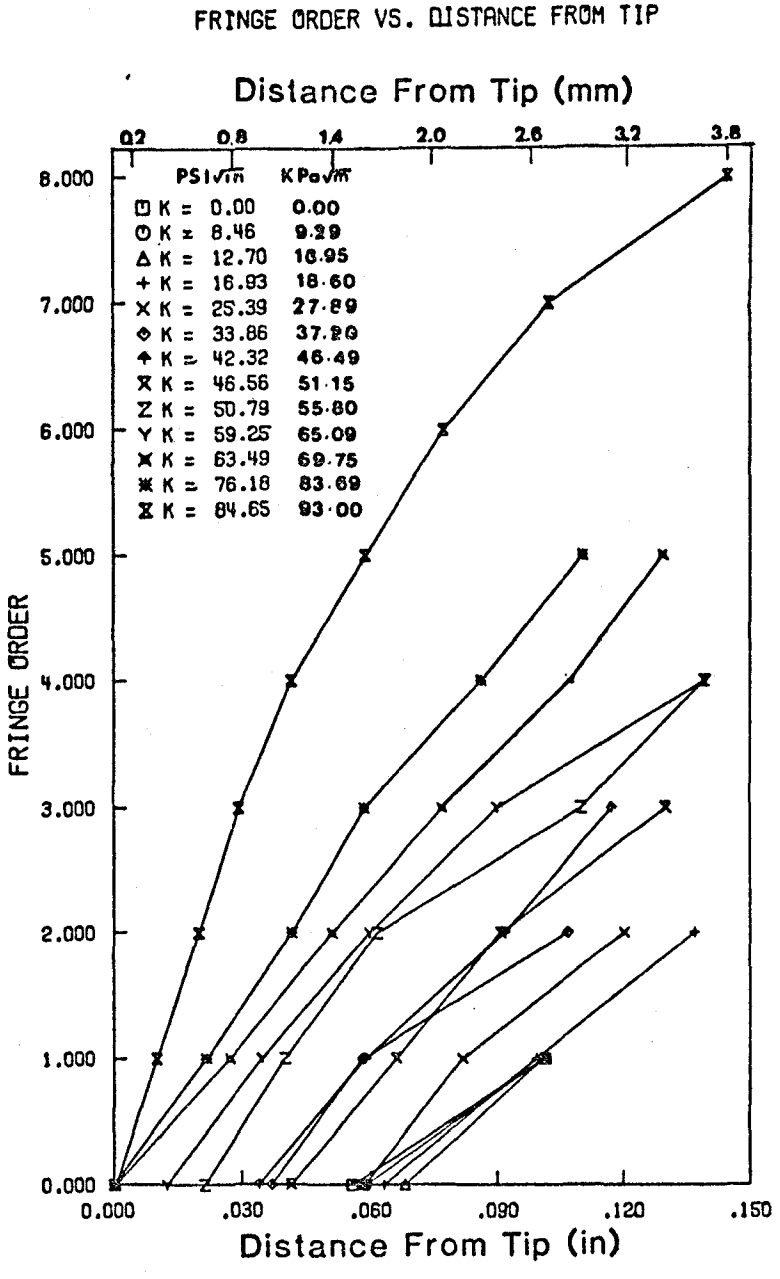

Figure 21: Free surface crack opening profiles as a function of applied load for specimen B-12 (100th cycle following the overload).

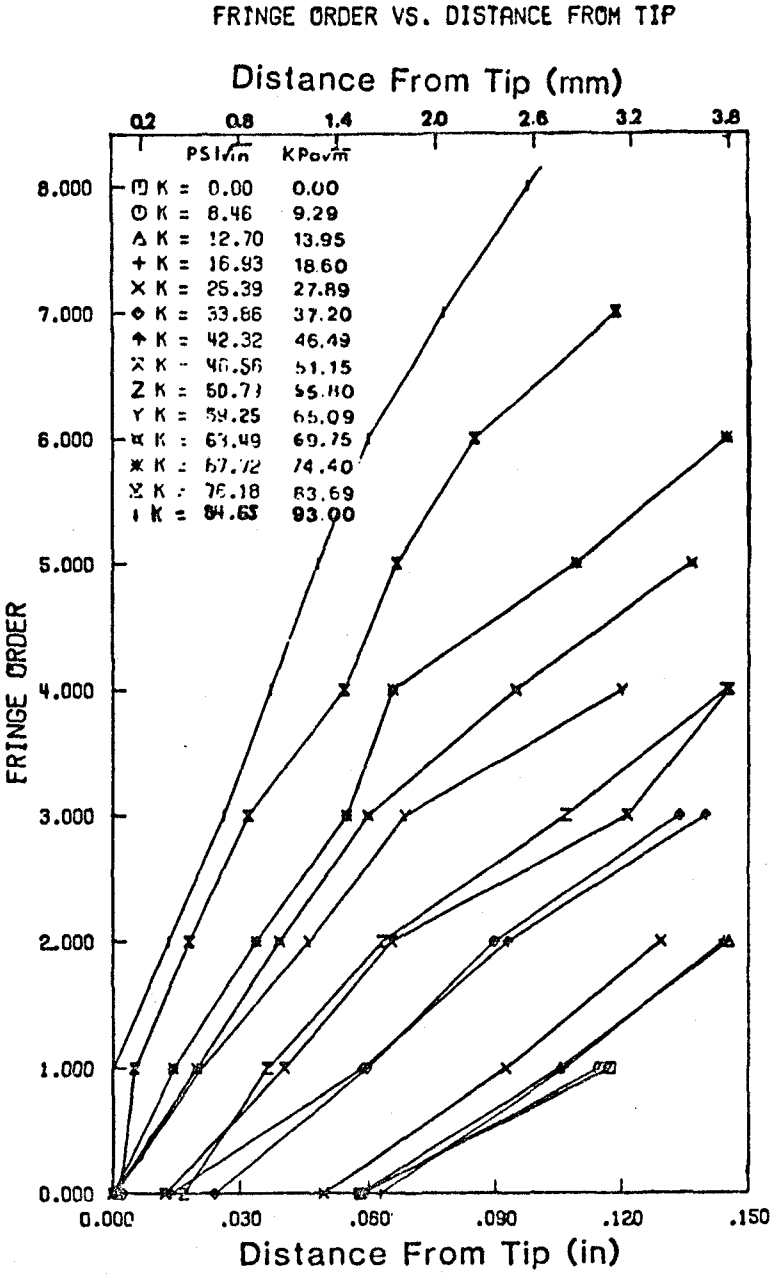

Figure 22: Free surface crack opening profiles as a function of applied load for Specimen B-12 (1000th cycle following the overload).

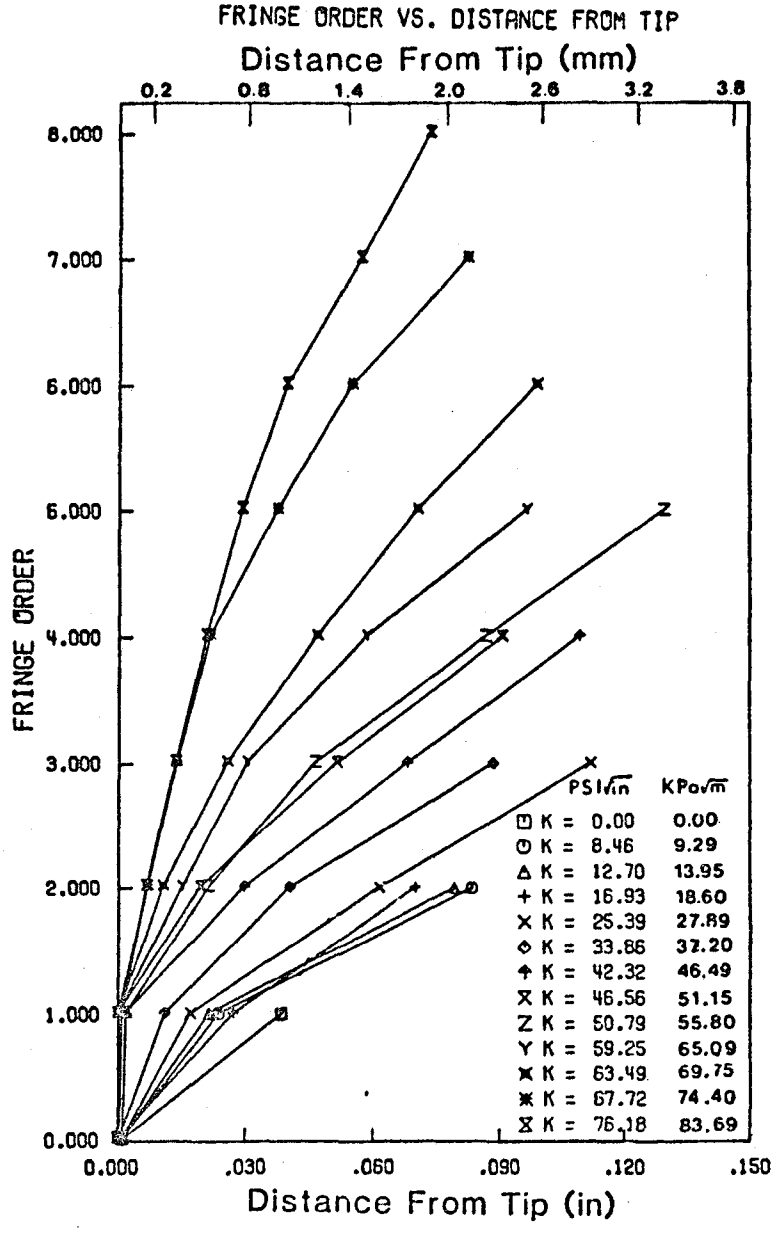

Figure 23: Midplane crack opening profiles as a function of applied load for specimen B-12 (1st cycle following the overload).

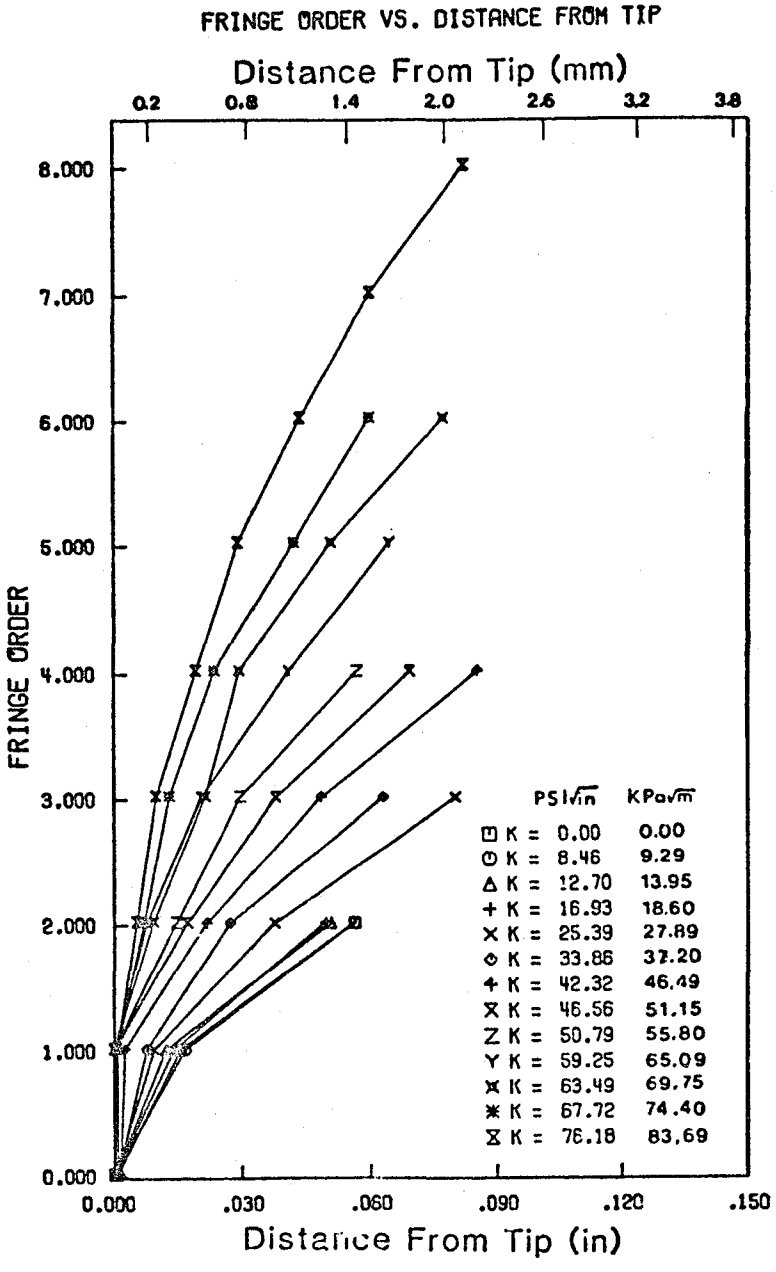

Figure 24: Midplane crack opening profiles as a function of applied load for specimen B-12 (10th cycle following the overload).

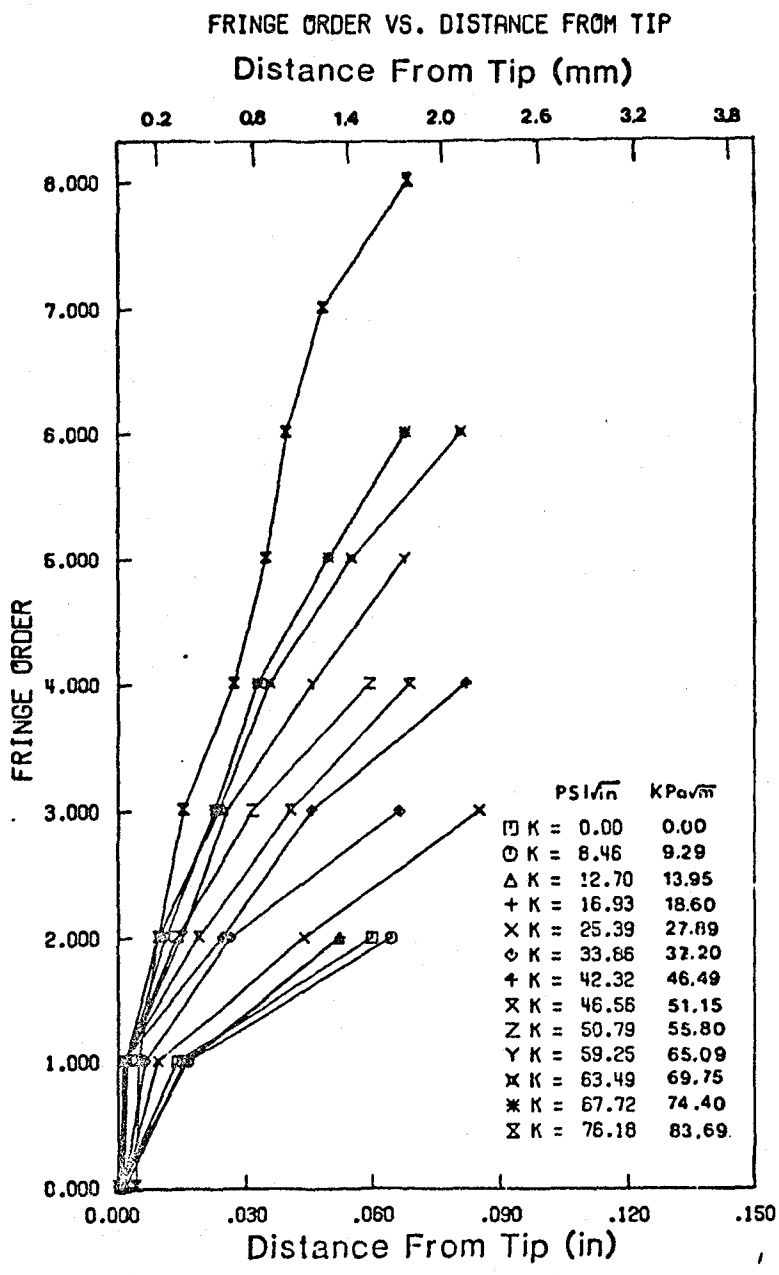

Figure 25: Midplane crack opening profiles as a function of applied load for specimen B-12 (100th cycle following the overload).

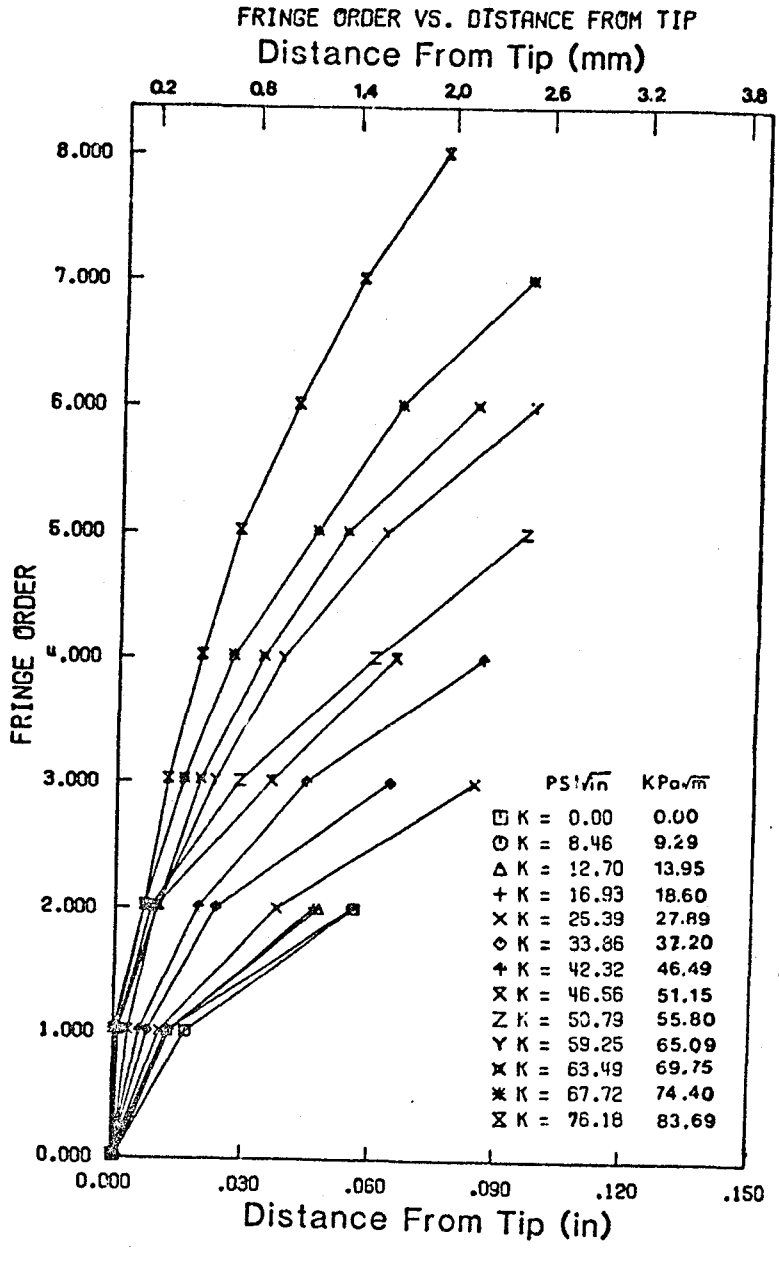

Figure 26: Midplane crack opening profiles as a function of applied load for specimen B-12 (1000th cycle following the overload).

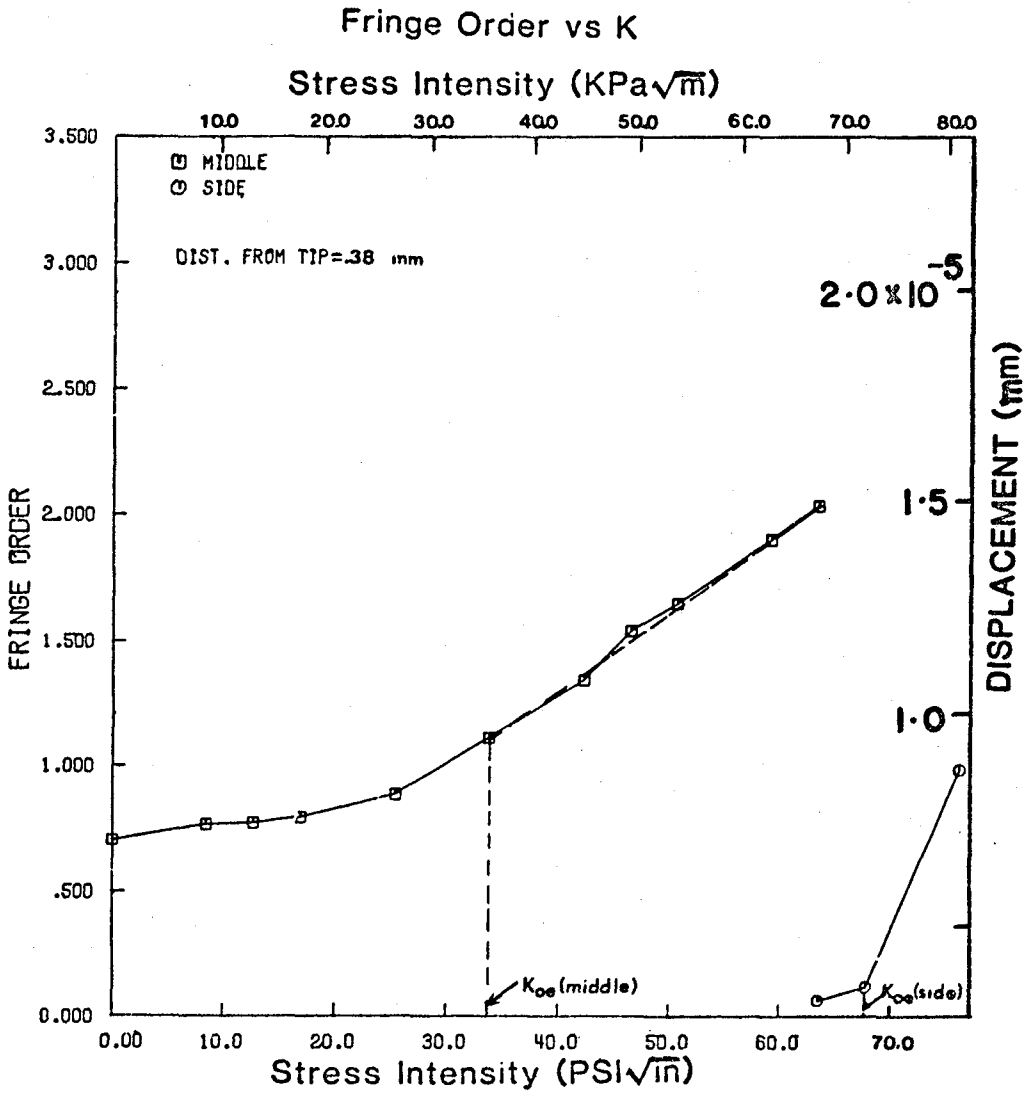

Figure 27: Crack tip separation measured as a function of applied load at a distance of 0.38 mm, behind the crack tip (steady state conditions).

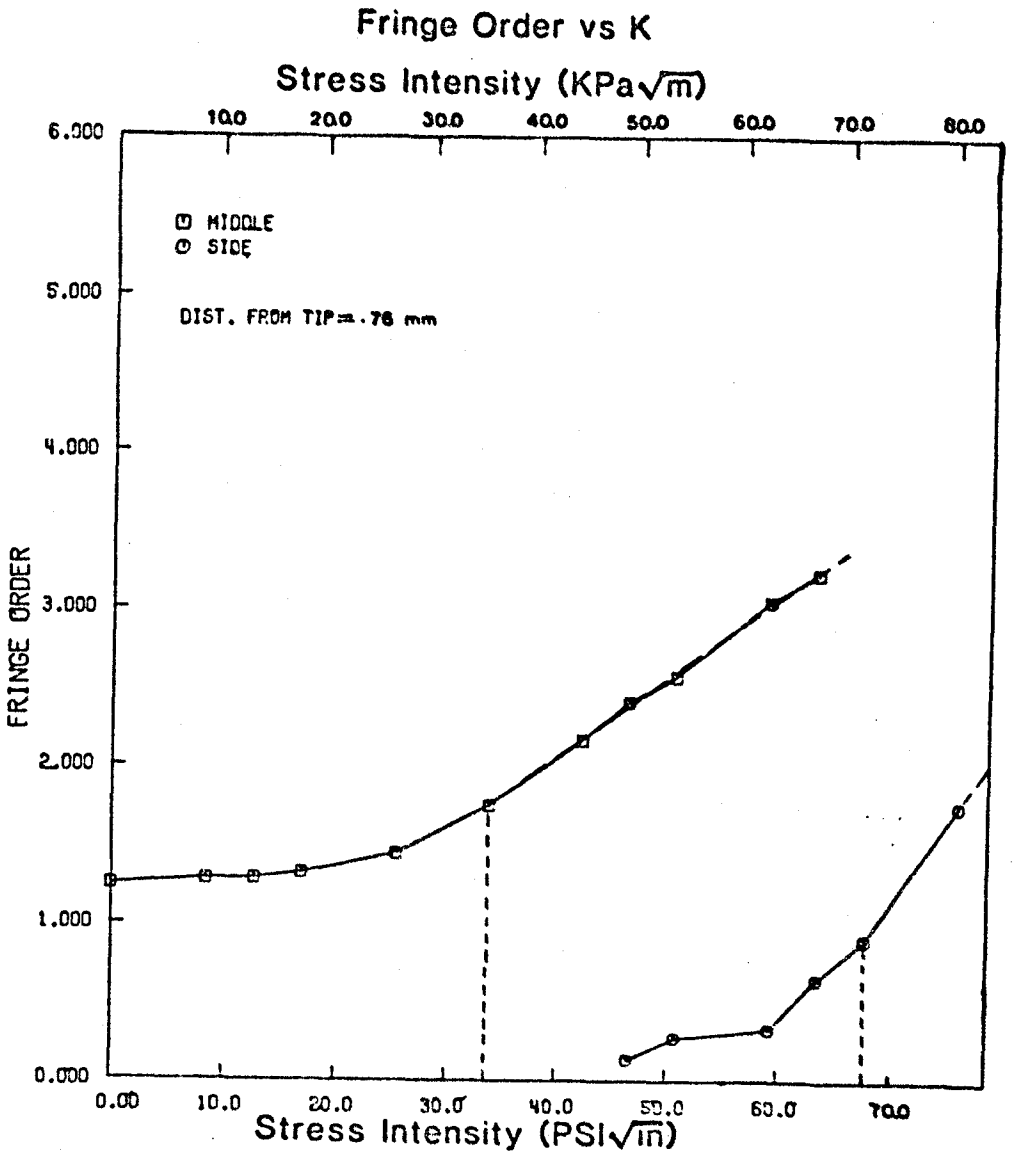

Figure 28: Crack tip separation measured as a function of applied load at a distance of 0.76 mm, behind the crack tip (steady state conditions).

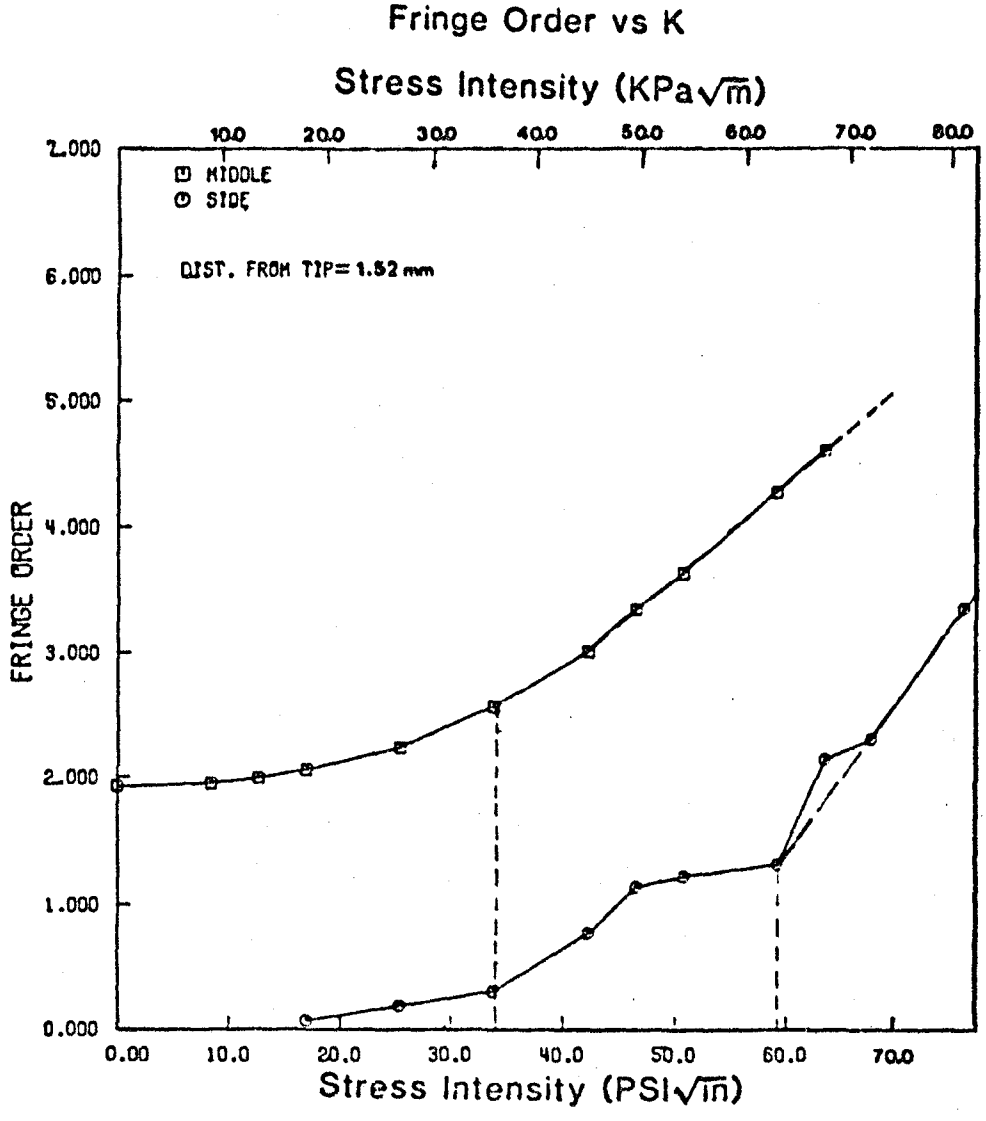

Figure 29: Crack tip separation measured as a function of applied load at a distance of 1.52 mm, behind the crack tip (steady state conditions).

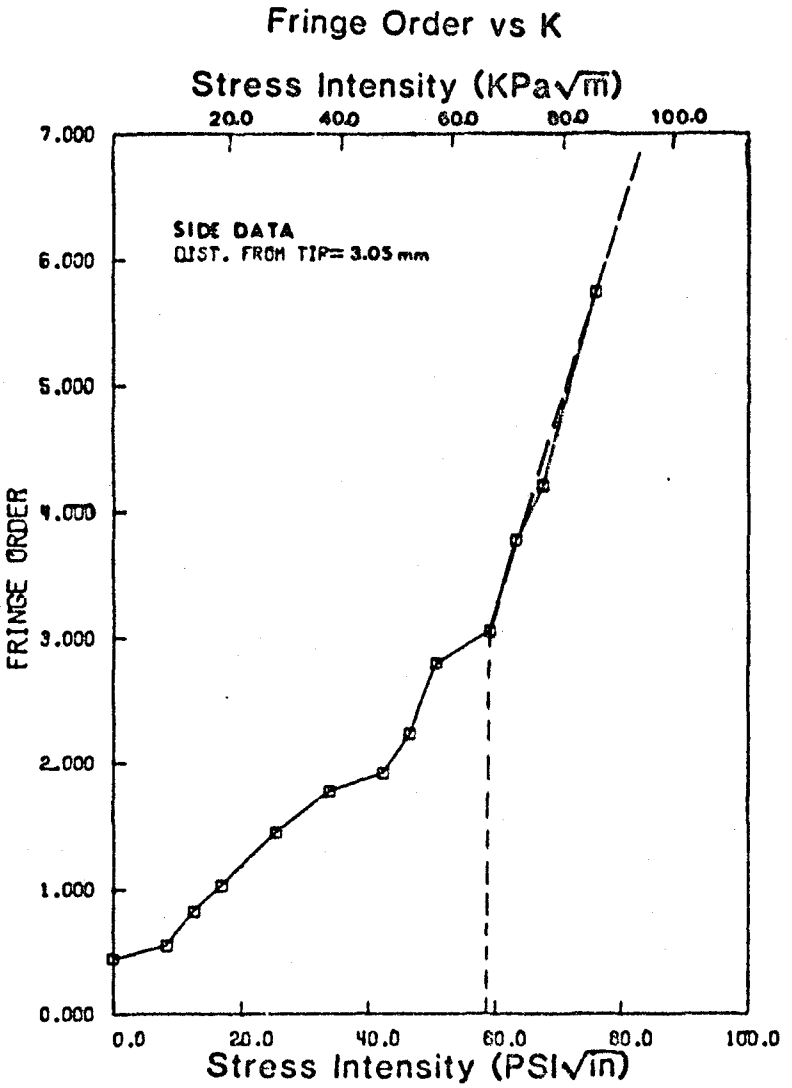

Figure 30: Crack tip separation measured as a function of applied load at a distance of 3.05 mm, behind the crack tip (steady state conditions).

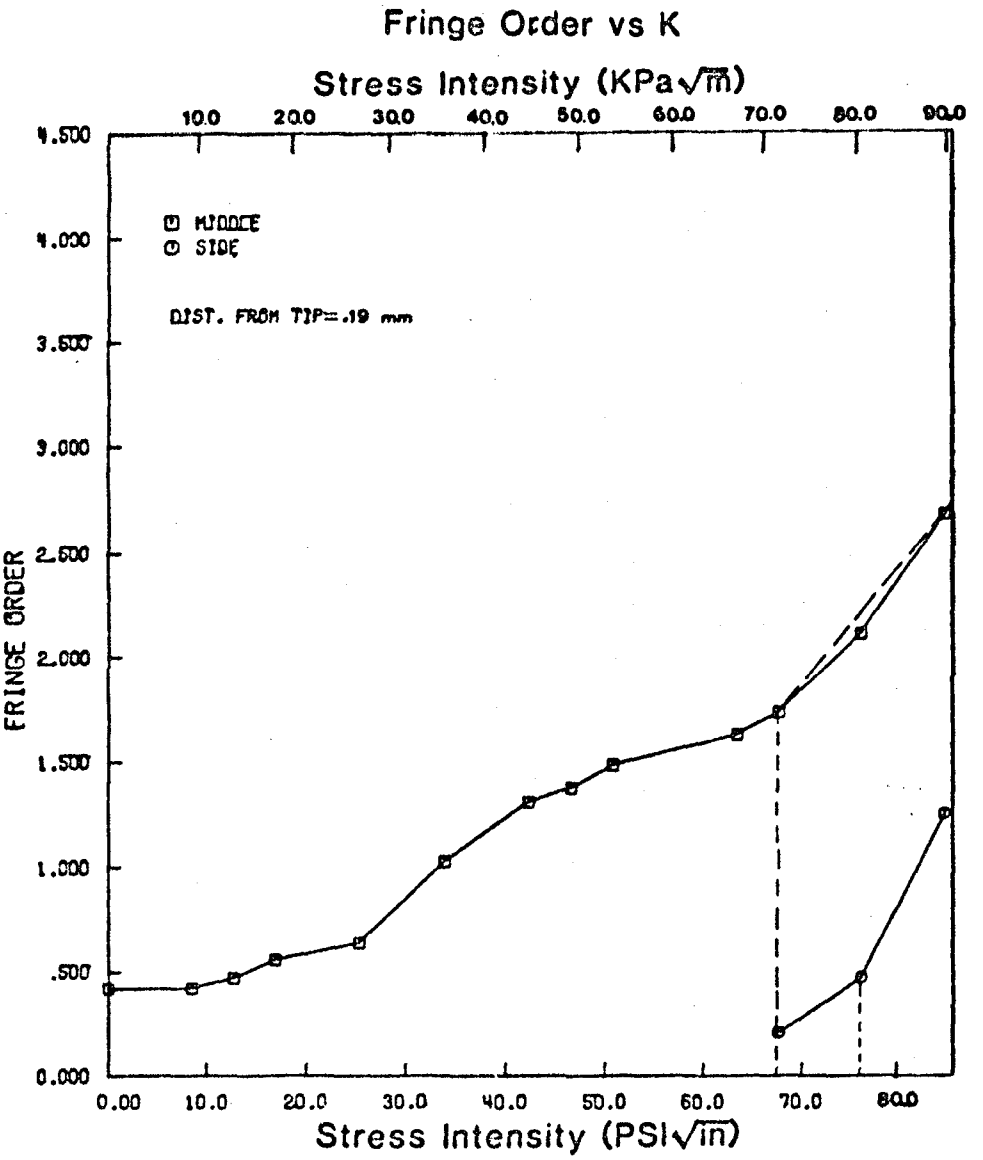

Figure 31: Crack tip separation measured as a function of applied load at a distance of 0.19 mm, behind the crack tip (10th cycle following the overload).

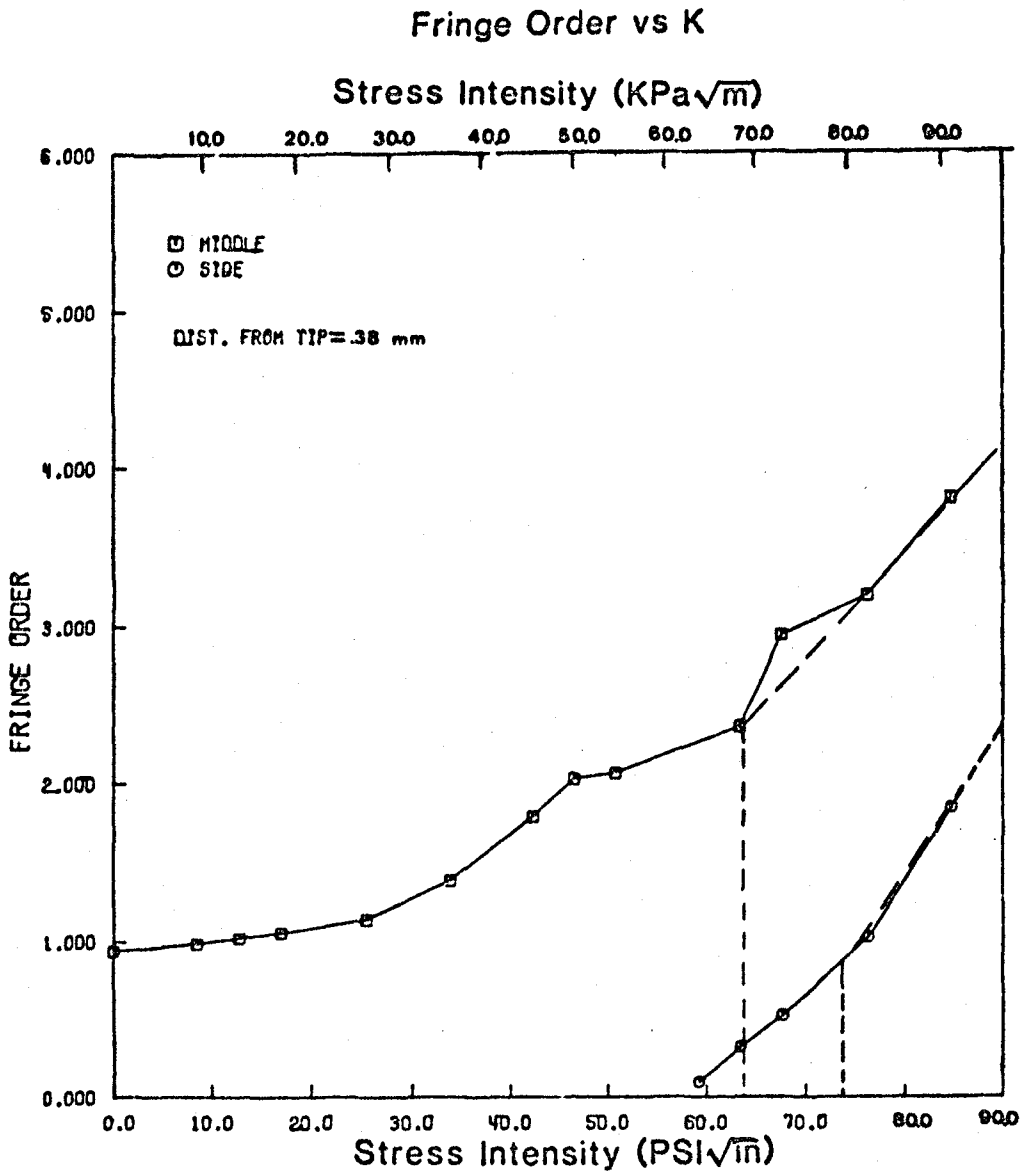

Figure 32: Crack tip separation measured as a function of applied load at a distance of 0.38 mm, behind the crack tip (10th cycle following the overload).

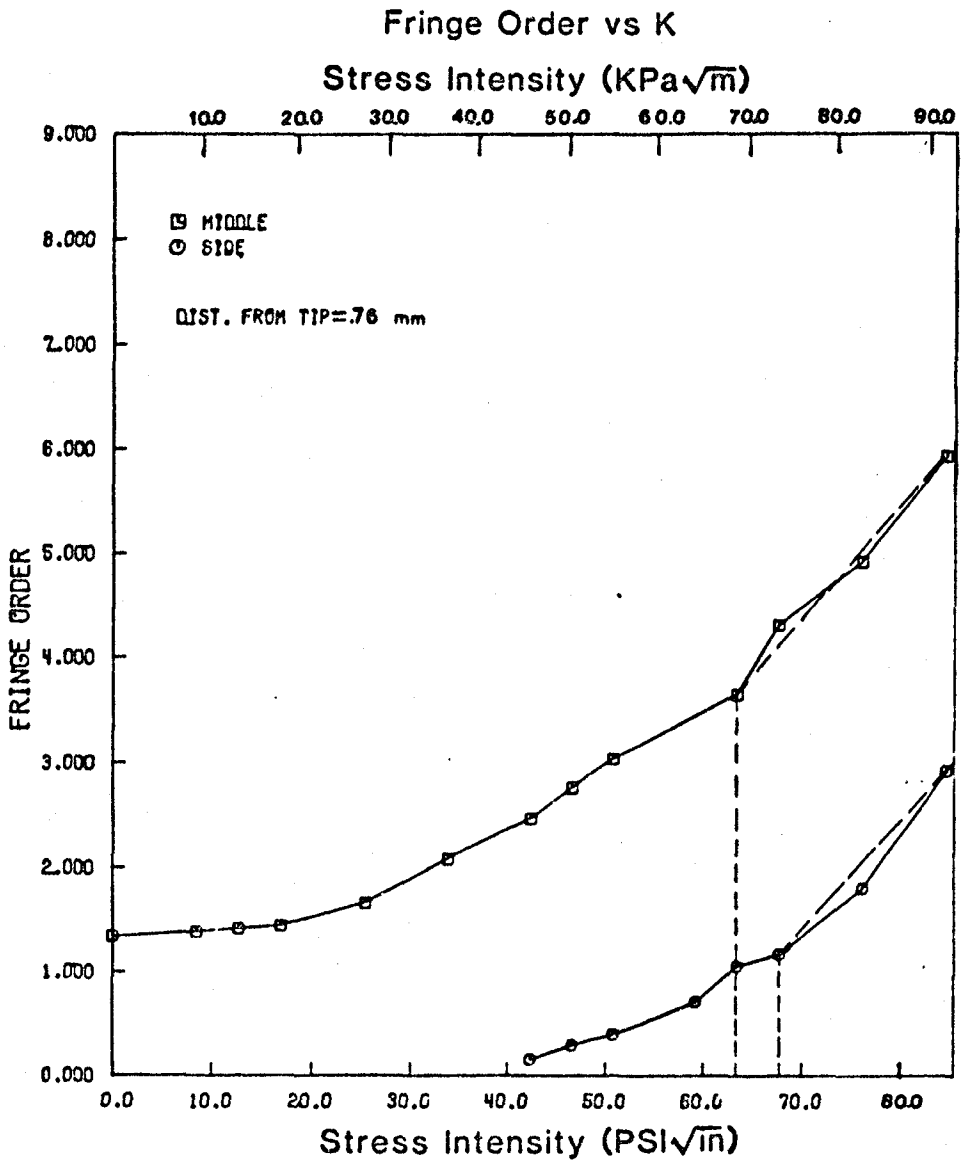

Figure 33: Crack tip separation measured as a function of applied load at a distance of 0.76 mm, behind the crack tip (10th cycle following the overload).

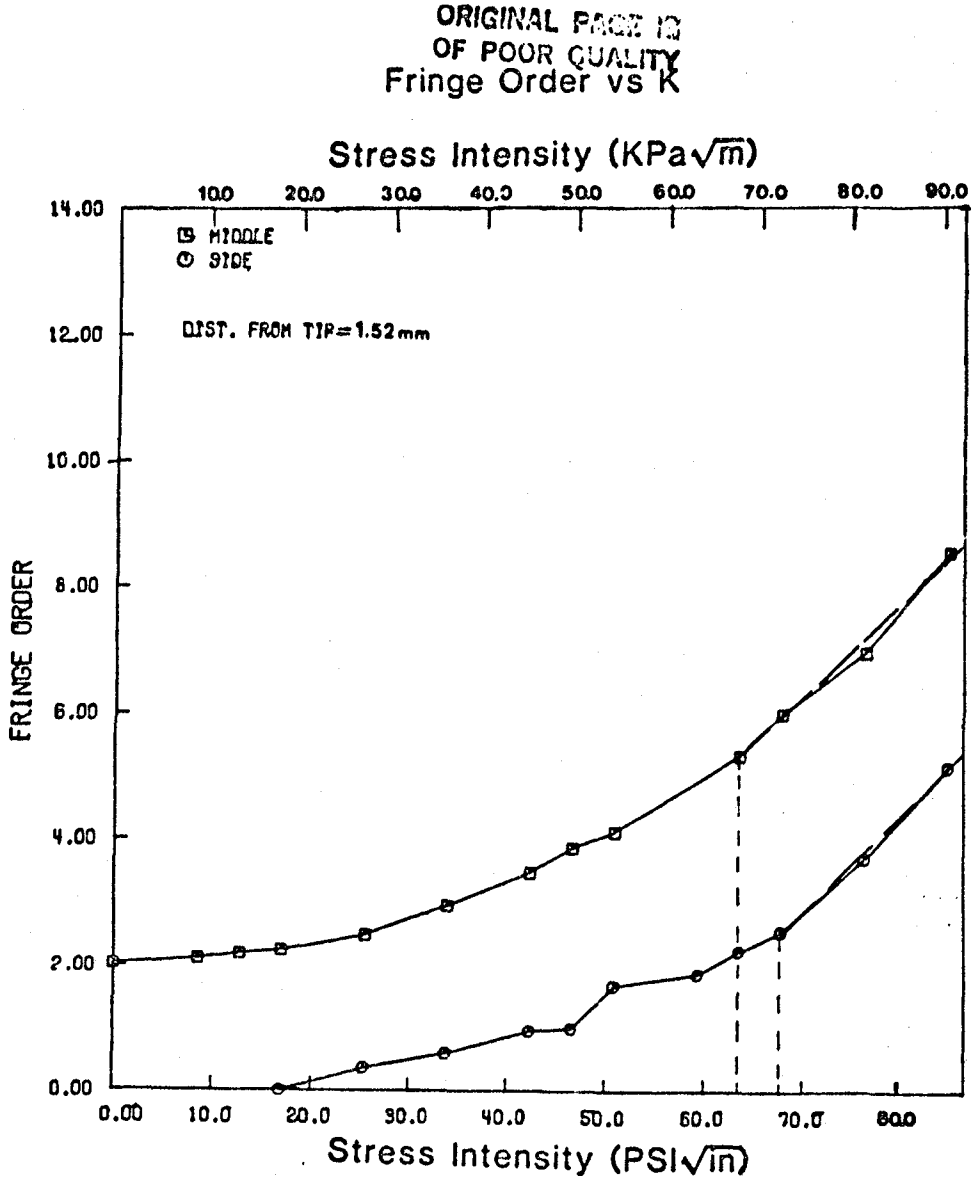

Figure 34: Crack tip separation measured as a function of applied load at a distance of 1.52 mm, behind the crack tip (10th cycle following the overload).

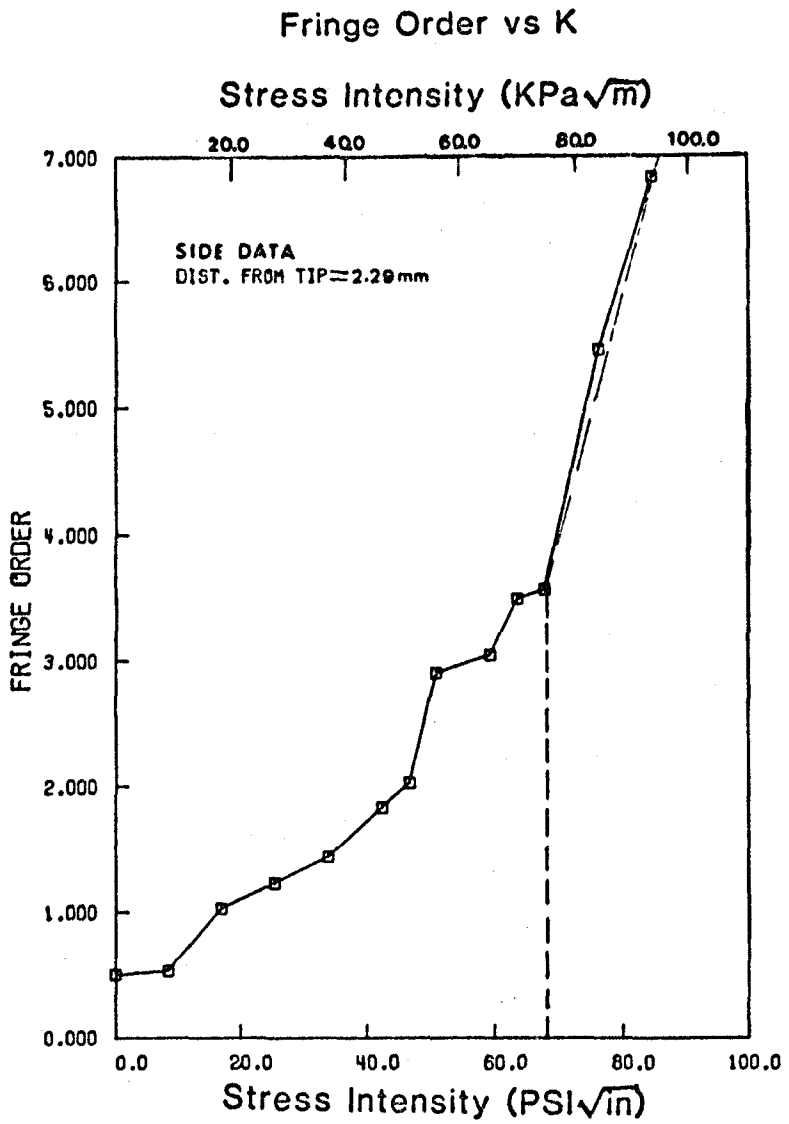

Figure 35: Crack tip separation measured as a function of applied load at a distance of 2.29 mm, behind the crack tip (10th cycle following the overload).

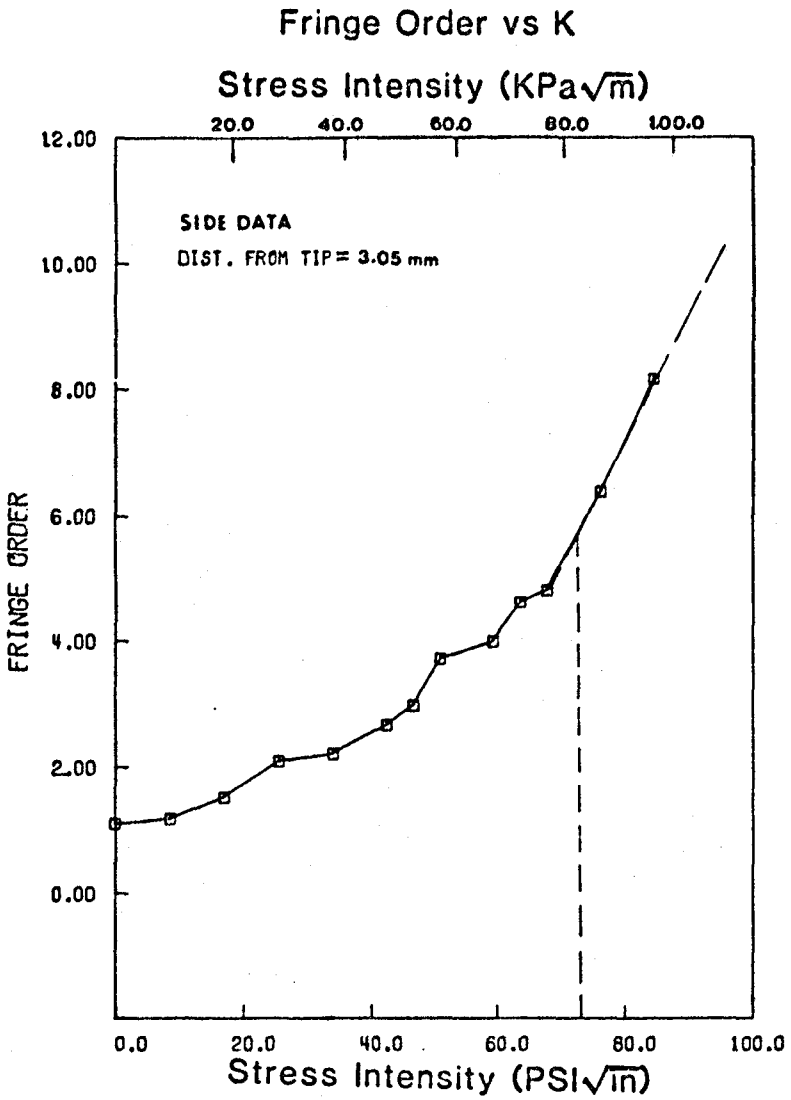

Figure 36: Crack tip separation measured as a function of applied load at a distance of 3.05 mm, behind the crack tip (10th cycle following the overload).

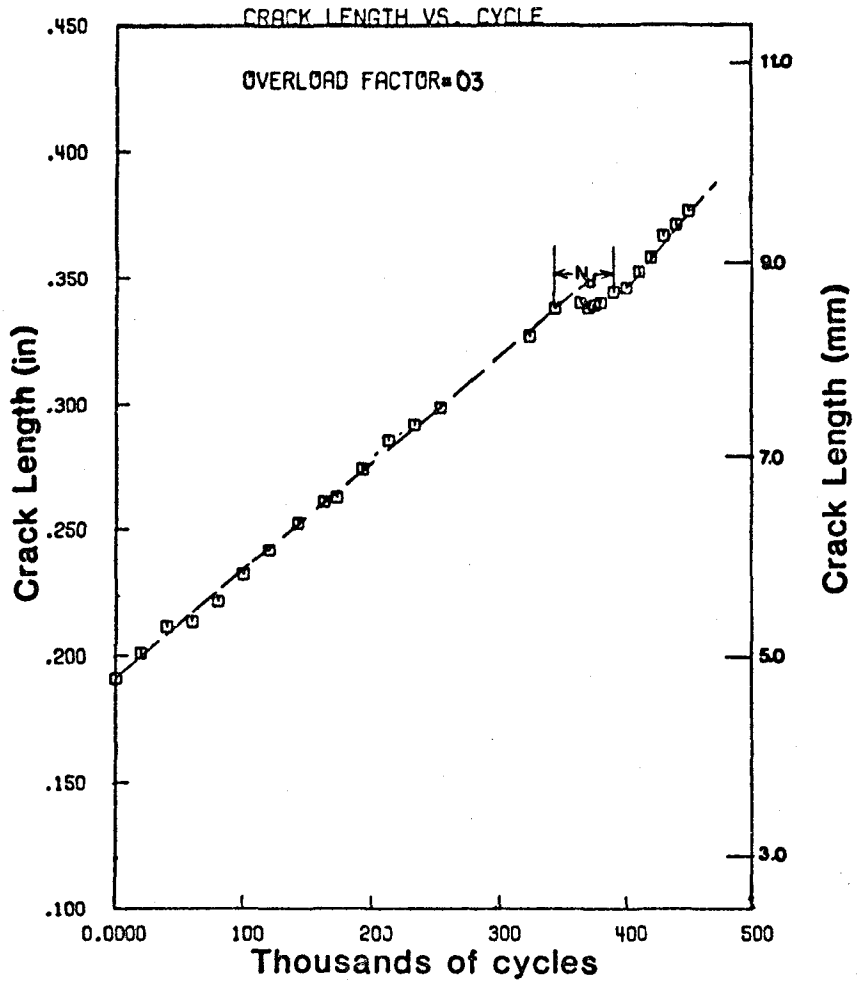

Figure 37: Average through-the-thickness fatigue crack length versus cycles curve for specimen B-13 (ΔK = 313 KPa-$m^{1/2}$, single peak overload = 339 KPa-$m^{1/2}$).

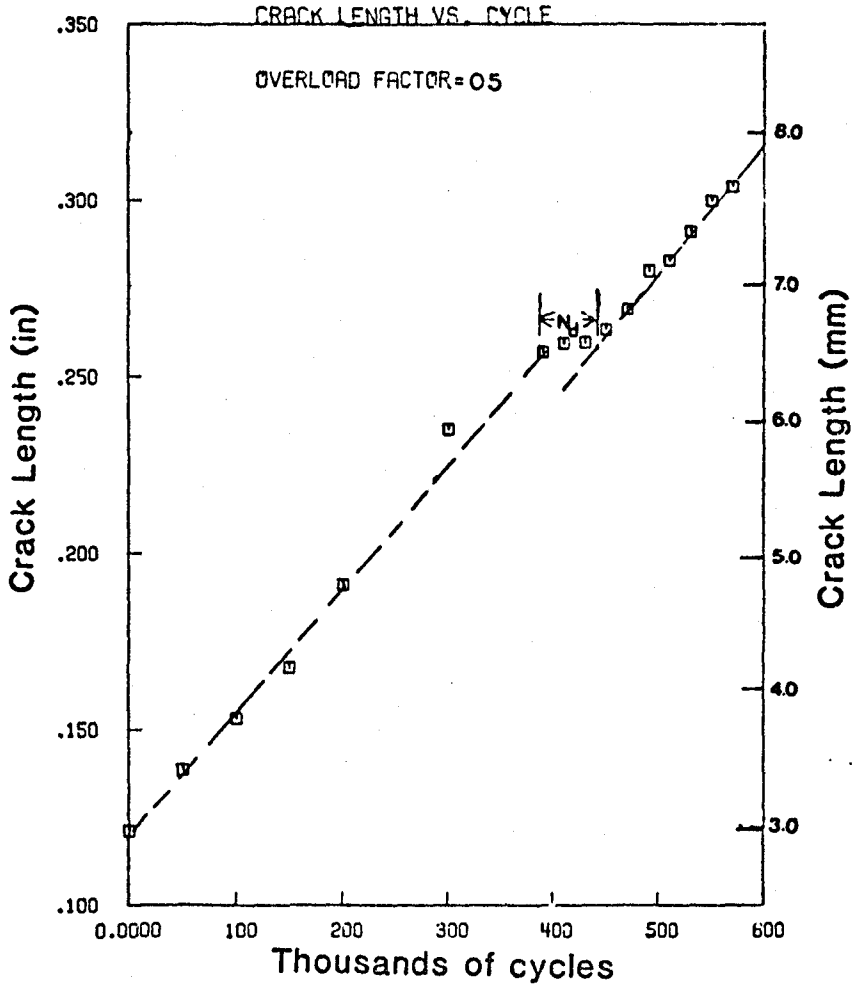

Figure 38: Average through-the-thickness fatigue crack length versus cycles curve for specimen B-14 (ΔK = 297 KPa-$m^{1/2}$, single peak overload = 1485 KPa-$m^{1/2}$).

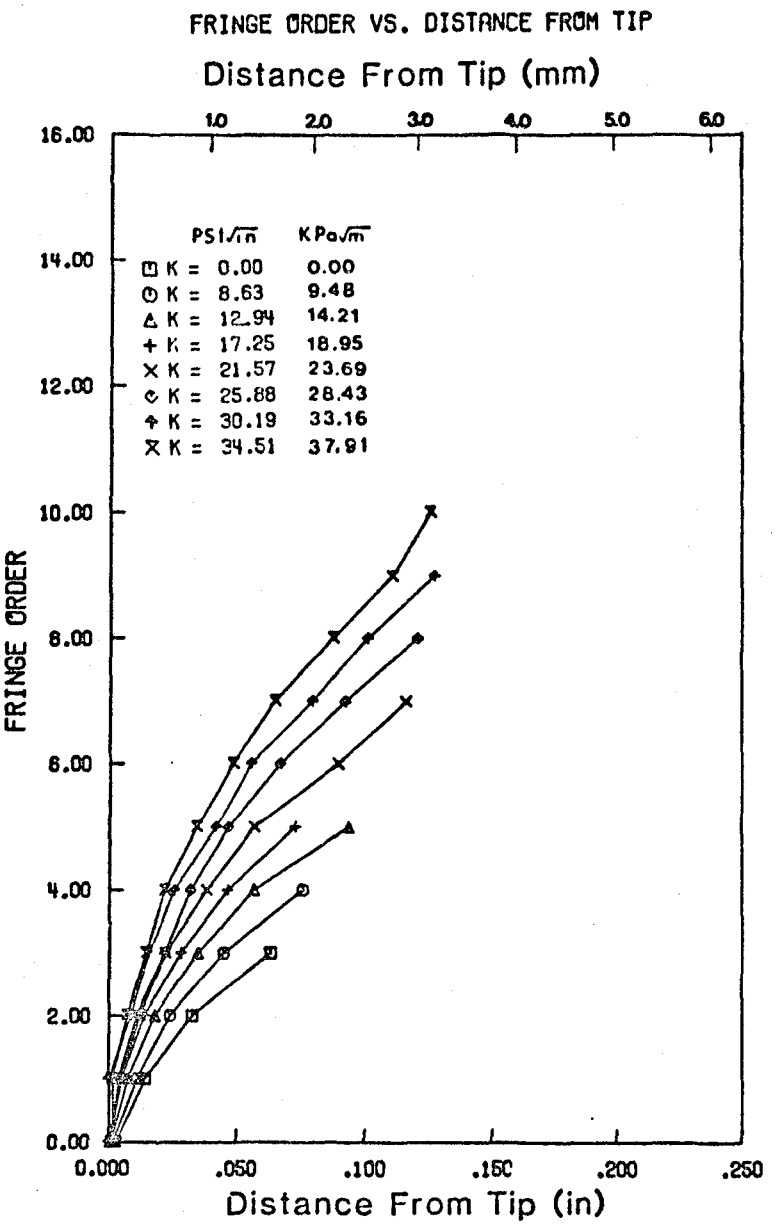

Figure 39: Midplane crack opening profiles as a function of applied load for specimen B-14 (steady state conditions).

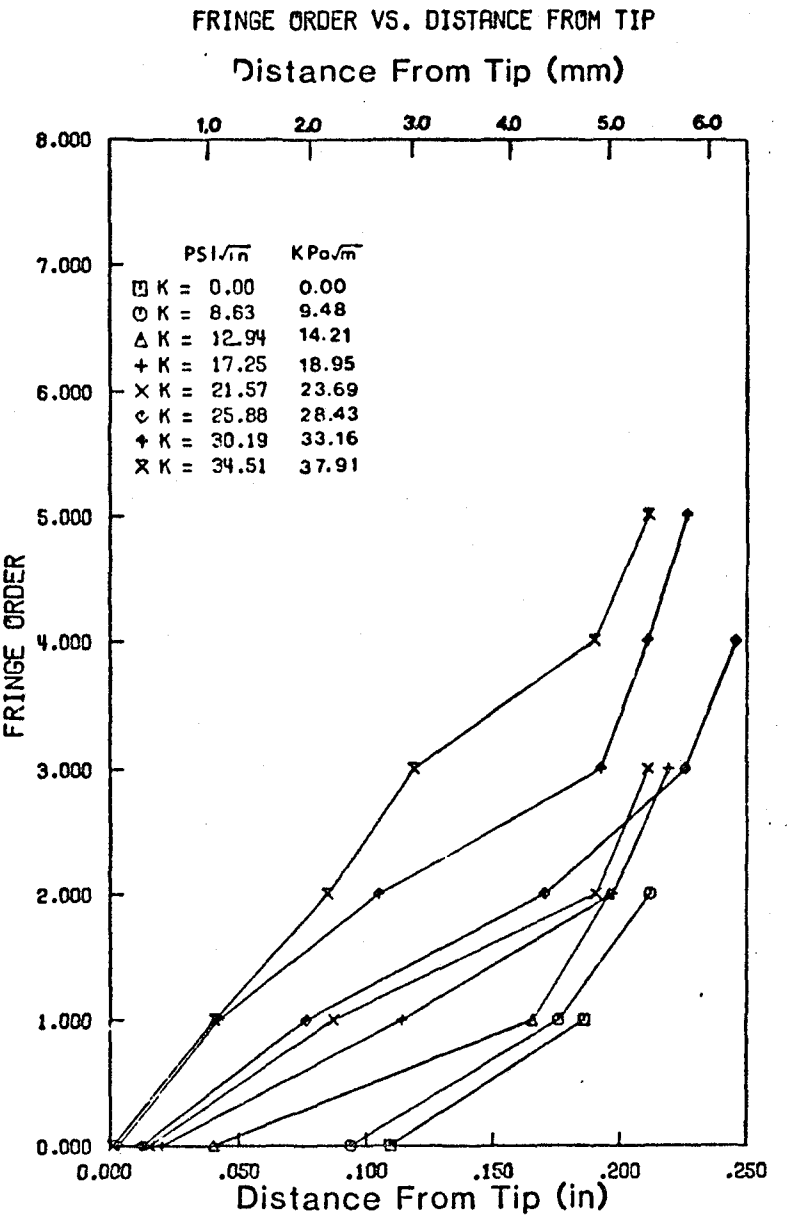

Figure 40: Free surface crack opening profiles as a function of applied load for specimen B-14 (steady state conditions).

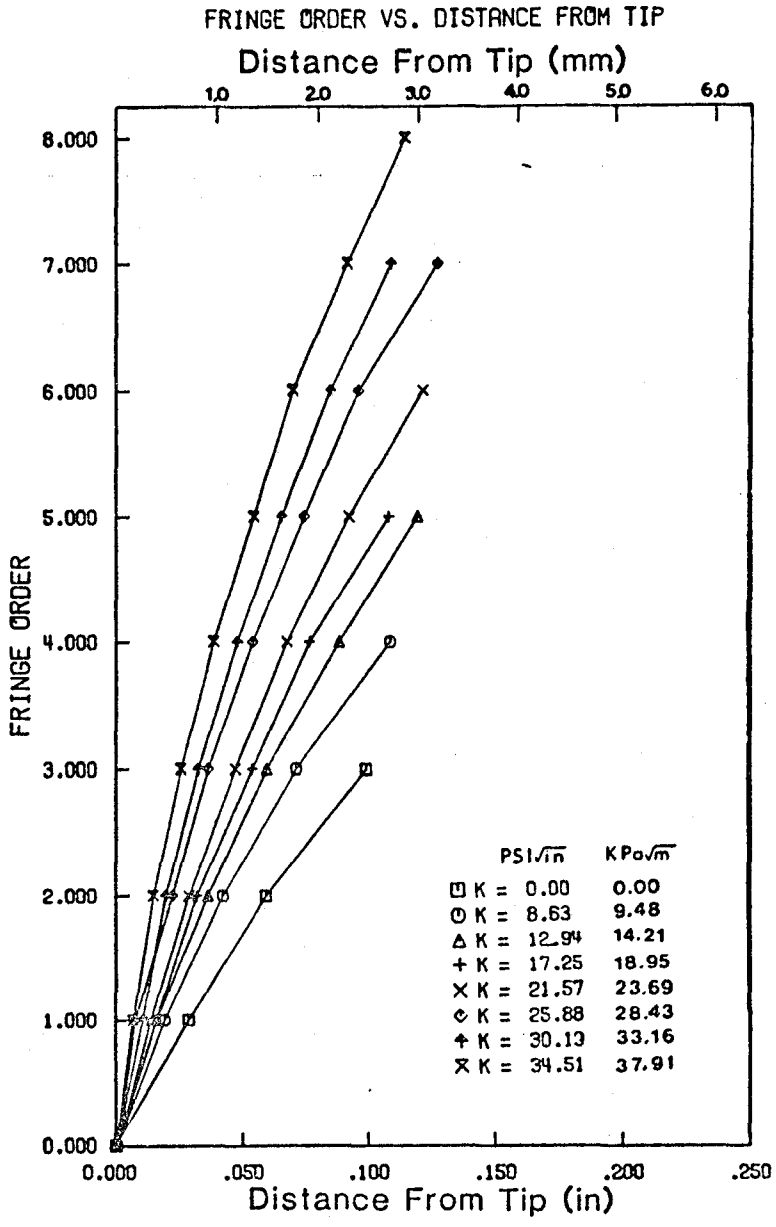

Figure 41: Midplane crack opening profiles as a function of applied load for specimen B-14 (1st cycle following the overload).

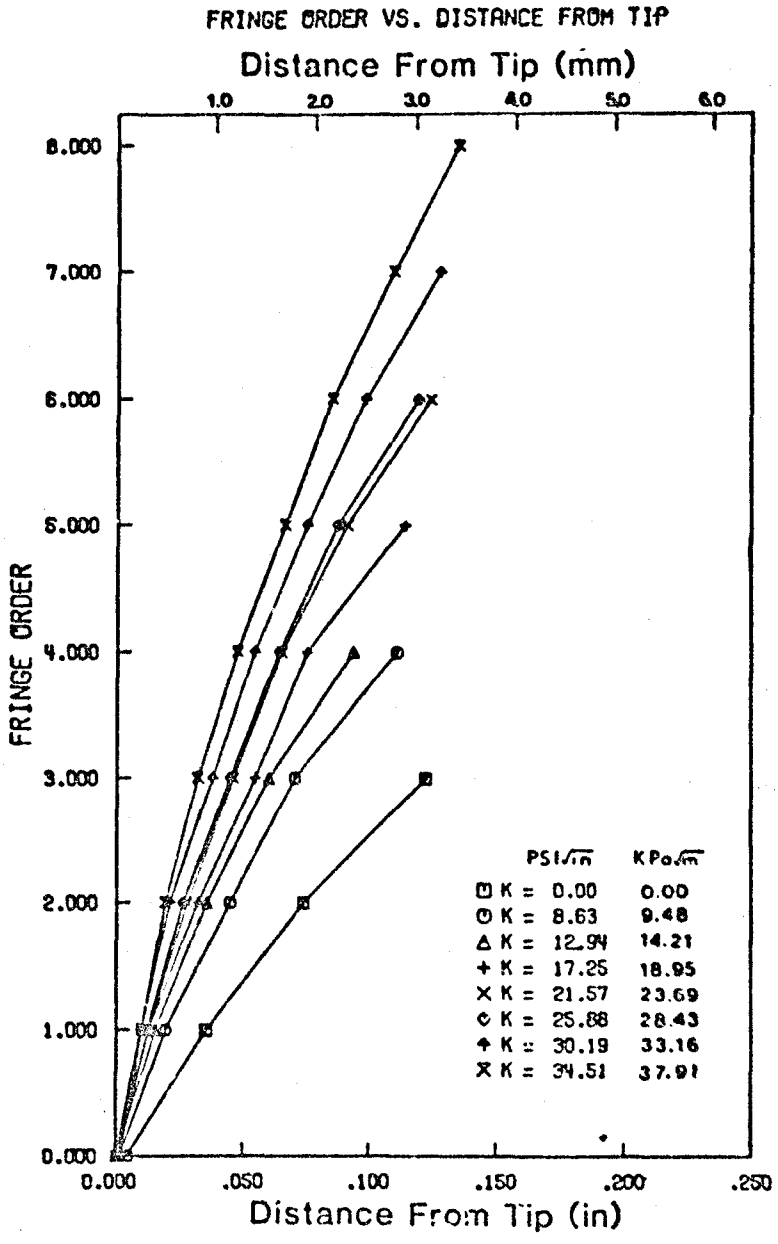

Figure 42: Midplane crack opening profiles as a function of applied load for specimen B-14 (10th cycle following the overload).

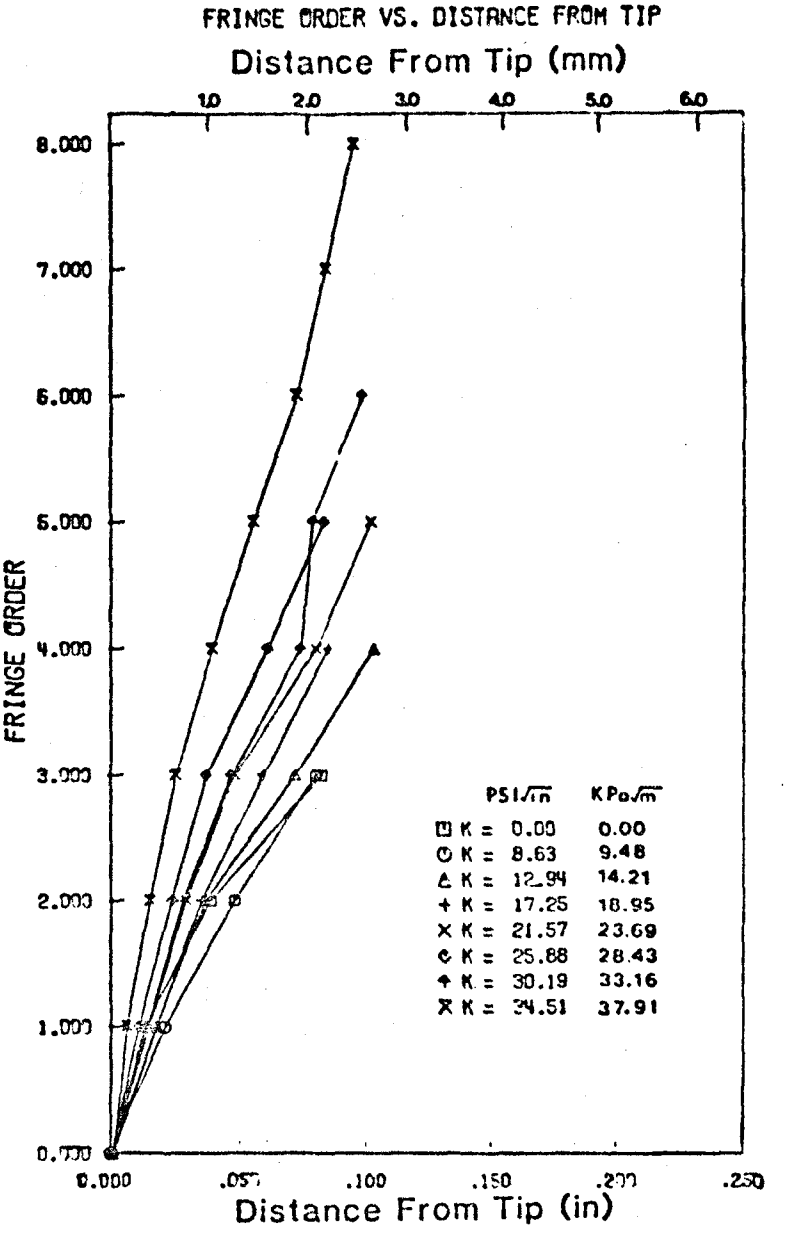

Figure 43: Midplane crack opening profiles as a function of applied load for specimen B-14 (1000th cycle following the overload).

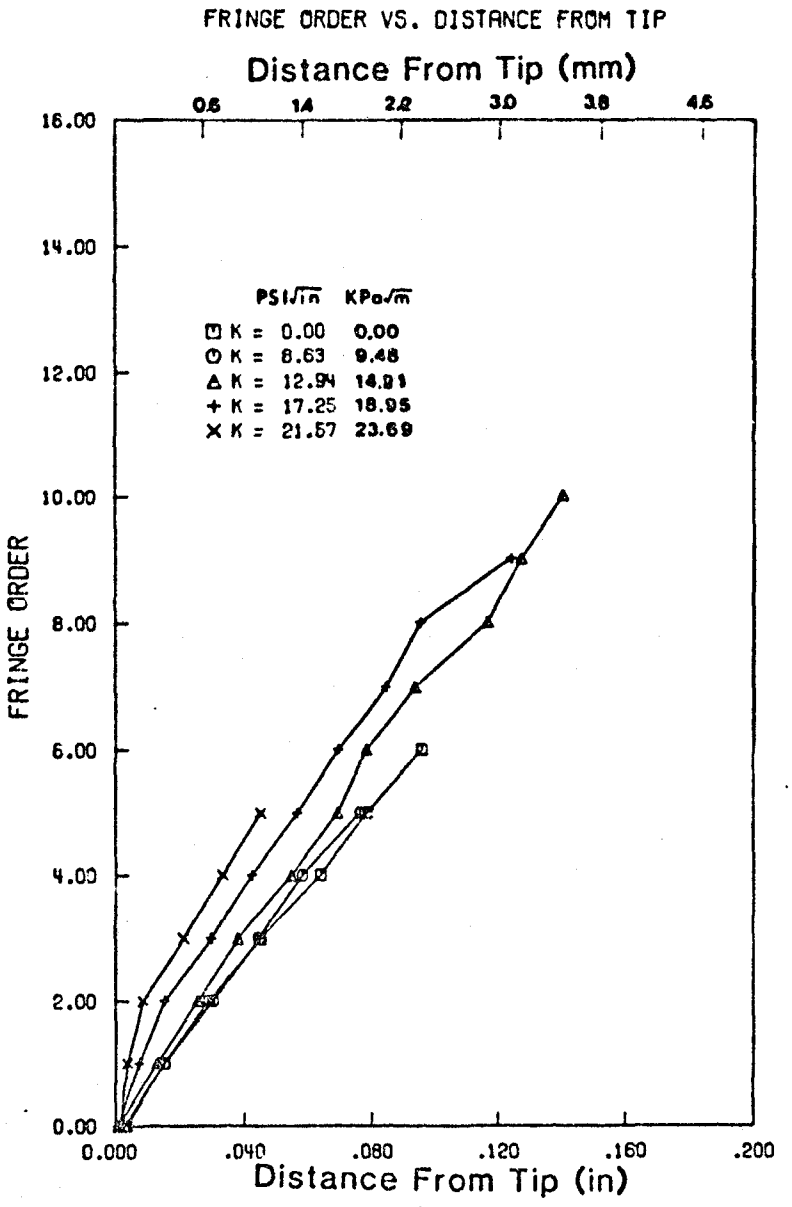

Figure 44: Free surface crack opening profiles as a function of applied load for specimen E-14 (1st cycle following the overload).

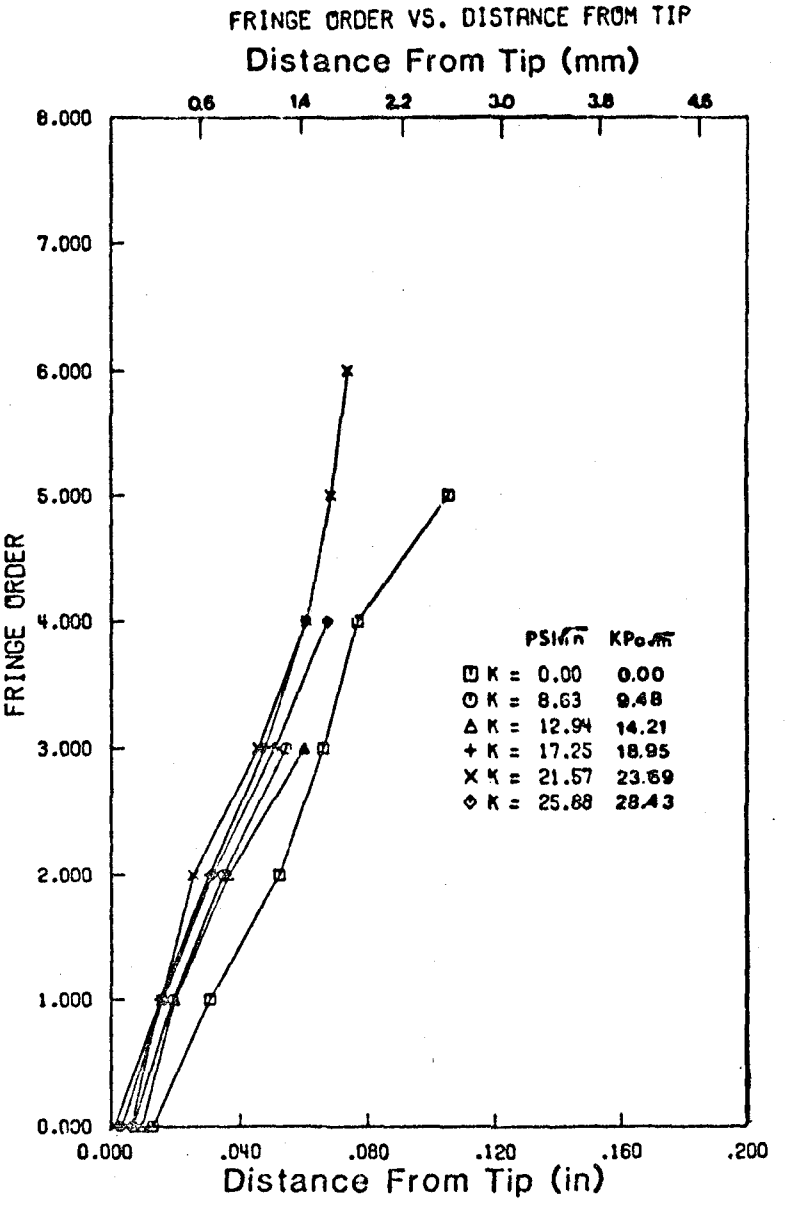

Figure 45: Free surface crack opening profiles as a function of applied load for specimen B-14 (10th cycle following the overload).

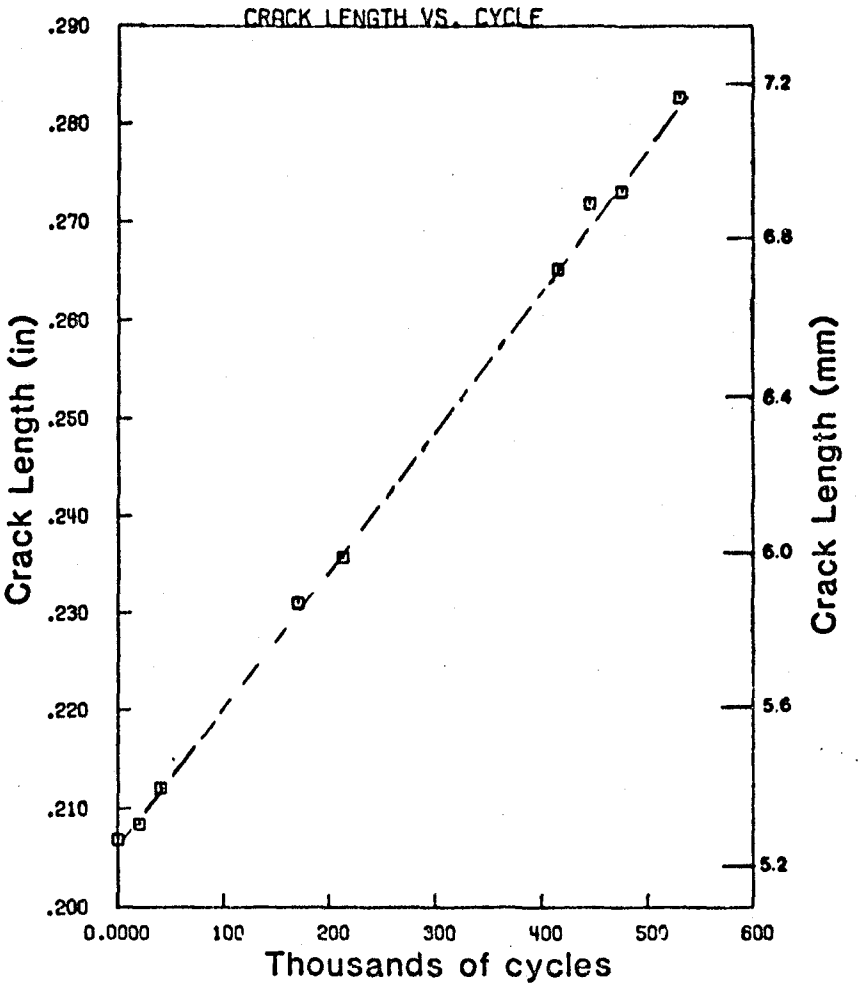

Figure 46: Average through-the-thickness fatigue crack length versus cycles curve for specimen B-15 (ΔK = 269 KPa-$m^{1/2}$, single peak overload = 1076 KPa-$m^{1/2}$). Note that this plot only contains the steady state behavior.

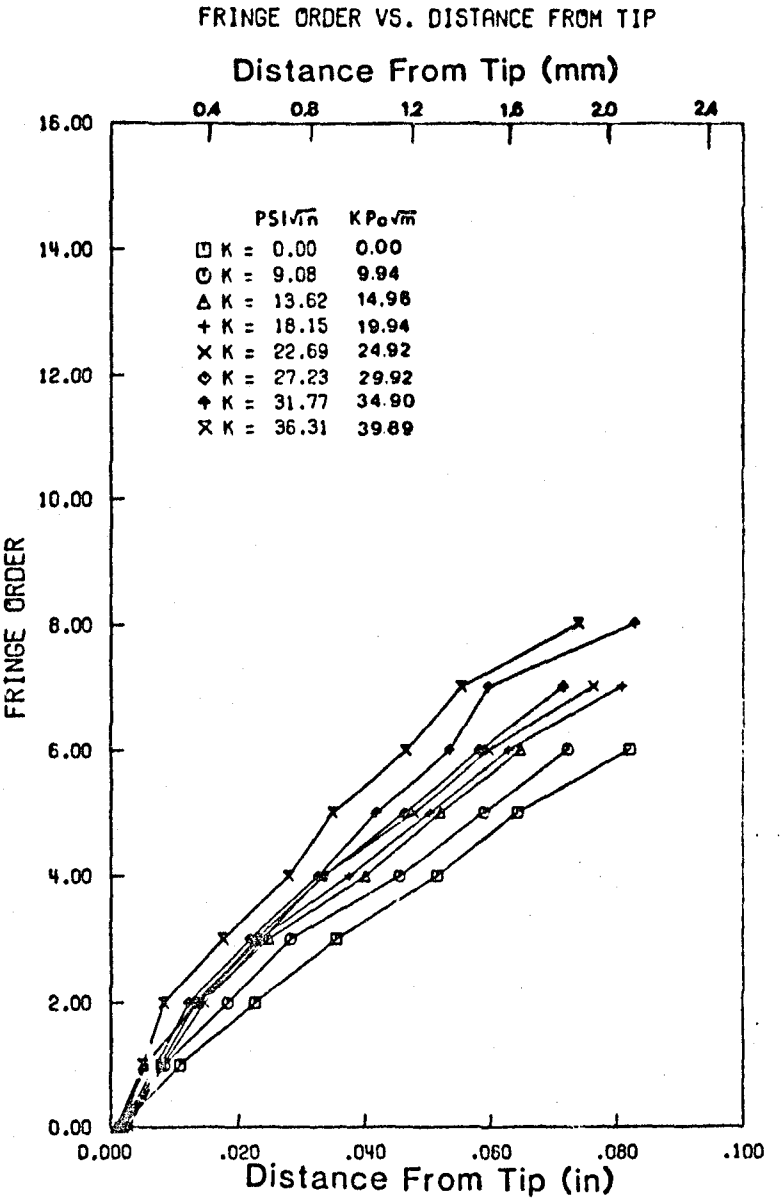

Figure 47: Midplane crack opening profiles as a function of applied load for specimen B-15 (Steady state conditions).

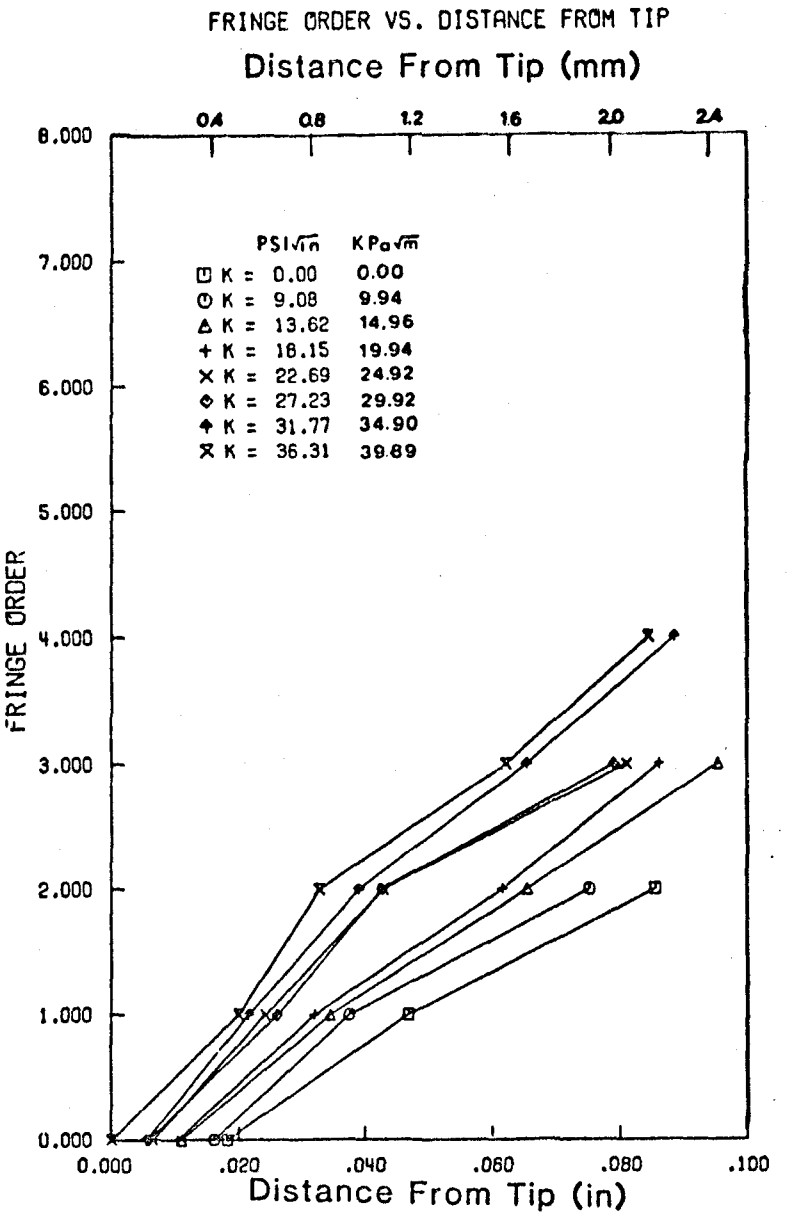

Figure 43: Free surface crack opening profiles as a function of applied load for specimen B-15 (steady state conditions).

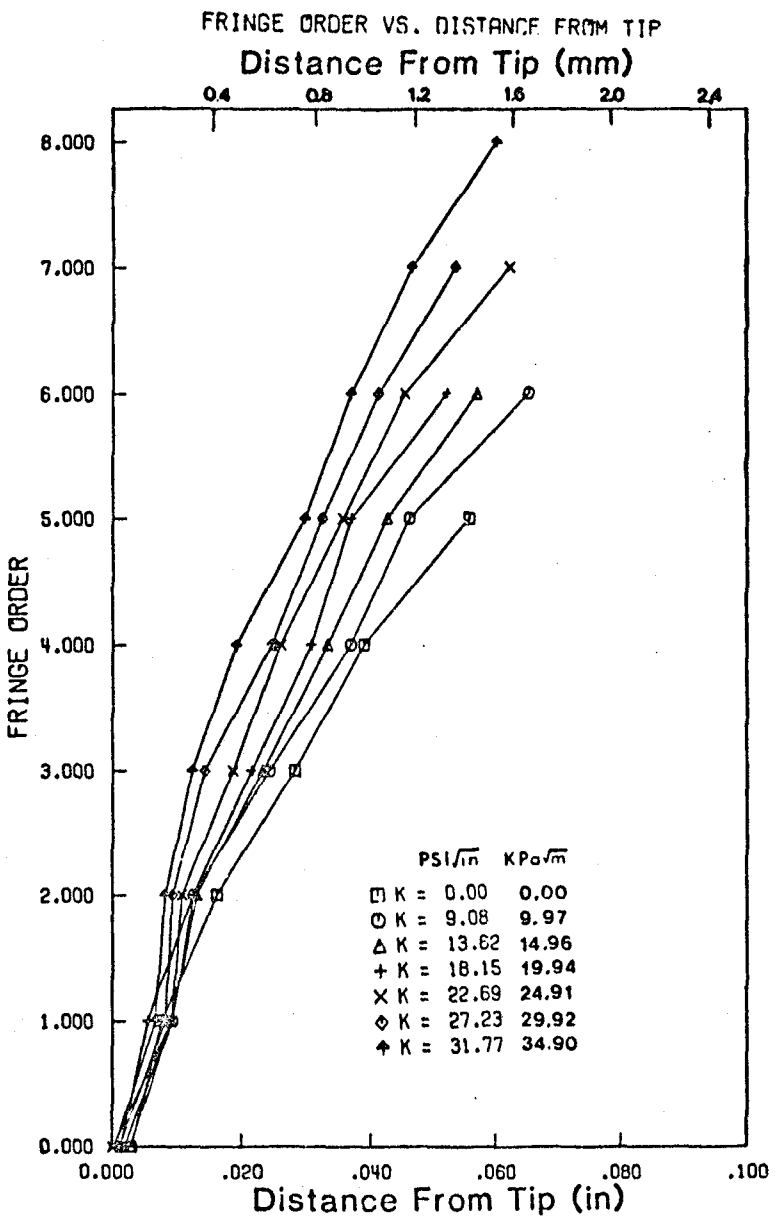

Figure 49: Free surface crack opening profiles as a function of applied load for specimen B-15 (1st cycle following the overload).

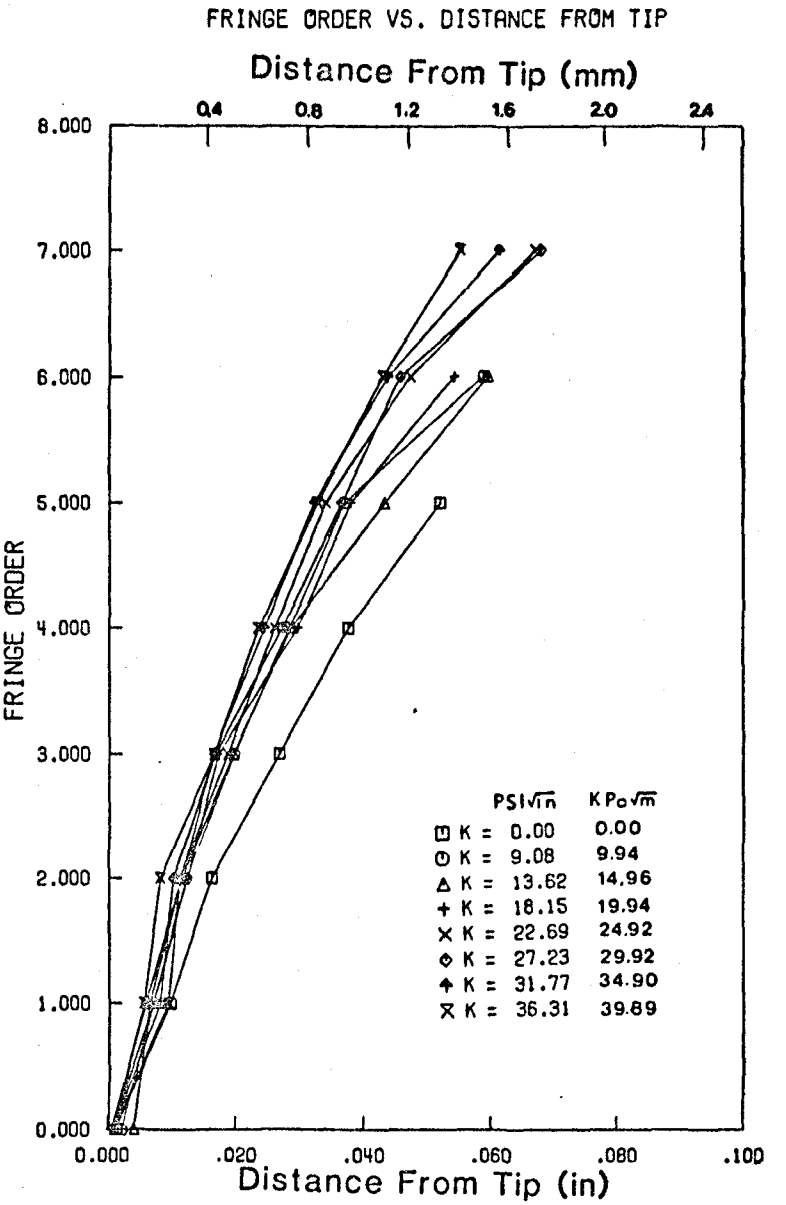

Figure 50: Free surface crack opening profiles as a function of applied load for specimen B-15 (10th cycle following the overload).

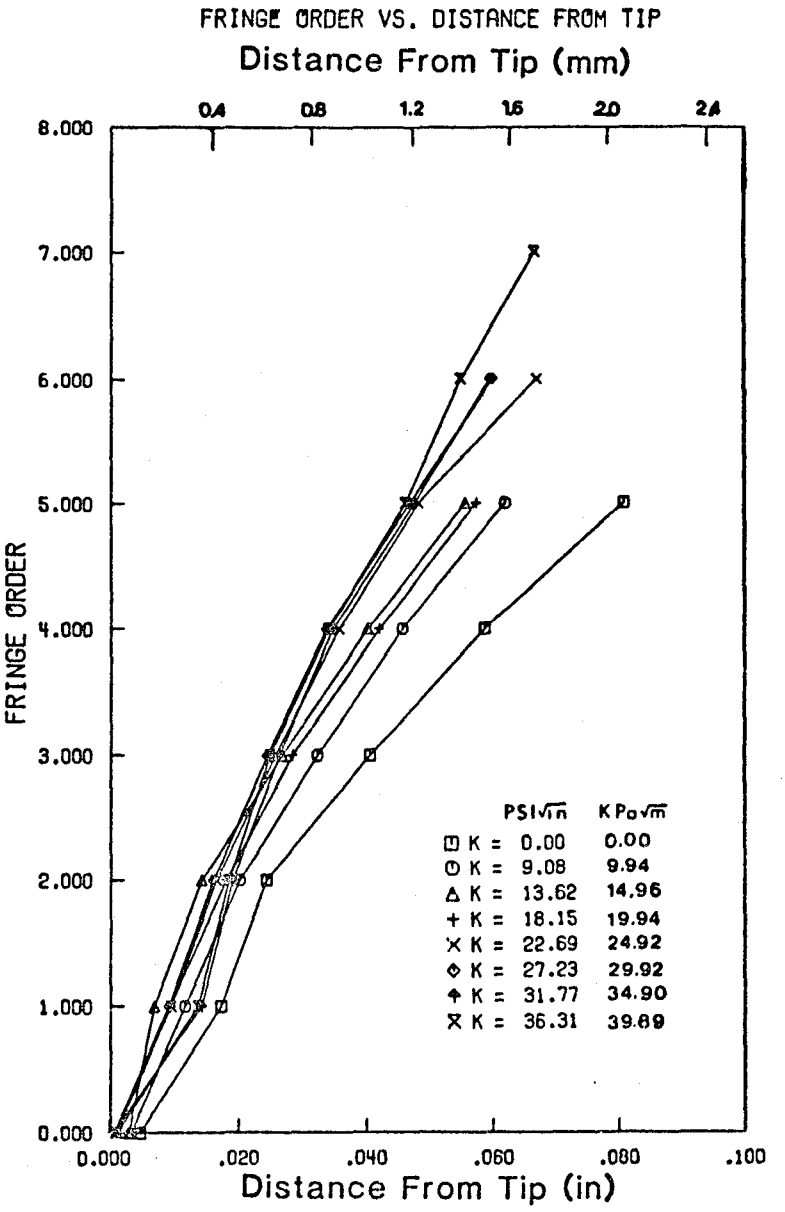

Figure 51: Free surface crack opening profiles as a function of applied load for specimen B-15 (100th cycle following the overload).

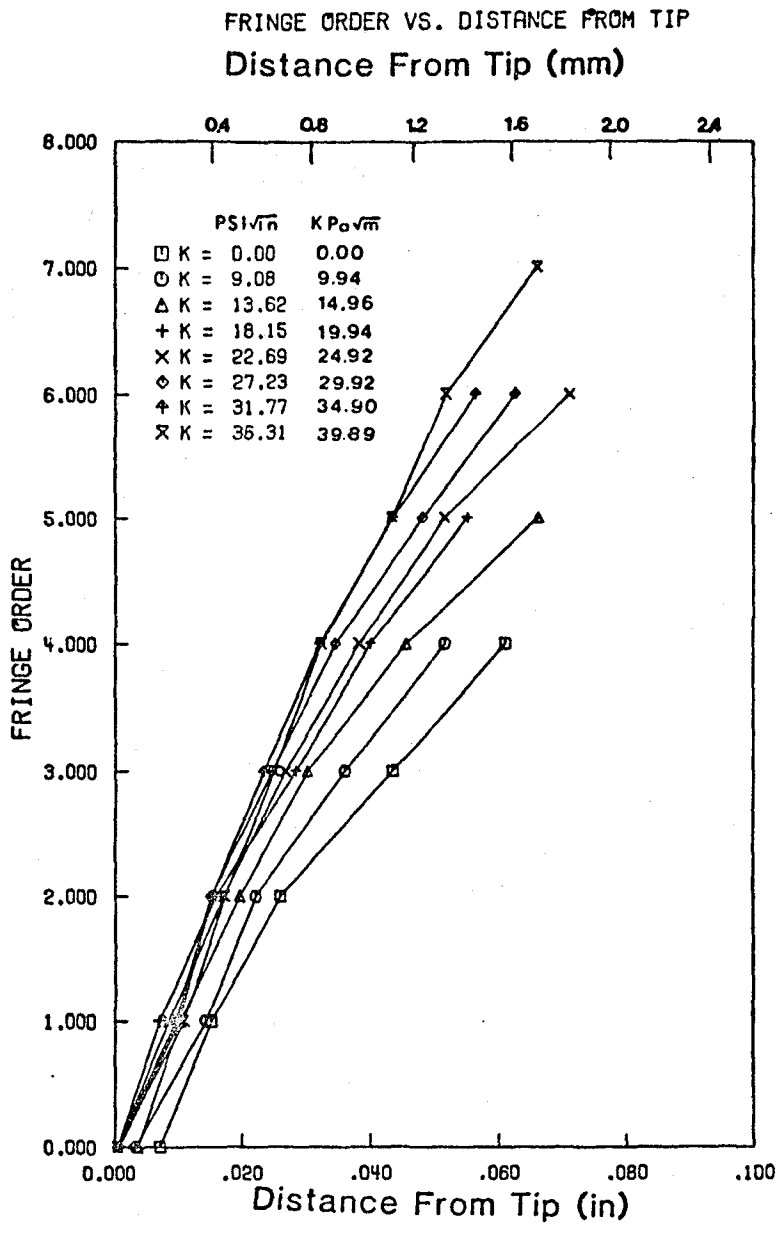

Figure 52: Free surface crack opening profiles as a function of applied load for specimen B-15 (1000th cycle following the overload).

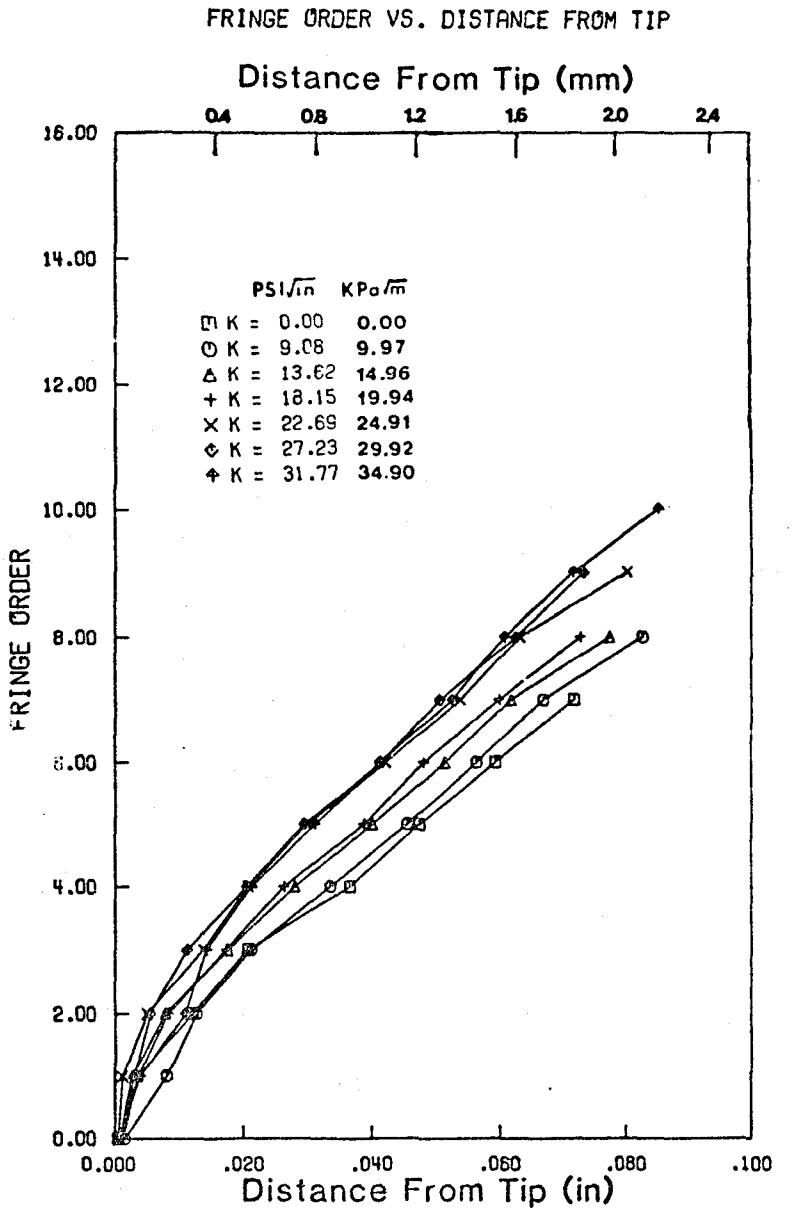

Figure 53: Midplane crack opening profiles as a function of applied load for specimen B-15 (1st cycle following the overload).

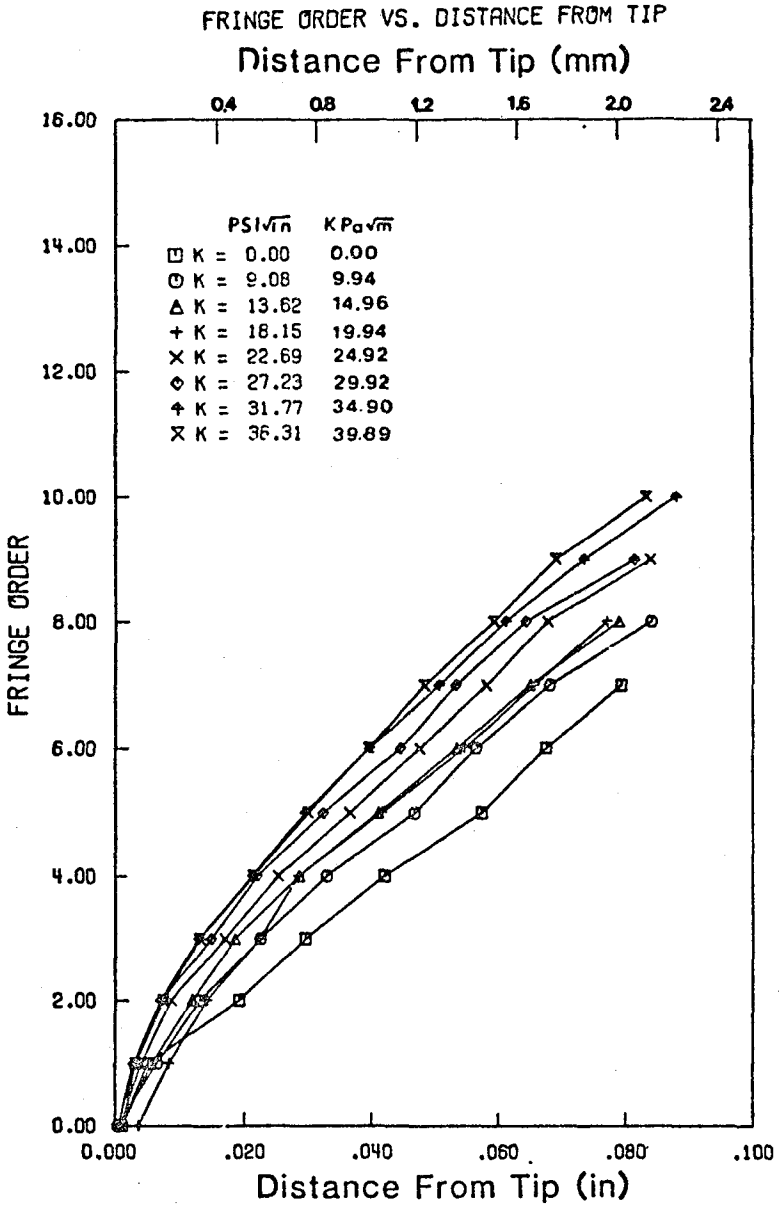

Figure 54: Midplane crack opening profiles as a function of applied load for specimen B-15 (10th cycle following the overload).

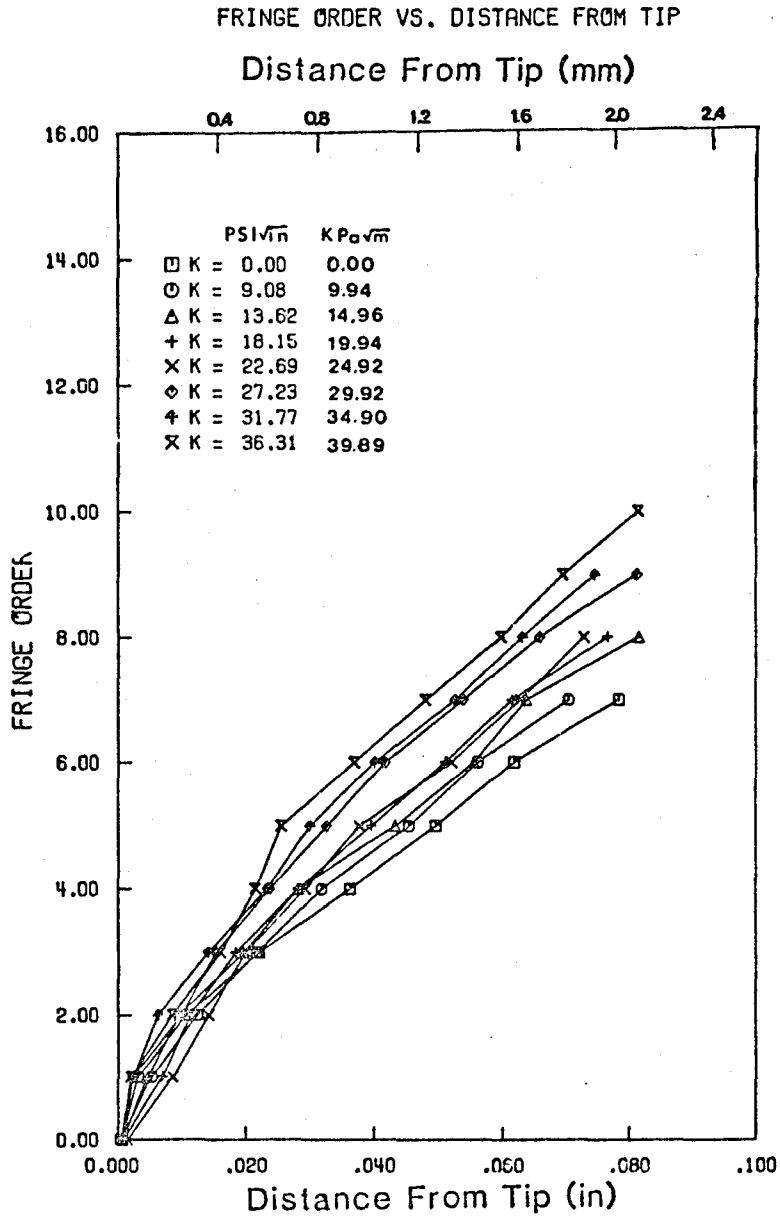

Figure 55: Midplane crack opening profiles as a function of applied load for specimen B-15 (100th cycle following the overload).

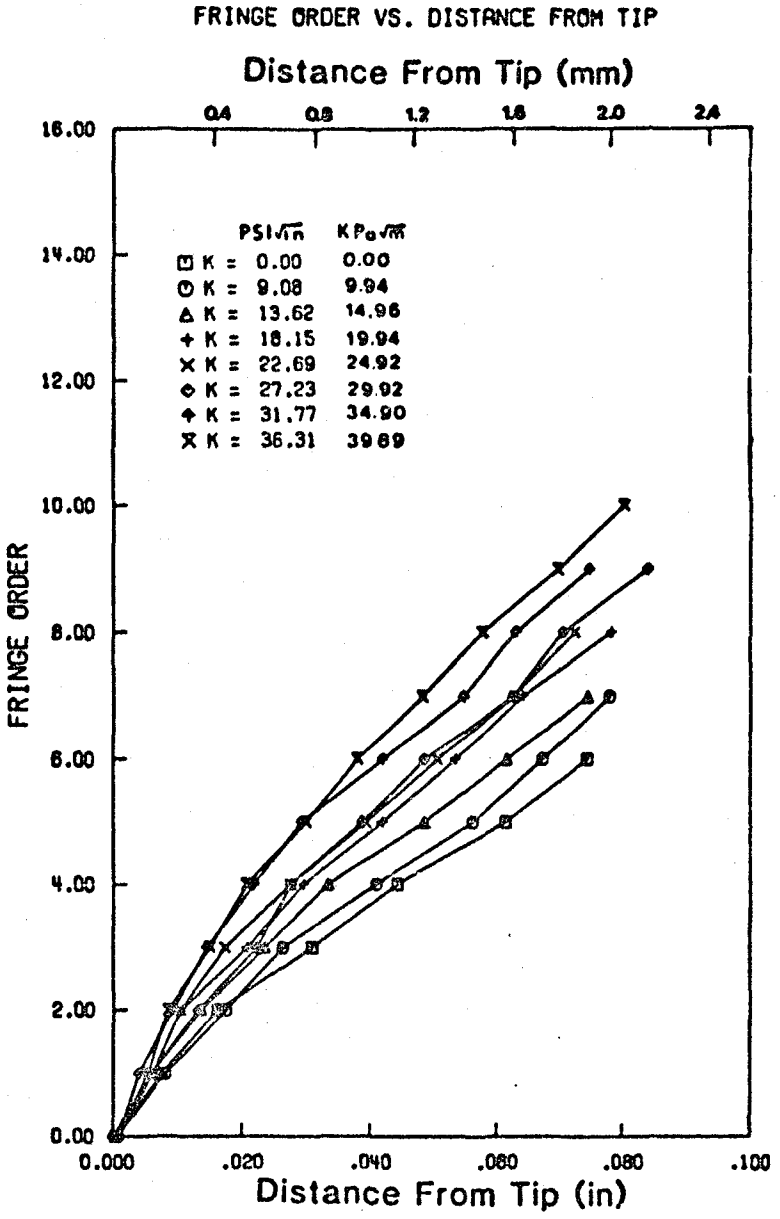

Figure 56: Midplane crack opening profiles as a function of applied load for specimen B-15 (1000th cycle following the overload).

C-2

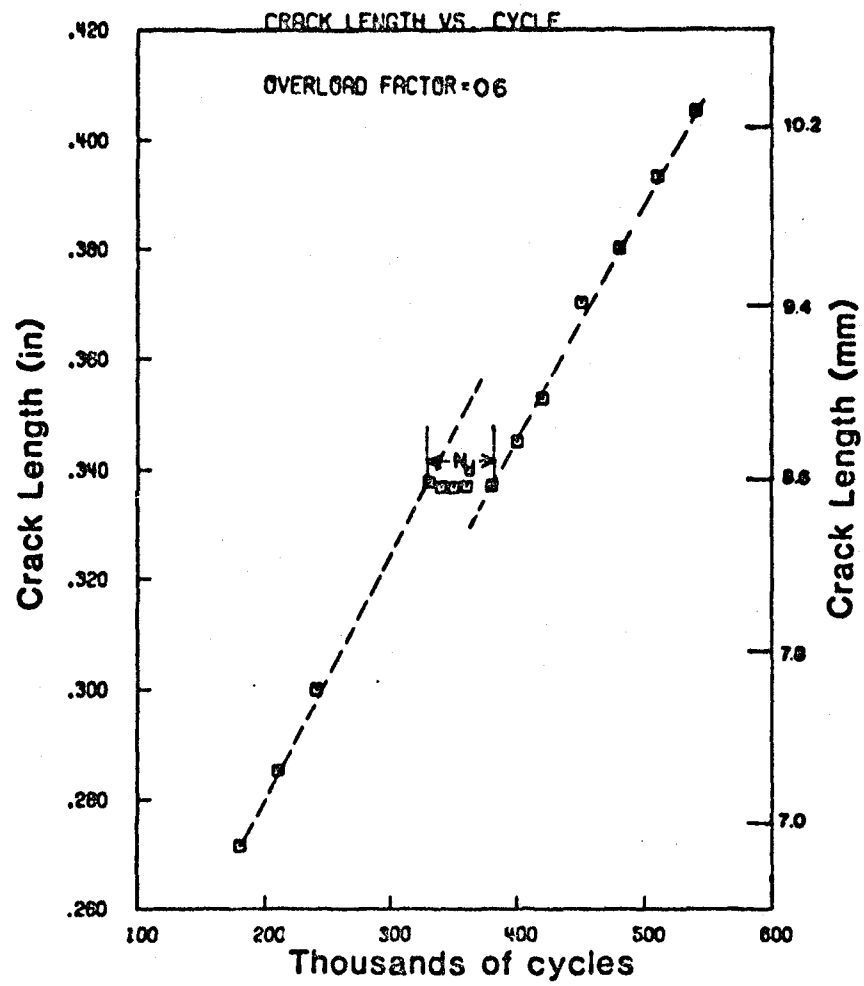

Figure 57: Average through-the-thickness fatigue crack length versus cycles for specimen B-16 (ΔK = 352 KPa-$m^{1/2}$, single peak overload = 2112 KPa-$m^{1/2}$).

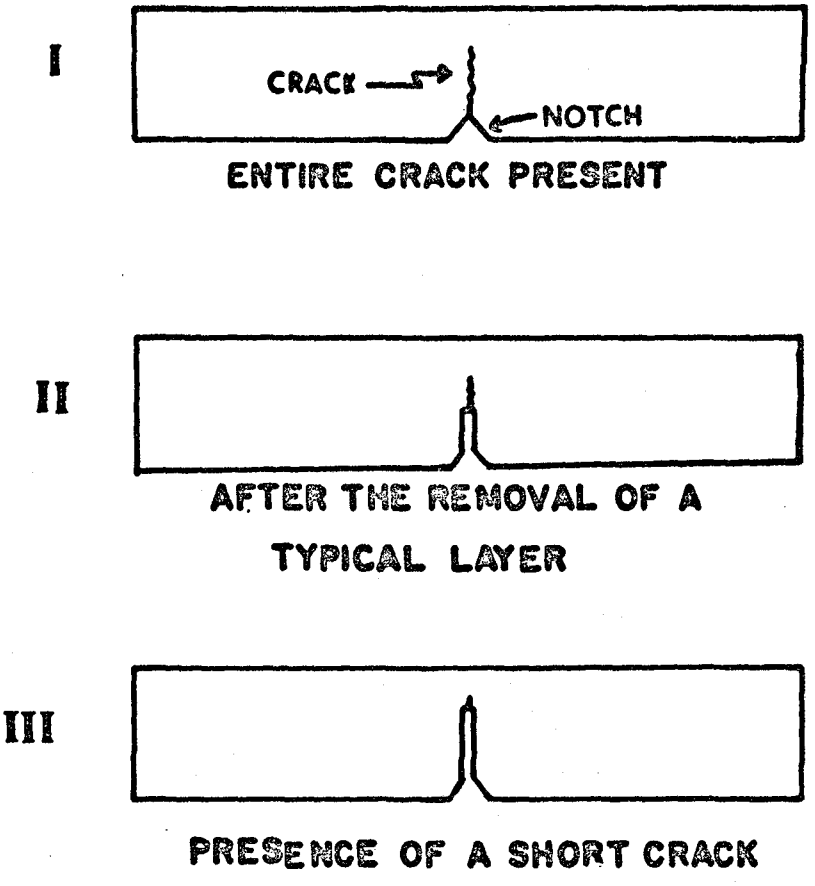

Figure 58: Schematic view of the crack following the removal of successive layers from the test specimen B-17.

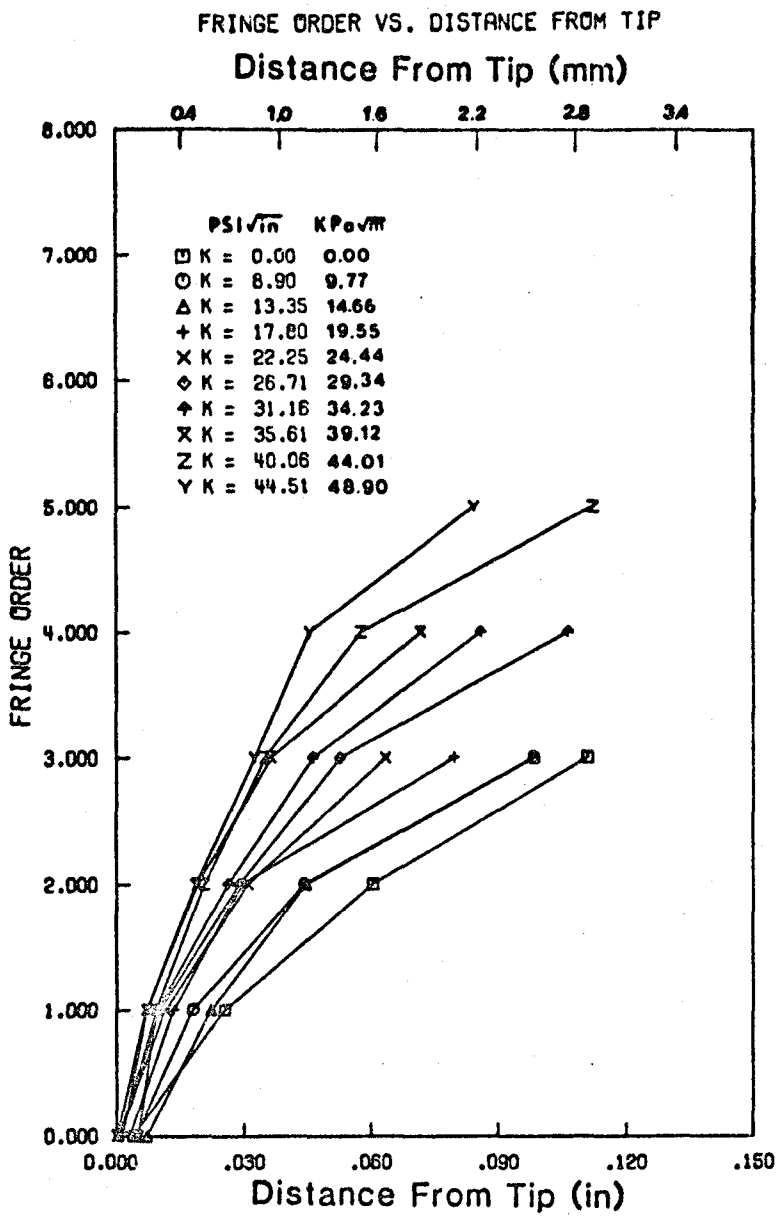

Figure 59: Midplane crack opening profiles as a function of applied load for specimen B-17 (steady state conditions).

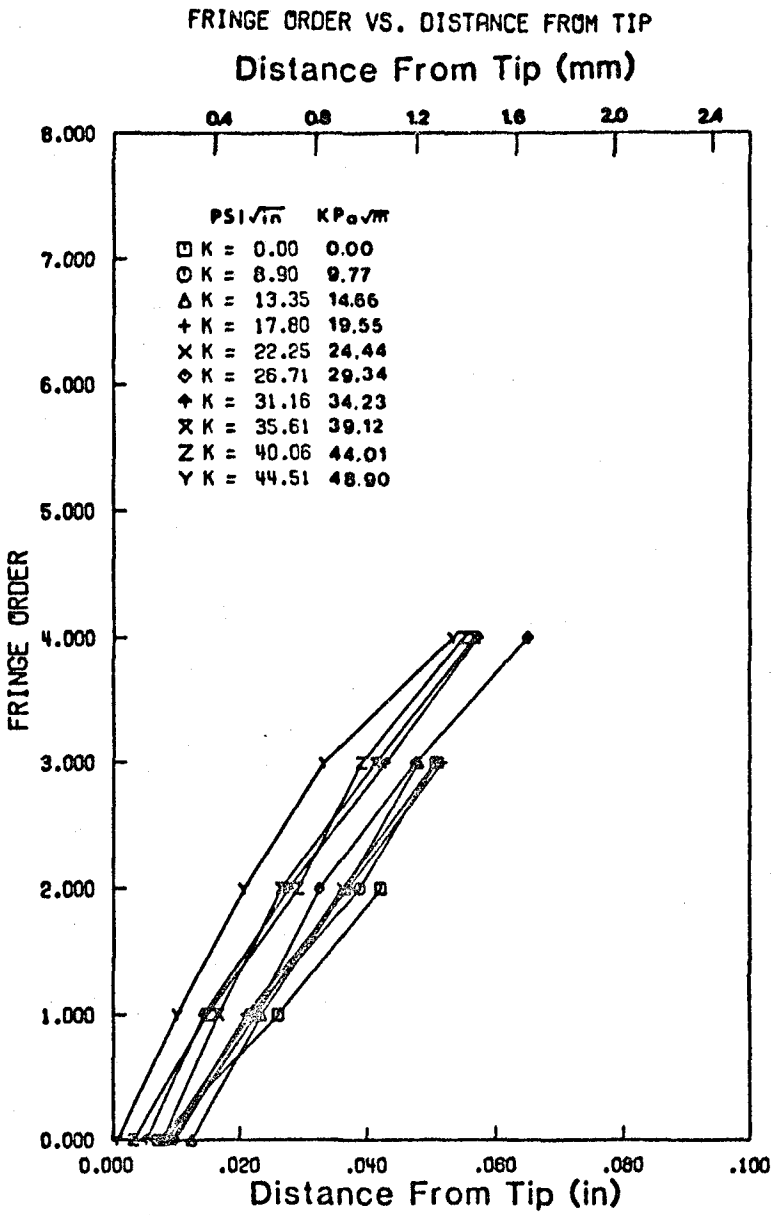

Figure 60: Free surface crack opening profiles as a function of applied load for specimen B-17 (steady state conditions).

CHAPTER 4

DISCUSSION OF RESULTS

4.1 CRACK RETARDATION

As discussed earlier, fatigue crack growth was retarded following application of the tensile overload to the polycarbonate test specimens. The crack tip appeared to be blunted by the peak load. Figure 61 shows the crack tip following the overload for Test B-12. Note that after 25-000 cycles following the overload, small individual flaws developed along the original (steady state) crack front, and after 45 000 cycles, a single through-crack front has been reestablished. Development of a new crack front and resumption of steady state crack growth at approximately 45 000 cycles following the overload, conforms to the delay period (N_d) in Figure 10. Crack tip blunting was seen in all overload tests in this project and was also observed in similar polycarbonate overload experiments reported in Reference 5.

In addition to the delay in the average fatigue crack growth rate following the overload cycle, crack tunneling was also observed. Although the tunneling also occurred during the steady state crack growth, it was more pronounced following the overload. Figures 62-63 compare crack growth behavior for the interior and the surface of Specimens B-14 and B-16. Although these tests had N_d values of approximately 50 000 cycles, the specimen surface crack dimension was more affected by the overload than the interior (middle) crack length. From these figures, it may be observed that, following the overload delay period, the interior crack growth rate returned to steady state conditions before

the surface crack growth rate. Thus, a retardation period based on the average crack length may not truly represent the crack delay across the specimen thickness.

4.2 CRACK PROFILES

Fatigue crack opening profiles were measured by optical interferometry at various times during the specimen life. The objective of these measurements was to characterize three-dimensional aspects of the fatigue crack closure phenomenon. As discussed previously, two different measures were obtained for the crack closure load. In one case, the minimum stress intensity factor required to physically separate the crack tip surfaces was determined from the crack opening profiles. This measure of crack closure is called the K_o load in this report and was determined at various points along the crack front through the specimen thickness. The second measure of crack closure, the elastic crack opening stress intensity level K_{oe}, is defined here as the minimum K value which causes the crack surfaces to separate in a linear elastic manner. As described earlier, the K_{oe} load is determined from the load/displacement records obtained at various locations behind the crack tip. All of the tests presented in this report indicate that the opening and the closing K_o and K_{oe} values measured at the specimen surface were higher than for the interior case.

Figures 64-67 present the K_o opening stress intensity factors measured at different locations along the crack front. In these figures, the K_o values are normalized with the baseline cyclic stress intensity, and distances from the specimen surface are normalized with specimen

thickness. The zero point on the abscissa for example, represents the specimen surface location while the 0.5 value represents the middle (interior) location. Figures 64-67 each contain two curves; one for steady state cycling and one for post-overload behavior. The difference in the opening load with location is expected from the plane strain/plane stress transition through the specimen.

The crack tip opening loads (K_o) following the tensile overload were found to be less than for the steady state case (Figures 64-66). This observation does not agree with the conventional closure mechanism for crack retardation which states that crack delay is due to elevation of the opening loads following the overload.

The reduction in the opening load following the overload in the present experiments may be due to crack tip blunting which causes the crack faces to be physically separated from each other. It was observed in Figures 64-66 that following the overload, the specimen interior remained open under zero load while the specimen surfaces required positive load to separate. The reduction in K_o at the specimen interior was greater than at the surface suggesting that the specimen interior suffered more blunting than the surface. Since the plastic zone is bigger at the specimen surface than the interior location, more plastic deformation is expected at the surface and the surface should be more affected by the blunting mechanism.

Since increased blunting of the specimen interior is not consistent with the plasticity arguments, another explanation may be in order for the drop in the opening load at the specimen interior following the

overload. Perhaps the specimen surface experiences plastic deformation during the opening phase of the overload cycle which causes the crack faces to come in contact at the surface but keeps the crack surfaces propped open in the specimen interior. Thus, the residual crack tip displacements along the interior crack front may be due in part to plastic deformation at the free surface and not necessarily to the blunting mechanism alone.

Table 2 presents the elastic crack opening stress intensity values (K_{oe}) for Test B-12. Figure 68 presents these linear K_{oe} values in a graphical form for the specimen surface while Figure 69 shows the behavior at the specimen interior. Recall that the K_{oe} value is defined here as the stress intensity level which causes the crack surfaces to separate in a linear elastic manner. This load is obtained from a plot of displacement versus applied load measured at a particular point behind the crack tip (recall Figures 27-36). Note from these figures that the K_{oe} values for the specimen surface are again higher than in the interior. As the distance from the crack tip increases, the elastic opening values decrease. Note that Figures 68 and 69 show the K_{oe} values for the specimen surface are again higher than in the specimen interior. As the distance from the crack tip increases, the elastic opening values decrease. This decrease in K_{oe} as one moves further from the crack tip has been observed earlier in metal specimens [40,55]. Following the overload, the elastic K_{oe} values increased although the crack tip separation load (K_o) decreased as discussed earlier.

Although the increase in K_{oe} following the tensile overload is consistent with the crack retardation phenomenon, it should be noted that

increases in the elastic opening K_{oe} values were more pronounced in the specimen interior than at the surface. Although the specimen interior experienced a greater elevation in K_{oe} following the overload than at the surface, the tunneling phenomenon was more pronounced after the overload (see Figures 62-63). The interior crack growth quickly resumed following the overload application suggesting that the interior K_{oe} value returned to the steady state case shortly following the overload cycle. On the other hand, large plastic deformation at the specimen surface would require a longer cycling period for K_{oe} values at the specimen surface to return to the steady state levels. Since the overload also blunted the crack tip and prevented interference fringe formation on the new crack faces following retardation, crack opening profiles could not be measured once crack growth resumed. Thus, the K_o and K_{oe} values could not be measured once the crack growth resumed following the retardation period.

4.3 STRAIN GAGE AND CLIP GAGE RESULTS

As discussed earlier, strain gages were mounted across the crack in an attempt to measure opening loads by both the fringe and strain gage methods. Fringe pattern pictures obtained with the strain gage mounted at the surface are shown in Figure 70. Note that the 0-order fringe does not behave in the same fashion for applied loads as observed in Figure 11 (the steady state case without strain gage). Figure 70 shows a cusp at the location of the strain gage, and the top right corner of the 0-order fringe never passes through the cusp. In essence, the 0-order fringe reaches the specimen surface crack tip without separating

the crack faces at the strain gage location. Since the strain gage influenced the crack opening profiles, it is obvious that the opening loads obtained from the strain gage data are not consistent with the interferometric measurements.

A clip gage was also mounted across the crack mouth at the notch of the specimen, but it was observed that the force exerted across the notch by the clip gage also affected the opening load. In this case, the crack tip opening loads were smaller since the tension of the clip gage applies a positive load at the specimen notch. The effect of the strain gage, and the clip gage may be due to the fact that the opening loads for the experiments are relatively small and that the polymer test material has a low modulus of elasticity.

4.4 CONTACT SURFACE REMOVAL

An experiment was conducted to determine the effect of fatigue crack length on the opening load. As discussed in section 3.2 (Test B-17), successive lengths of crack surfaces were removed (Figure 58), and the resulting fringe patterns were analyzed. Although the quality for the fringe photographs following the removal of a typical layer are poor and are not reproduced in this report, it was possible to make crack displacement measurements from the 35 mm negatives. The fringe patterns following the removal of one layer are circular whereas the original fringe patterns were semi-circular as shown in Figure 11. For the shorter crack lengths (measured from the notch root), the 0-order fringe did not reach the crack tip until relatively high loads. This elevation in the opening K value for the shorter crack is inconsistent with the plastic wake theory, which would expect shorter cracks to have a smaller plastic wake region behind the crack tip. Removal of this plastic wake should reduce the closure effect and decrease the opening stress. The fact that the opening load increased for shorter cracks may be due to possible residual stresses induced by machining successive layers from the crack. Detailed examination of this point was beyond the scope of the current program.

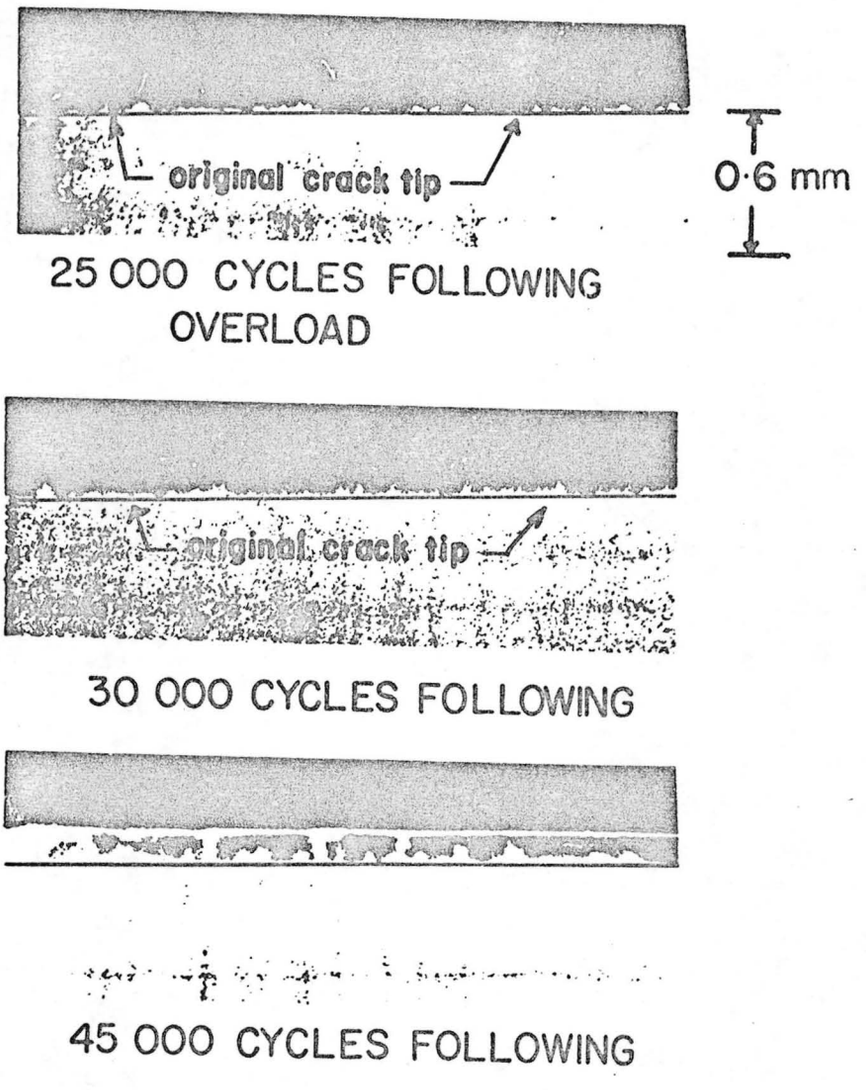

Figure 61: Photographs of blunted crack tip for 25 000, 30 000, and 45 000 cycles following the overload for specimen B-12.

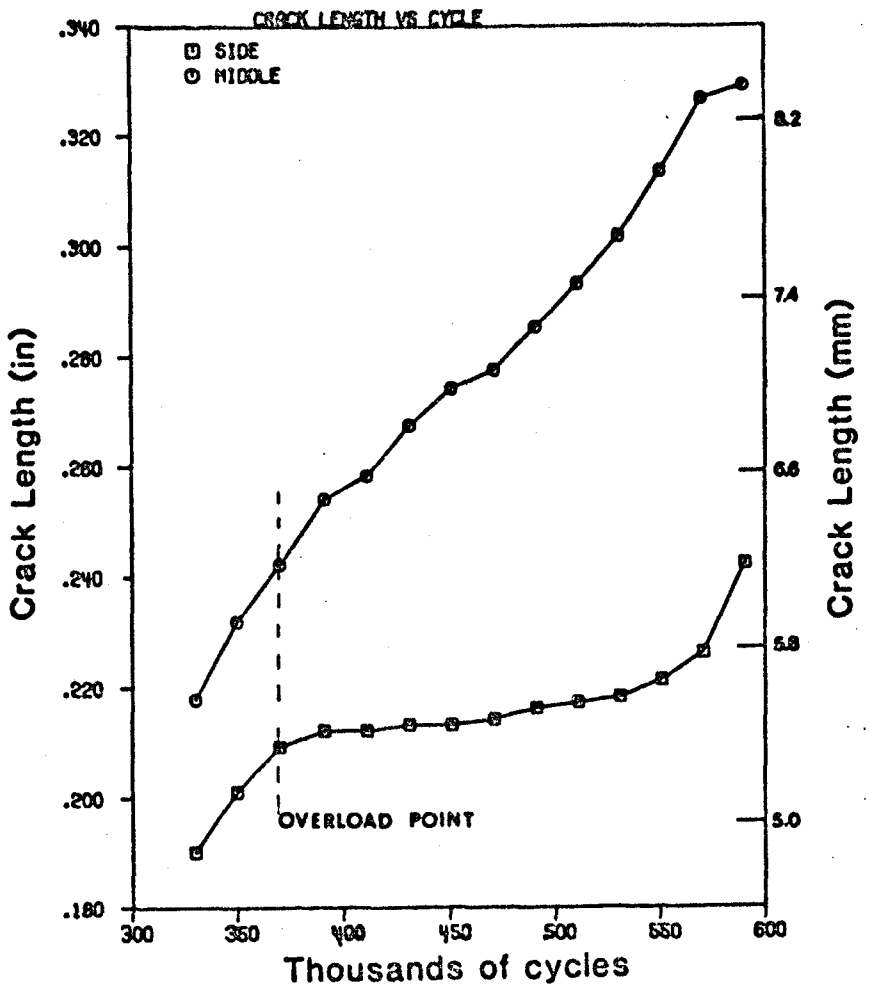

Figure 62: Comparison of the cyclic growth of crack dimensions measured at the surface and middle of specimen B-14 (ΔK = 297 KPa-$m^{1/2}$, overload = 1485 KPa-$m^{1/2}$).

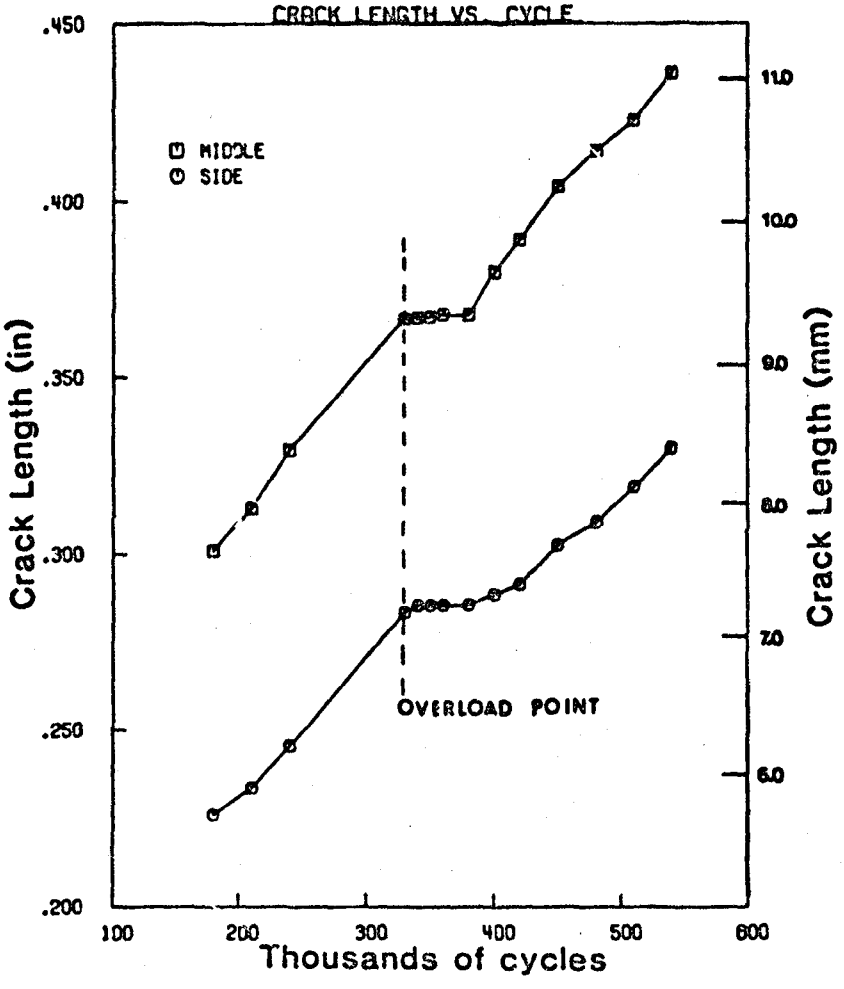

Figure 63: Comparison of the cyclic growth of crack dimensions measured at the surface and middle of specimen B-16 (ΔK = 352 KPa-$m^{1/2}$, overload = 2112 KPa-$m^{1/2}$).

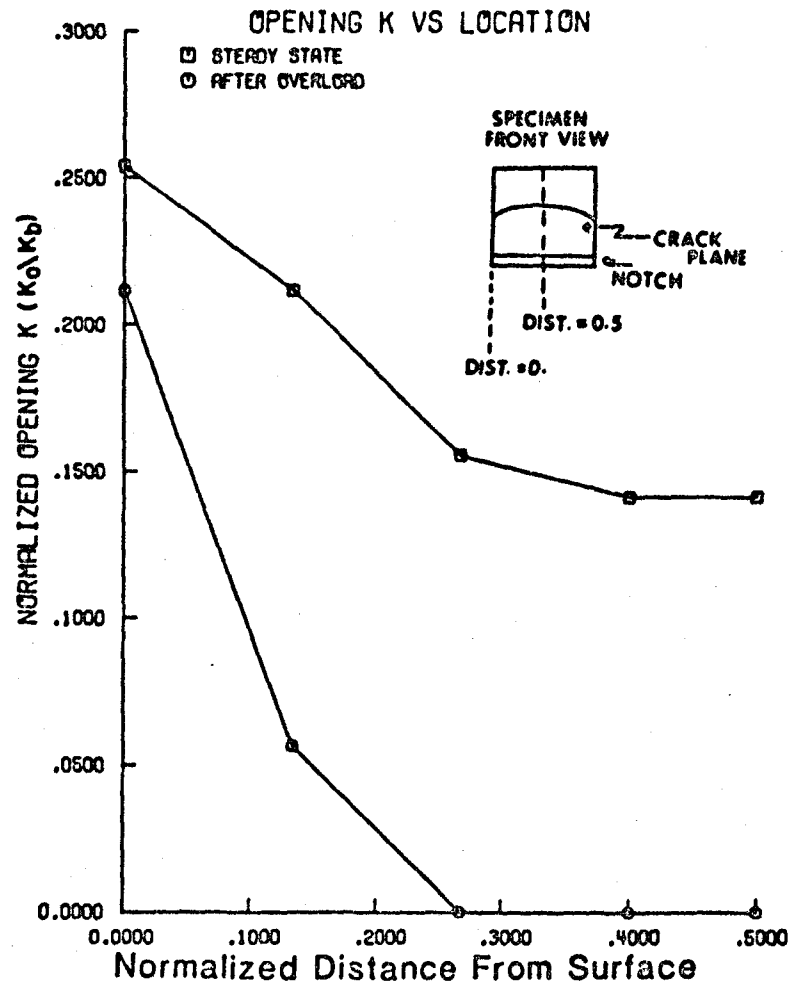

Figure 64: Comparison of dimensionless crack opening load measured at various points through the specimen thickness before and after overload (Test B-12).

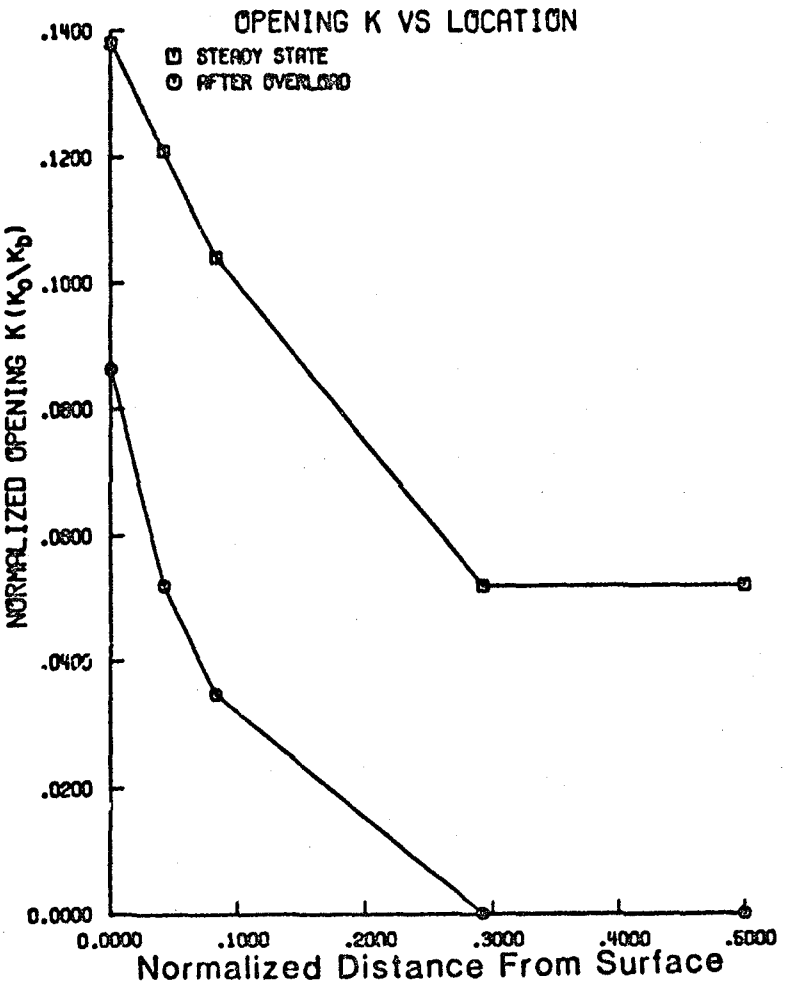

Figure 65: Comparison of dimensionless crack opening load measured at various points through the specimen thickness before and after overload (Test B-14).

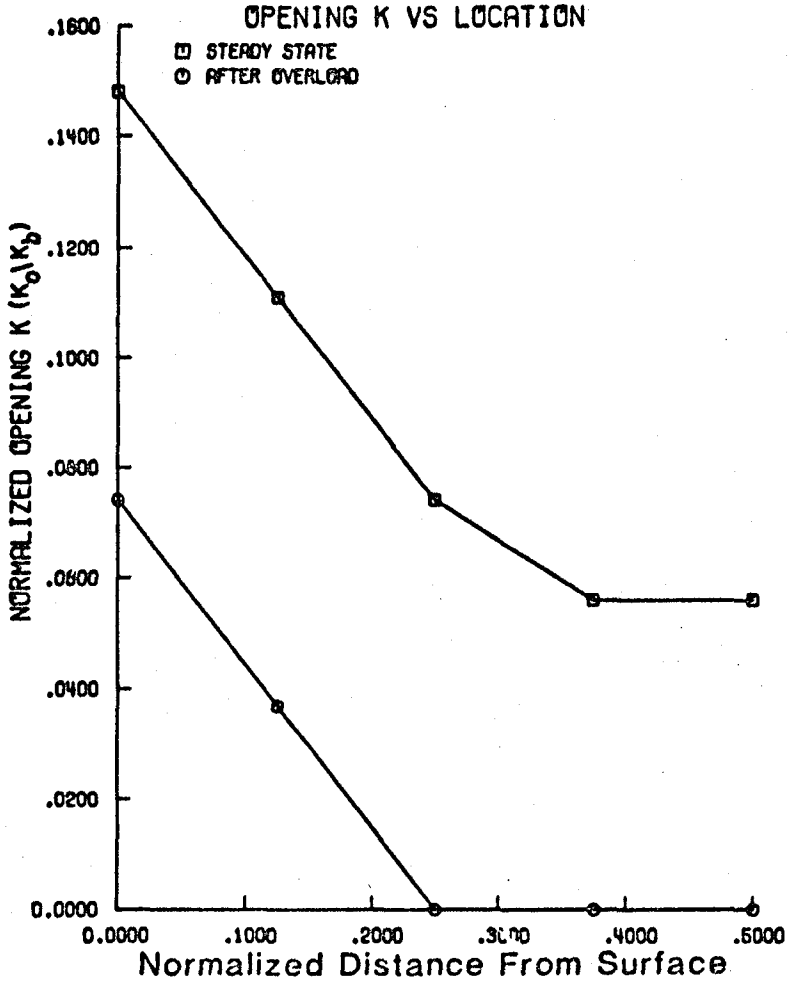

Figure 66: Comparison of dimensionless crack opening load measured at various points through the specimen thickness before and after overload (Test B-15).

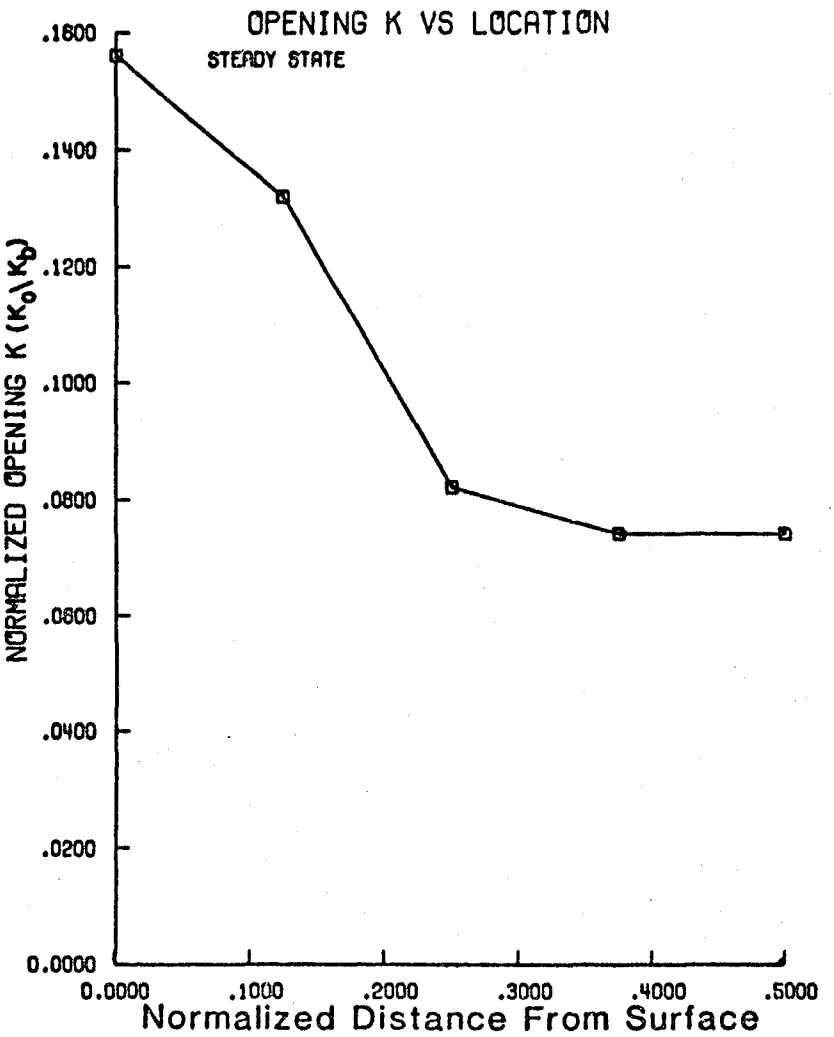

Figure 67: Comparison of dimensional crack opening load measured at various points through the specimen thickness for steady state case (Test B-17).

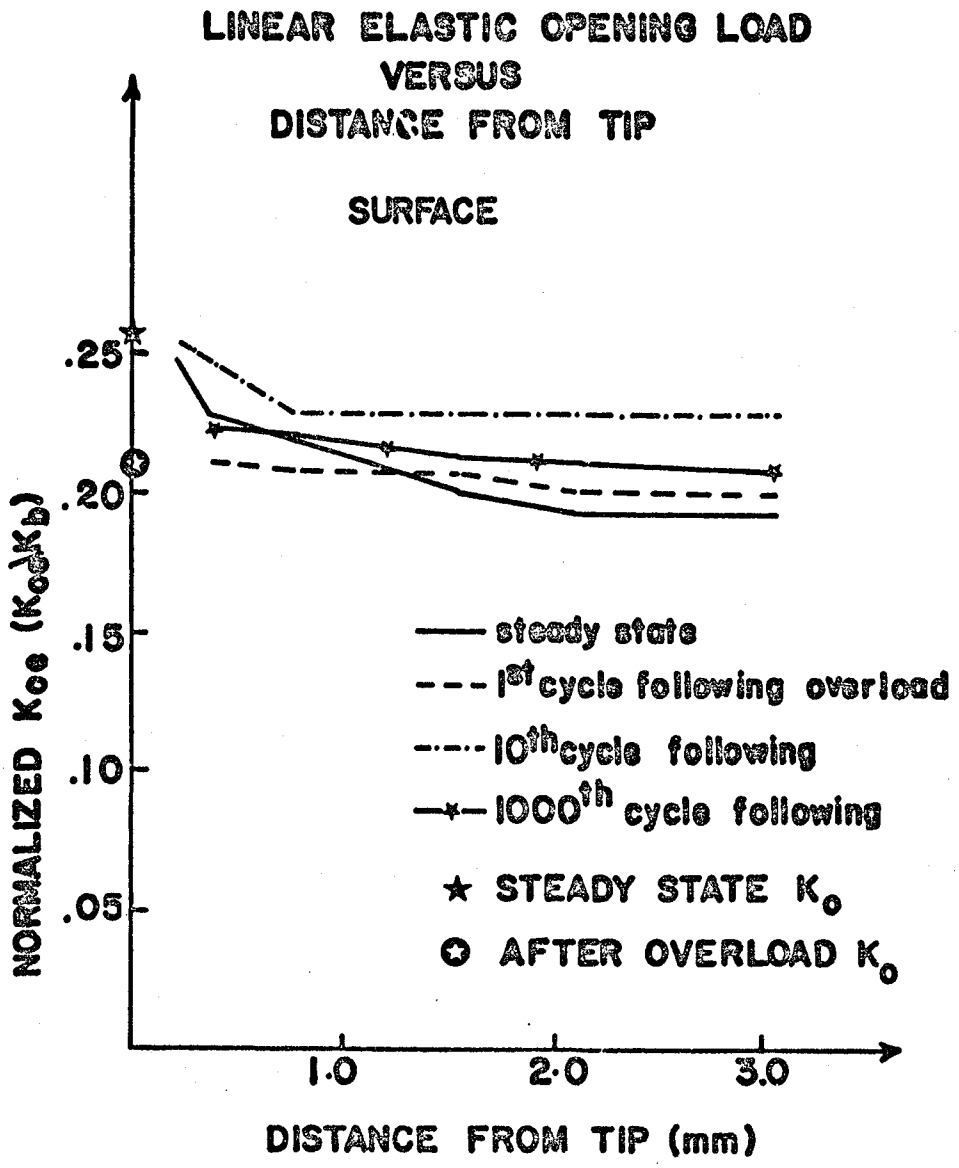

Figure 68: Comparison of dimensionless elastic crack opening load (K_{oe}) measured at various distances from the crack tip for the specimen surface.

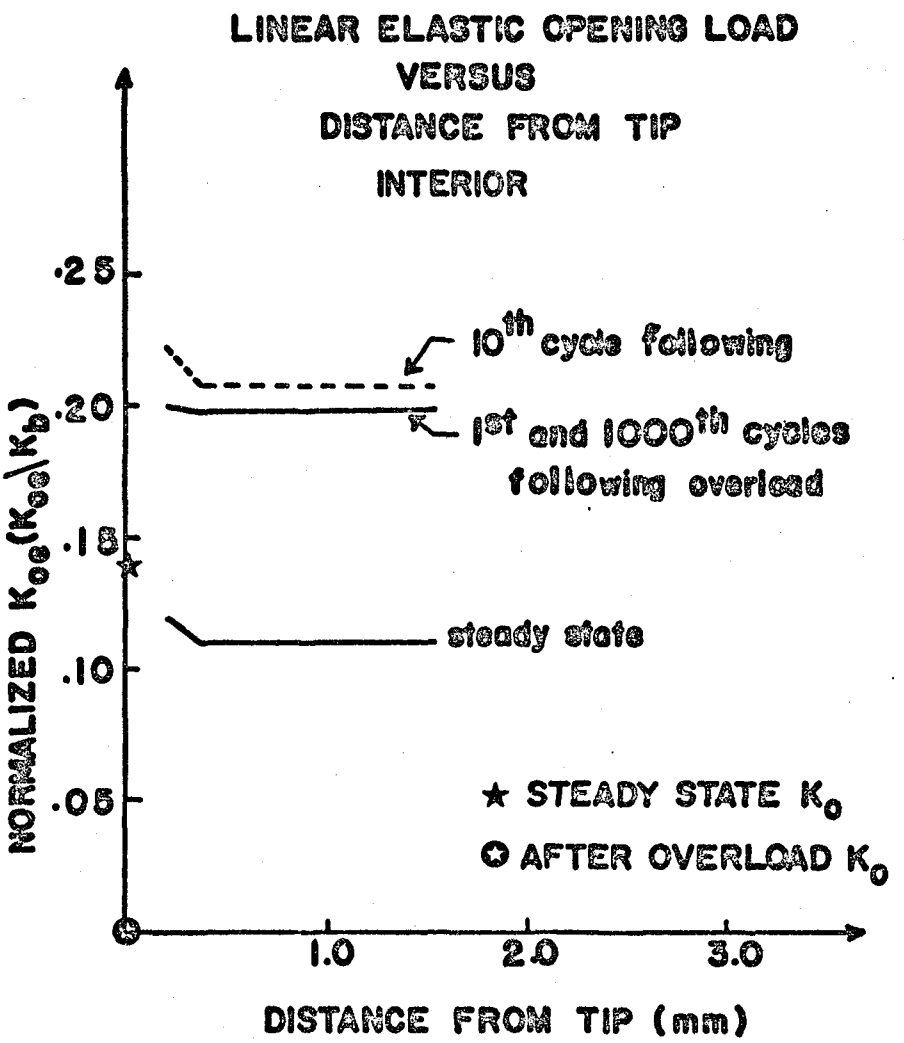

Figure 69: Comparison of dimensionless elastic crack opening load (K_{oe}) measured at various distances from the crack tip for the specimen interior.

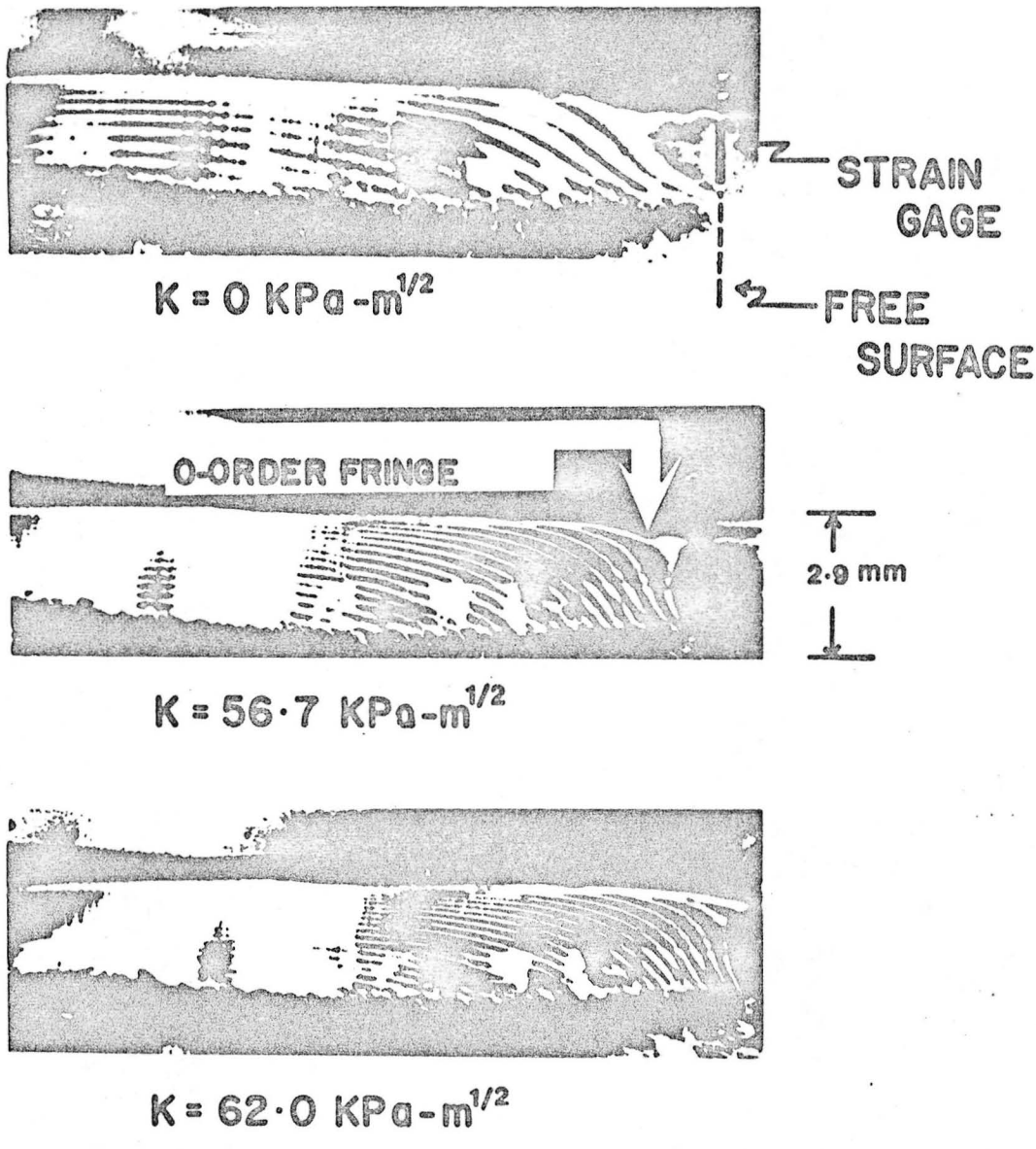

Figure 70: The crack opening profiles for the steady state case with a strain gage mounted across the crack at 0.0, 56.7, and 62.0 KPa-$m^{1/2}$.

CHAPTER 5

CONCLUDING REMARKS

Fatigue cracks were grown in polycarbonate specimens under conditions of constant ΔK and were subjected to tensile overloads to determine the fatigue crack retardation behavior. The cracks were examined under a monochromatic light source to create optical interference fringe patterns which were used to measure the crack closure effect in the test specimens. The crack opening profiles were obtained as a function of applied load and were compared before and after the tensile overloads. The following conclusions may be drawn from these experiments.

A tensile overload was shown to significantly delay subsequent fatigue crack growth in polycarbonate specimens grown under conditions of constant ΔK.

The reinitiation of separate crack growth sites along the crack tip following the overload suggests that crack tip blunting contributes to the mode of fatigue crack retardation in polycarbonate.

The increased difference between crack growth rates at the surface and interior of the specimen results in more tunneling following the overload.

The crack opening load at the specimen surface is significantly higher than in the interior, which explains the difference in crack growth rates between the surface and the interior of the specimen. This difference in opening K values is expected from the plastic zone variation resulting from plane stress (surface) and plane strain (interior) conditions.

The interference patterns obtained from these experiments suggest that the stress intensity value which causes crack surface displacements is nearly same for crack opening as closing , both at the specimen surface and in the specimen interior.

Although the crack tip separation load (K_o) decreased following the overload application, the load at which the crack opens and closes elastically (K_{oe}) increased following the overload. This latter behavior is consistent with the fatigue crack retardation phenomenon observed in these experiments. Following the tensile overload application, the specimen interior experienced a higher elevation in the elastic opening loads than the specimen surface. The more pronounced tunneling effect following the overload suggests that the effective cyclic stress intensity factor at the specimen interior returns to the steady state level faster than the value at the specimen surface.

The strain and crack opening displacement gage techniques influenced crack opening behavior in the present experiments. Future attempt to use these methods with fatigue cracks grown at low cyclic stress intensity factors in polycarbonate specimens should take special precautions to ensure that the measurement technique does not alter the specimen behavior.

REFERENCES

[1] Elber, W., "The Significance of Fatigue Crack closure", Damage Tolerance in Aircraft Structures, ASTM STP 486, pp. 230-242 (1971).

[2] Wheeler, O.E., "Spectrum Loading and Crack Growth", Journal of Basic Engineering, Vol. 94, Series D, No. 1 (1972).

[3] Willenborg, J., Engle, R.M., and Wood, H.A., "A Crack Growth Retardation Model Using an Effective Stress Concept", TM-71-1-FBR, Air Force Flight Dynamic Laboratory (Jan 1971).

[4] Vroman, G.A., "Analytical Prediction of Crack Growth Retardation Using a Residual Stress Intensity Concept", Los Angeles Division, North American Rocakewll Paper (May 1971).

[5] Banasiak, D.F., Grandt, A.F., Jr., and Montulli, L.T., "Fatigue Crack Retardation in Polycarbonate", Journal of Applied Polymer Science, Vol. 21, pp. 1297-1309 (1977).

[6] Elber, W., "Fatigue Crack Closure Under Cyclic Tension", Engineering Fracture Mechanics, Vol. 1, No. 4, pp. 705-718 (1970).

[7] Fleck, N.A., and Smith, R.A., "Crack Closure-Is It Just a Surface Phenomenon?", International Journal of Fatigue, Vol. 4, No. 3, pp. 157-160 (July 1982).

[8] Paris, P.C., "Twenty Years of Reflection on Questions Concerning Fatigue Crack Growth, Part 1: Historical Observations and Perspectives, "Fatigue Thresholds", Vol. 1, EMAS Publication Ltd, Warley, U.K., pp. 1-10 (1981).

[9] Fuchs, H.O., and Stephens, R.L, Metal Fatigue in Engineering, John Wiley and Sons (1980).

[10] Saff, C., "F-4 Service-Life Tracking Program (Crack Growth Gages)", Technical Report AFFDL-TR-79-3148, Air Force Flight Dynamic Laboratory, WPAFB, Ohio, (Dec 1979).

[11] Mills, W.J., and Hertzber, R.W., "The Effect of Sheet Thickness on Fatigue Crack Retardation in 2024-T3 Aluminum Alloy", Engineering Fracture Mechanics, Vol. 7, No. 4, pp. 705-711 (1975).

[12] Chanani, G.R., "Fundamental Investigation of Fatigue Crack Growth Retardation in Aluminum Alloys", Technical Report AFML-TR-76156, Air Force Material Laboratory, WPAFB, Ohio (September 1976).

[13] Bernard, P.J., Lindley, T.C., and Richards, C.E., "Mechanics of Overload Retardation During Fatigue Crack Propagation", Fatigue Crack Growth Under Spectrum Loads, ASTM STP 595, American Society for Testing and Materials, pp. 78-97 (1976).

[14] Macha, D.E., Grandt, A.F., Jr., and Wicks, B.J., "Effects of Gas Turbine Engine Load Spectrum Variables on Crack Propagation", Effect of Load Spectrum Variables on Fatigue Crack Initiation and Propagation, ASTM STP 714, American Society for Testing and Materials (1980).

[15] Matsuoka, S., and Tanaka, K., "Influence of Sheet Thickness on Delayed Retardation Phenomenon in Fatigue Crack Growth in HT80 Steel and A5083 Aluminum Alloy", Engineering Fracture Mechanics, Vol. 13, No. 2, pp. 293-306 (1980).

[16] Hess, J.P., Grandt, A.F., Jr., and Dumanis, A., "Effect of Side-Grooves on Fatigue Crack Retardation", Fatigue of Engineering Materials and Structures, Vol. 6, No. 2, pp. 189-199 (1983).

[17] Walker, W., and Beevers, C.J., "A Fatigue Crack Closure Mechanism in Titanium", Fatigue of Engineering Materials and Structures, 1, pp. 135-148 (1979).

[18] Morris, W.L., James, M.R., and Buck, O., "A Simple Model of Stress Intensity Range Threshold and Crack Closure Stress", Engineering Fracture Mechanics, Vol. 18, No. 4, pp. 871-877 (1983).

[19] Minakawa, K., and McEvily, A.J., "On Crack Closure in Near-Threshold Region", Scripta Metallurgica, Vol. 15, pp. 633-636 (1981).

[20] Beevers, C.J., Carlson, R.L., Bell, K., and Starke, E.A., "A Model for Fatigue Crack Closure", Engineering Fracture Mechanics, Vol. 19, No. 1, pp. 93-100 (1984).

[21] Mayes, I.C., and Baker, T.J., "An Understanding of Fatigue Threshold Through the Influence of Non-Metallic Inclusion in Steel", Fatigue of Engineering Materials and Structures, 4 (1), pp. 79-96 (1981).

[22] Suresh, S., and Ritchie, R.O., "A Geometrical Model for Fatigue Crack Closure Induced by Fracture Surface Morphology", Metallurgical Transactions, 13A, pp. 1627-1631 (1982).

[23] Ritchie, R.O., Suresh, S., and Moss, C.M., "Near-Threshold Fatigue Crack Growth in 2 1/2 Cr-Mo Pressure Vessel Steel in Air and Hydrogen", Journal of Engineering and Material Technology, Transaction of ASME, Series H, 102, pp. 293-299 (1980).

[24] Suresh, S., Zamiski, G.F., and Ritchie, R.O., "Oxidation and Crack Closure. An Explanation for Near Threshold Corrosion Fatigue Crack Growth Behaviour", Metallurgical Transaction, 12A, pp. 1435-1443 (1981).

[25] Banerjee, S., "A Review of Crack Closure", Technical Report AFWAL-TR-84, Air Force Wright Aeronautical Laboratories, Wright-Patterson Air Force Base, Ohio (January 1984).

[26] Newman, J.C., Jr., "Prediction of Fatigue Crack Growth Under Variable-Amplitude and Spectrum Loading Using a Closure Model", Design of Fatigue and Fracture Resistant Structures, ASTM STP 761, P.R. Abelkis and C.M. Hudson, Eds., American Society for Testing and Materials, pp. 255-277 (1982).

[27] de Koning, A.U., "A Simple Crack Closure Model for Prediction of Fatigue Crack Growth Rates Under Variable-Amplitude Loading", Fracture Mechanics: Thirteenth Conference, ASTM STP 743, Richard Roberts, Ed., American Society for Testing and Materials, pp. 63-85 (1981).

[28] Newman, J.C., Jr., "A Finite-Element Analysis of Fatigue Crack Closure", Mechanics of Crack Growth, ASTM STP 590, American Society for Testing and Materials, pp. 281-301 (1976).

[29] Fleck, N.A., "The Use of Compliance and Electrical Resistance Techniques to Characterize Fatigue Crack Closure", CUED/MATS/TR.89, Engineering Department, Cambridge University (January 1982).

[30] Mohoney, M.W., and Paton, N.E., "Closure: An Explanation for Fatigue Crack Growth Rate Acceleration/Retardation Due to Overloads in Austenitic Stainless Steels", Fracture 1977, ICF-4, 2, Waterloo University Press, Waterloo, Canada, pp. 1081-1089 (1977).

[31] Irving, P.E., Robinson, J.L., and Beevers, C.J., "A Study of the Effects of Mechanical and Environmental variables on Fatigue Crack Closure", Engineering Fracture Mechanics, 7, pp. 619-630 (1975).

[32] Schimdt, R.A., and Paris, P.C., "Threshold for Fatigue Crack Propagation and the Effects of Load Ratio and Frequency", Program in Flaw Growth and Fracture Toughness Testing, ASTM STP 536, pp. 79-94 (1973).

[33] Buck, O., Ho, C.L., and Marcus, H.L., "Plasticity Effects in Crack Propagation", Engineering Fracture Mechanics, 5, pp. 23-24 (1973).

[34] Gan, D., Weertman, J., "Crack Closure and Crack Propagation Rates in 7050 Al.", Engineering Fracture Mechanics, 15, (1-2), pp. 87-106 (1981).

[35] Frandsen, J.D., Inman, R.V., and Buck, O., "A Comparison of Acoustic and Strain Gauge Techniques for Crack Closure", International Journal of Fracture, 11, pp. 345-348 (1975).

[36] Mahulikar, D.S., and Marcus, H.L., "Fatigue Crack Closure and Residual Displacement Results in Al Alloys", Engineering Fracture Mechanics, 3, pp. 257-264 (1981).

[37] Fleck, N.A., Smith, I.F.C., and Smith, R.A., "Closure Behaviour of Surface Cracks", Fatigue of Engineering Materials and Structures, 6 (3), pp. 225-239 (1983).

[38] Shih, T.T., and Wei, R.P., "A Study of Crack Closure in Fatigue", Engineering Fracture Mechanics, 6, pp. 19-32 (1974).

[39] Sharpe, W.N., Jr., "Interferometric Surface Strain Measurements", International Journal of Non-Destructive Testing, 3, pp. 57-76 (1971).

[40] Sharpe, W.N., Jr., Grandt, A.F., Jr., "A Preliminary Study of Fatigue Crack Retardation Using Laser Interferometry to Measure Crack Surface Displacements", Mechanics of Crack Growth, ASTM STP 590, American Society for Testing and Materials, pp. 302-320 (1976).

[41] Unangst, K.D., Shih, T.T., and Wei, R.P., "Crack Closure in 2219-T851 Aluminum Alloy", Engineering Fracture Mechanics, 9, pp. 725-734 (1977).

[42] Schijve, J., "Four Lectures on Fatigue Crack Growth", Engineering Fracture Mechanics, 11, pp. 167-221 (1979).

[43] Sunder, R., and Dash, P.K., "Measurement of Fatigue Crack Closure Through Electron Microscopy", International Journal of Fatigue, 4, pp. 97-105 (1982).

[44] Bowles, C.Q., "An Experimental Technique for the Vacuum Infiltrating of Cracks with Plastic and Subsequent Study in the SEM", Technical Report LR-249, Delft University of Technology, Department of Aeronautics Engineering (June 1977).

[45] Bachmann, V., and Munz, D., "Fatigue Crack Evaluation With the Potential Method", Engineering Fracture Mechanics, 2, pp. 61-71 (1979).

[46] Sommer, E., "An Optical Method for Determining the Crack-Tip Stress Intensity Factor", Engineering Fracture Mechanics, Vol. 1, pp. 705-718 (1970).

[47] Crosley, P.B., Mostovoy, S., and Ripling, E.J., "An Optical Interference Method for Experimental Stress Analysis of Cracked Structures", Engineering Fracture Mechanics, Vol. 3, pp. 421-433 (1971).

[48] Pitoniak, F.J., Grandt, A.F., Jr., Montulli, L.T., and Packman, P.F., "Fatigue Crack Retardation and Closure in Polymethylmethacrylate", Engineering Fracture Mechanics, Vol. 6, pp. 663-670 (1974).

[49] Packman, P.F., "The Role of Interferometry in Fracture Studies", Experimental Techniques in Fracture Mechanics, SESA Monograph 2, A.S. Kobayash Ed. (1975).

[50] Halliday, D., Resnick, R., Physics Part 2, John Wiley and Sons Publication, Third Edition (1978).

[51] Barker, D.B., Fourney, M.E., "Three-Dimensional Speckle Interferometric Investigation of the Stress-Intensity Factor Along a Crack Front", Engineering Fracture Mechanics, Vol. 17, No. 7, pp. 241-247 (July 1977).

[52] Liechti, K.M., and Knauss, W.G., "Crack Propagation at Material Interfaces: 1. Experimental Technique to Determine Crack Profiles", Experimental Mechanics, Vol. 22, pp. 262-269 (July 1982).

[53] Gray, T.G.F., McKelvie, J., MacKenzie, P., and Walker, C.A., "Interferometric Measurement of J For Arbitrary Geometry an Loading", International Journal of Fracture 24 (1984) R 109-R 114.

[54] Minakawa, K., Newman, J.C., Jr., and McEvily, A.J., "A Critical Study of the Crack Closure Effect on Near-Threshold Fatigue Crack Growth", Fatigue of Engineering Materials and Structures, Vol. 6, No. 4, pp. 359-365 (1983).

[55] Ohta, A., Kosuge, M., and Sasaki, E., "Change of Fatigue Crack Closure Level with Gauge Location Along Crack Line", International Journal of Fracture, Vol. 15, pp. R53-R57 (1979).

END

DATE

FILMED

SEP 26 1984